Influence of Process Parameters on the Tack Behaviour of Dry Fibre Materials in the Context of Automated Dry Fibre Placement

Irene Eby

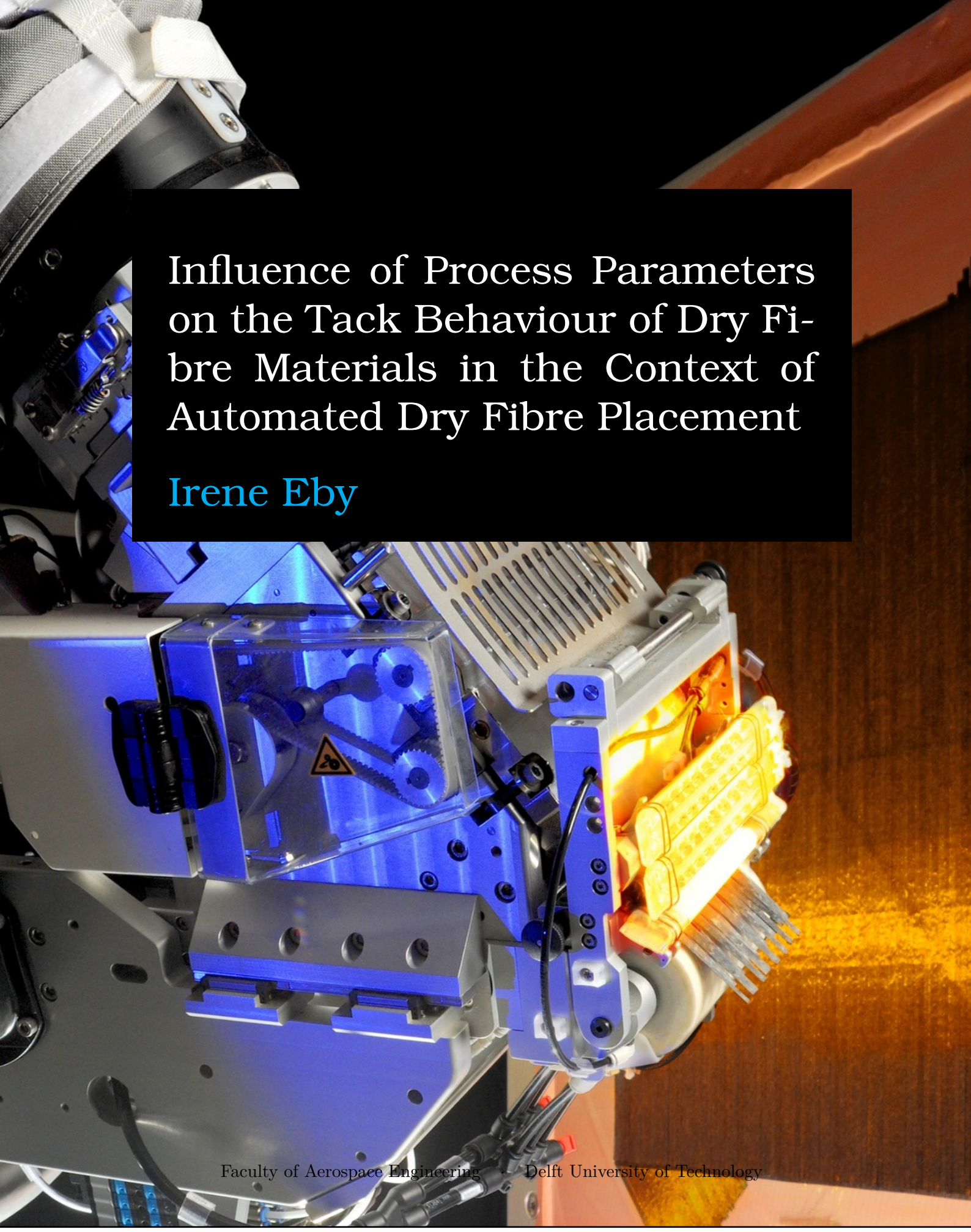

Faculty of Aerospace Engineering · Delft University of Technology

TU Delft Delft University of Technology

Influence of Process Parameters on the Tack Behaviour of Dry Fibre Materials in the Context of Automated Dry Fibre Placement

Master of Science Thesis

For obtaining the degree of Master of Science in Aerospace Engineering
at Delft University of Technology

Irene Eby

26-11-2024

Faculty of Aerospace Engineering · Delft University of Technology

The work in this thesis was done in collaboration with the German Aerospace Centre (DLR), centre for lightweight production technology, Stade. Their cooperation is gratefully acknowledged.

Delft University of Technology
Faculty of Aerospace Engineering
Department of Aerospace Structures and Materials

GRADUATION COMMITTEE

Dated: 26-11-2024

Chair holder:

Dr. JJE (Julie) Teuwen

External examiner:

Dr. B. (Bariș) Çağlar

Academic Supervisor:

Dr. ir. DMJ (Daniël) Peeters

Industry Supervisor:

Dipl. Ing. Dominik Delisle

Acknowledgments

Firstly, I would like to express my sincere gratitude to my academic supervisor, Dr. ir. DMJ (Daniël) Peeters, for his unwavering support, insightful guidance, and invaluable feedback throughout the journey of completing this thesis. His expertise and encouragement were instrumental in helping me refine my ideas and delve deeper into the topic, pushing me to think critically and approach my work from multiple perspectives.

I would also like to extend my sincere gratitude to my industry supervisor ir. Dominik Delisle, at the German Aerospace Centre (DLR). His practical insights and support during my time at the DLR were invaluable, ensuring I had the resources needed to carry out my research effectively. His approachable nature and prompt assistance made the process smoother, and I am particularly grateful for his help in overcoming the challenges I encountered. Working with him at DLR was a pleasure, and I am thankful for the opportunity to gain hands-on experience in such a collaborative environment.

Additionally, I would like to thank the staff and fellow interns at DLR for their support and hospitality throughout my time there. Their assistance and willingness to share their knowledge made my experience at DLR enjoyable. I am particularly grateful to those who contributed to my project, whether by offering technical insights, providing resources, or simply creating a welcoming environment. Their professionalism and commitment to research inspired me, and I am fortunate to have worked alongside such dedicated individuals.

I am also grateful to my thesis defence committee including Dr. Julie Teuwen and Dr. B. (Bariș) Çağlar for taking the time to read, review, and evaluate my work, as well as for showing genuine interest in my research.

Lastly, I would like to extend my heartfelt thanks to my family, partner, his family, and my friends. Their belief in me and constant motivation helped me persevere, even during the most challenging moments of this journey. I am also deeply grateful to every single coffee molecule that fuelled my late nights and early mornings.

Delft, University of Technology — Irene Eby
26-11-2024

Summary

With the increasing demand for manufacturing sustainable aerospace parts, along with cost-effectiveness and preciseness. Automated Dry Fibre Placement(ADFP) has emerged as a promising solution. ADFP combines these goals and enables the production of precise and cost-effective aerospace components with the potential for reduced defects. Tack, which is the adhesion between fibre layers during deposition, plays an important role in achieving high-quality preforms. Tack is essential for securely holding down the plies. Insufficient tack leads to final part defects like wrinkling contributing to the stability of the final part.

This study investigates the influence of nip point temperature, layup speed, and compaction force on the tack behaviour of Hexcel HiTape® dry fibre material during the Automated Dry Fibre Placement (ADFP) process. It also assesses the applicability of an existing tack model, developed for Solvay TX1100 dry fibre material, to the Hexcel HiTape®, possessing a different binder distribution and different fibre architecture. Tack was evaluated using 90-degree peel tests for specimens manufactured using different parameter combinations. Initial statistical analysis of the main parameter effects and interactions used a 2-level factorial design of experiments. To investigate the non-linear behaviour of the parameters, this design was extended to a 3-level face-centred central composite design of experiments.

The results show that temperature is the most dominant factor affecting tack, with higher temperatures significantly increasing tack forces due to binder activation and polymer diffusion at the interface. Layup speed also had a notable influence, with higher speeds leading to increased tack forces, which contrasts with the inverse relationship predicted by the existing model. This is likely due to the material architecture of Hexcel HiTape ®, where faster speeds reduce binder seepage through perforations, allowing more binder to remain at the interface. Compaction force had a minor impact on tack behaviour and the results of this analysis deemed the effect to be statistically insignificant. Additionally, while interaction effects between the parameters were analysed, they were not statistically significant at the 95% confidence level. The findings suggest that the independent contributions of temperature and velocity are key, but deviations from expected behaviour may be due to material-specific characteristics such as perforations and fibre structure. The behaviour of the material in relation to the statistically significant parameters shows that there is non-linearity.To test the generalisability of the model, the existing tack model for Solvay TX1100 dry fibre was applied to Hexcel HiTape ®. This model did not fit the data of Hexcel HiTape ® material. The observed positive relationship between speed and tack, contrary to the Solvay TX1100

model's inverse relationship, shows the need to adapt the model to Hexcel HiTape ® and indicates limitations in generalising tack models across dry fibre materials. Additionally, fibre fraying of Hexcel HiTape® was also observed during peel tests, marking a finding that warrants further investigation to help quantify the effect, aiding in understanding the dry fibre material behaviour.

Table of Contents

List of Figures

List of Tables

Glossary

List of Abbreviations

Abbreviation	**Description**
AFP	Automated Fibre Placement
ADFP	Automated Dry Fibre Placement
ATP	Automated Tape Placement
FRP	Fibre Reinforced Plastic composites
LCM	Liquid Composite Moulding
CFRP	Carbon Fibre Reinforced Polymers
VARTM	Vacuum Assisted Resin Transfer Moulding
VBO	Vacuum Bag Only
RTM	Resin Transfer Moulding
OoA	Out of Autoclave
IR	Infrared
RT	Room Temperature
PEEK	Polyether Ether Ketone
PET	Polyethylene terephthalate
NCF	Non-Crimp Fabric
HDPE	High Density Polyethylene

List of Symbols

Symbol	Description
σ	Tack Strength or Stress
$\sigma_{\max}$	Maximum tack stress at maximum adhesion
Db	Degree of Bonding
Dh	Degree of Healing
Dic	Degree of Intimate Contact
MC	Critical Molecular Weight
tr	Reptation Time
tw	Welding Time
c	Constant
F	Compaction Force
i	Subscript for item
T	Nip Point Temperature
T_g	Glass Transition Temperature
T_m	Melting Temperature
v	Layup Speed
$w_(adh)$	work of adhesion
F_B	Fibre Bend Force
F_S	Total Peel force
F_T	Tack force

Chapter 1

Introduction

Composite materials have become essential in aerospace manufacturing by combining high strength with low weight, meeting the industry's demands for both performance and sustainability. As the need for environmentally friendly solutions grows, lightweight composite construction offers significant potential for reducing pollution through more fuel-efficient aircraft, without compromising safety or durability. Fibre-reinforced plastic composites (FRPs), in particular, provide high specific mechanical properties, allowing for substantial weight reductions while maintaining structural integrity. This weight savings is especially valuable in commercial aviation, where it translates into notable fuel savings and reduced carbon emissions over an aircraft's lifespan. [20] [21] [22].

Efficient manufacturing of FRP components is important to achieving sustainability benefits. Liquid Composite Moulding(LCM) techniques are gaining popularity as they are significantly cheaper owing to the method's reduced labour cost and energy efficiency due to the possibility of automation [23]. This process enables the manufacture of large complex-shaped components in a single cycle. [24].

LCM uses preforms that can be manufactured using AFP (Automated Fibre Placement) techniques. High-volume production of large-scale Aerospace grade components is possible with LCM technology. Currently, most parts are manufactured using conventional semi-finished textile products like non-crimp fabric(NCF) or woven fabrics usually using hand layup techniques. However, these materials due to their flat, areal shape, can generate high levels of scrap of -up to 50% [25], making it challenging to achieve load-specific orientations within the preforms. To overcome these limitations, ADFP can be employed.

Automated Dry fibre Placement (ADFP), which is an advanced fibre placement technology, allows for the precise deposition of dry fibre tapes in variable directions and positions. This process creates a near-net-shape preform with a defined fibre orientation in each layer, optimising the anisotropic properties of the material to meet specific mechanical requirements while minimising mass [26]. The final resin infusion and curing processes often include using an autoclave or LCM process. ADFP reduces the handling of fibres during the preform stage

and provides more flexibility in manufacturing as compared to traditional fibre placement methods like hand layup.

ADFP should not be confused with AFP which is Automated fibre placement.AFP typically uses prepreg materials or fibres pre-impregnated with resin for fibre deposition. In contrast, ADFP uses bindered dry fibre material that is coated with binder that provides tack during fibre placement.

An increasing interest in using dry fibre materials for primary structural components in newer commercial aircraft projects has been observed [27]. This interest is driven by the advantages of dry fibre material, like the absence of out-time due to the stability of the binder at room temperature. Out-time refers to the period, a prepreg material can remain at room temperature before it must be used or returned to storage. Thermoset prepreg materials need to be refrigerated below their cure initiation temperature and when exposed to room temperature, the resin matrix begins to react and slowly cure, thus limiting their handling and storage time outside refrigeration. Therefore, dry fibre materials can help lower production costs by reducing energy consumption and lower material wastage due to the extended life span.

In both processes of AFP and ADFP, the fibres are deposited, using a heating source to heat up the matrix material and the compaction roller on the robotic head presses the incoming material onto the warm substrate resulting in the melting of the matrix/binder in the case of thermoplastic and curing(in case of thermoset), resulting in sticking of the two layers of plies together, creating tack [28].

Tack is essential in ensuring that the individual layers bond securely and stay in place during the manufacturing process. It is especially critical when depositing the fibre layers on curved or complex tool surfaces, where the tows can experience stretching and compression forces. Inconsistent tack can lead to defects, such as wrinkles or dents, which can compromise the product's final quality [29].

To mitigate these defects, it is crucial to understand the influence of process conditions on the tack properties of the dry fibre material.

Tack is influenced by various process parameters [17]. The complex interplay between these parameters necessitates detailed analysis to optimise the ADFP process for consistent and defect-free manufacturing. Currently, there is limited knowledge of the tack behaviour of dry fibre materials during the ADFP process. Most existing models for tack behaviour have been developed for prepreg materials. These models may not be directly applicable to dry fibre materials. This research aims to fill this knowledge gap by systematically investigating the influence of key process on the tack behaviour of dry fibre material in the ADFP process. This is also done by investigating the validity of a previously proposed model for the Solvay TX1100 dry fibre material based on a thermoplastic prepreg material model. This research will assess whether this existing tack model for the Solvay TX1100 dry fibre material can be used for the Hexcel HiTape ® dry fibre material with a different material architecture and binder type or if a new model needs to be developed to account for the unique behaviour if any of this material.

By providing a detailed understanding of how process parameters influence tack in Hexcel HiTape ® dry fibre material, this research will contribute to the development of a more

efficient and reliable manufacturing process for dry fibre materials. The insights gained will not only improve the quality and consistency of FRP components produced using ADFP but also support the broader sustainability goals and use of the technology in applications ranging from aerospace to automotive industries.

Chapter 2 kicks off with an in-depth review of the existing literature, establishing the essential background for the study. Moving forward, Chapter 3 pinpoints the research gaps and sets the stage by outlining the study's objectives research questions and hypothesis. Chapter 4 then explains the methodology of the experiments' setup, including the procedures for specimen manufacturing and subsequent testing. In Chapter 5, the results and discussion section, the focus shifts to presenting and interpreting the results. Chapter 6 concludes the study by summarizing the findings. while Chapter 7 offers suggestions for further research.

The figure 1.1 illustrates the planning of the project

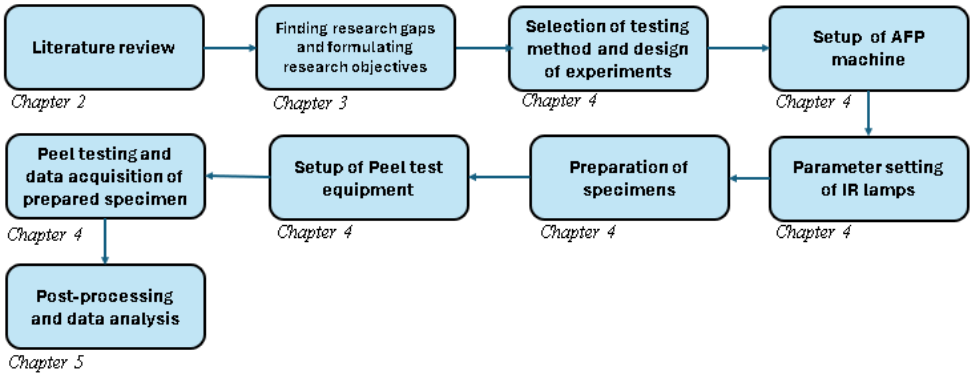

Figure 1.1: Planning of project

Chapter 2

Literature Review

This chapter provides a comprehensive overview of current research in AFP and ADFP technologies, beginning with an exploration of these processes and materials used in sections 2.1 and section 2.2 Section 2.3 delves into the concept of tack formation, highlighting its significance in ensuring proper adhesion during ADFP. Section 2.4 reviews various methods used to measure tack, while section 2.5 analyses the key process parameters: nip point temperature, layup speed, and compaction force, along with their interactions. The insights gained from this review help to identify gaps in the existing research and establish the foundation for the formulation of the research objectives and hypotheses.

2.1 Automated fibre Placement

In the last century, commercial production and industrialization of aluminium have been optimised, to produce large structural aerospace components. While, the development and industrialisation of pre-impregnated fibres or prepregs have only been in commercial use for the last 30 years, while dry fibre materials emerged even more recently. Automated Fibre Placement (AFP) has been developed to automate the placement of fibres in different directions and positions. This allows for an efficient layer-wise deposition to create high-quality preforms with defined fibre orientation in each layer.

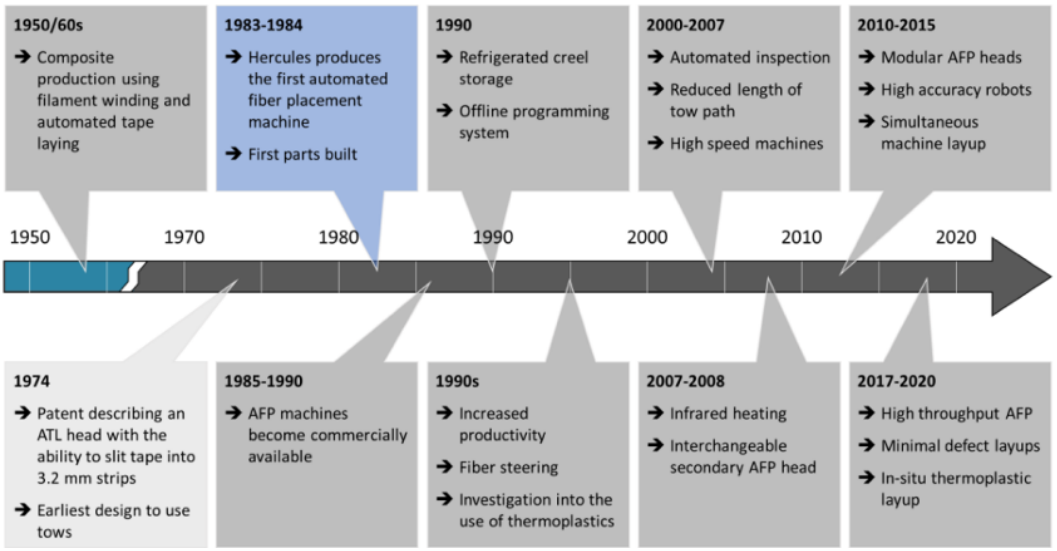

Figure 2.1: Developments in AFP technology [1]

Figure 2.1 demonstrates the key technological developments in AFP over the years, demonstrating how the technology has progressed to its current state. Modern AFP systems are found to achieve minimal defects during layup. The integration of robotics, real-time monitoring and state-of-the-art heating systems ensure that the fibre placement is accurate, and results in minimal wrinkling or fibre misalignment [5]. Compared to traditional methods like hand layup. AFP offers higher precision and productivity ensuring reduced defects such as fibre wrinkling and misalignment. A high level of precision and sufficient tack is essential to reduce the defects in the preforms that could compromise the final part strength. [30]

AFP technology has been employed to manufacture over 1000 composite structures for spacecraft Ariane V, Antares, Pegasus, Delta II, Atlas V, and Delta IV. [31] The use of the high precision and part quality of AFP technology has also been seen in the manufacture of military-grade weapons bay doors for the F-35 Lightning II and wing sections for the B-2 Spirit bomber. [31]Commercial applications of AFP include its use in the Boeing 787 Dreamliner and Airbus A350 XWB [31] [32].

AFP system Overview

An AFP system typically consists of a robotic gantry or an articulated arm that is attached to a layup head as seen in Figure 2.2.

This fibre placement head includes multiple components: heating elements, compaction rollers to press the fibres onto the substrate or tooling surface, and integrated cutting blades inside the AFP head for precise fibre trimming.

The material used in deposition is of high strength-to-weight ratio material. Unidirectional tows are bundles of continuous fibres or filaments made of carbon, glass or other high-performance materials. Each tow is typically 3.175mm to 38.1 mm wide [33], and up to 32 tows can be deposited simultaneously to optimise production. In most AFP applications,carbon fibre reinforced polymers (CFRP) are used due to their excellent strength-to-weight ratios.

The unidirectional tows are fed through the tape head. The tows are carried away from the creel to the tool surface. The heating system preheats both the fibre material and substrate

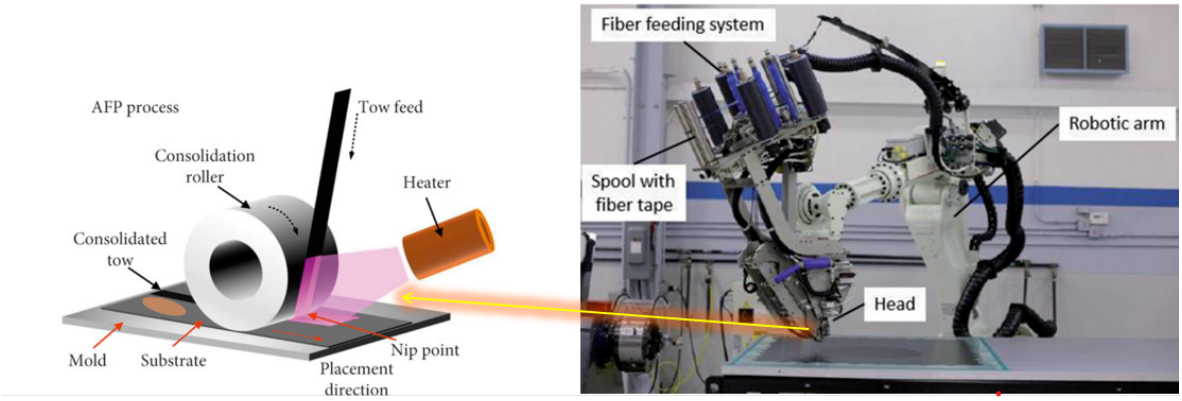

Figure 2.2: Overview of the Automated Fibre Placement (AFP) process (left) and a robotic AFP system (right) with key components highlighted. [2] [3]

while softening the resin matrix above its melting temperature T_m for thermoplastic material and T_g for thermoset materials. There are a plethora of heating systems employed in AFP, including LASER, IR lamps, hot gas torches, and Flashlamp heating systems like humm3® flashlamp that heats up the material using pulsed light. A summary of heating systems used in AFP is shown in table 2.1

Heating Element	Function	Advantages	Drawbacks
Hot Gas Torch	Transfers heat through forced convection. Used for preheating and consolidation, particularly when high temperatures are required for effective bonding [34].	Low capital cost, easy integration with AFP head [35, 36].	Low energy efficiency [37], potential oxidation at high temperatures unless inert gas (e.g., nitrogen) is used, significantly increasing operating costs [36].
Infrared (IR) Heater	Transfers heat primarily through radiation, effective for heating the outer surface of powder-impregnated fibres, but requires good thermal management to avoid inefficiencies [38].	Inexpensive, easy to operate, can output focused heating that performs better than a hot gas torch [36].	Delayed heating process when heat transfer passes through the outer veil to the fibres through convection [38]. Inconsistent heating due to residual heat [39].
Laser	Provides fast and precise heating at the nip point [36], essential for high-temperature consolidation of advanced composites like carbon/PEEK [40].	High radiation intensity allows fast, localized heating; supports very high line speeds due to high power ratings [41]; reduced oxidation with modern diode lasers [36].	High cost, complex setup requiring careful consideration of laser angle, beam profile, and distance to nip point; additional processing parameters and safety measures are needed [42].
Ultrasonic Welding	High-frequency, low-amplitude ultrasonic vibrations generate heat through surface friction, leading to polymer melting and bonding [43].	Short processing time, localized heating with low energy requirements, effective for thermoplastic composites [37, 44].	Performance depends significantly on material properties (e.g., stiffness, hardness) [44].
Flashlamp (humm3®)	Utilizes pulsed light technology to provide rapid, controlled heating, allowing for high-speed fibre placement with precise thermal management [45].	Very high heating rate, excellent temperature control, comparable to high-powered lasers but without restrictive safety requirements [46].	Emerging technology with limited broader application studies [46].

Table 2.1: Summary of Heating Elements Used in AFP

Compaction rollers then apply pressure to the incoming heated material and press it down,

ensuring it conforms to the underlying tool surface or previously laid laminate, known as the substrate. Adhesion between layers is achieved by precisely controlling various process parameters, such as nip point temperature, speed, and compaction force which are tailored based on the specific tow material.

The tool is usually placed with a release film for separation of the produced preform from the tool surface. The separation is also ensured by coating the tool with a release agent if the tows are being deposited directly on the tool surface. The tool surface is not limited to a horizontal flat surface, but can also be on a curved tool surface. This can be introduced into the system both horizontally and vertically.

AFP is advantageous as it can be used to manufacture preforms with complex geometries. For curved tooling and complex geometry, the fibres have to be steered according to the contours while being deposited. AFP is most suitable for fibre steering applications, as significantly narrower tapes are deposited. This is different from Automated Tape placement (ATP), another fibre placement manufacturing technology which deposits wider tapes, usually used for flat or simpler structures. During fibre steering for certain components that possess complex tooling geometry, the narrower tapes deposited using AFP help reduce the formation of wrinkles in the material and additionally reduce material waste. The precision of narrow tows reduces the likelihood of material overhang or excess outside the tool's contour, a common issue with the wider tapes used in Automated Tape Placement (ATP) processes. Wider tapes, while efficient for large flat surfaces, can lead to excess material extending beyond the intended boundaries, which must then be trimmed. This can be seen in figure 2.3.

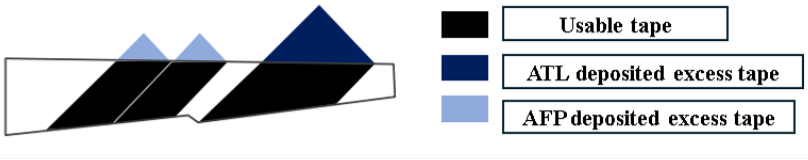

Figure 2.3: Comparison of contour fitting and excess material between narrow tows AFP and wide tapes in ATP [4]

This trimming not only increases material waste but also adds unnecessary weight to the component if not entirely removed. By using narrow tapes, manufacturers can minimise waste and achieve closer-to-net-shape layups, enhancing the component's performance by maintaining a good contour accuracy without the additional weight from excess material.

2.1.1 Materials used in AFP manufacturing

In AFP, the choice of materials is critical to achieving the desired structural properties, manufacturing efficiency, and cost-effectiveness. The primary materials used in AFP are thermoset prepreg, thermoplastic prepreg, and dry fibre. Each material type has distinct characteristics that influence its suitability for specific AFP applications [4].

Material	Processing Temperature	Material Storage	Curing
Thermoset	Low	Frozen	Autoclave/Oven
Thermoplastic	High	Room Temp	*In-situ*/Autoclave
Dry Fiber	High	Room Temp	Infusion

Figure 2.4: Characteristics of different materials used in Automated fibre placement [1]

Thermoset prepreg material

Thermoset prepregs, composed of fibres pre-impregnated with thermoset resin, have been a foundational material in AFP since the process was developed. The low gel point of thermoset resins allows these materials to be laid up at room temperature with minimal heating requirements [47]. Once the resin reaches its gel point, a chemical cross-linking reaction initiates, ultimately creating a rigid, durable structure after curing. This ease of handling at lower temperatures makes thermoset prepregs suitable for applications requiring high strength and stability. However, the low curing threshold also necessitates careful storage in refrigerated conditions to prevent unintended curing reactions. Thermoset prepregs have a limited shelf life, requiring strict inventory control and adding logistical complexity. Additionally, full curing typically requires high-pressure autoclaves or ovens to achieve maximum mechanical properties, which increases both processing time and manufacturing costs [48].

Thermoplastic prepreg material

Thermoplastic prepregs consist of fibres impregnated with high-viscosity thermoplastic resins, which offer advantages in terms of recyclability and durability. Unlike thermosets, thermoplastic resins do not cure chemically; instead, they melt upon heating and solidify upon cooling. This property enables thermoplastic composites to be reshaped, facilitating recycling and repair. Thermoplastic prepregs are therefore well-suited for applications that require high-temperature resistance and reprocessability. [49] Processing thermoplastic prepregs requires high temperatures and pressures, often exceeding several hundred degrees Celsius, to achieve full consolidation. Specialised equipment, such as autoclaves or heated presses, is needed, increasing manufacturing costs. However, thermoplastic prepregs allow for in-situ consolidation in AFP, which can streamline the production process by forming parts directly during layup. Additionally, thermoplastic prepregs are stable at room temperature, eliminating the need for refrigerated storage and providing a longer shelf life compared to thermoset materials. However, these materials are typically more expensive and require higher processing requirements like high temperature and high-pressure equipment, which leads to increased energy costs.

2.1.2 Dry fibre materials

Dry fibre materials are non-impregnated unidirectional carbon fibre tows coated with binder and may contain a mesh veil that is typically thermoplastic glass fibre or carbon fibre [29]. Unlike prepreg materials, which come impregnated with a resin matrix in the material, dry fibres have a binder system. The binder particles can be applied powdered/sprayed on the fibres. This can cause the binder to be unevenly distributed, leading to localised bonding during consolidation as certain areas are binder-rich and certain regions where the binder is not present at all. Another method is coating the fibres with a veil of binder, the thickness of the veil applied can differ across the fibre resulting in binder-rich and binder-poor regions.

One key advantage of dry fibre material is its extended shelf life. The binder remains inactivated at room temperature, reducing the need for cold storage. This improved storability makes dry fibre material easier to handle logistically and more cost-effective compared to prepregs, which require refrigeration and must be processed within a particular time

frame after thawing to prevent the resin from curing immaturely, causing potential material wastage. [50] Moreover, dry fibres allow for a longer processing window, as the binder is activated through heating during the layup process. This flexibility contrasts with that of thermoset prepregs, where processing must occur within a limited window after thawing. [1]

Another advantage of dry fibre is its ability to be steered easily without tow bending or shearing because there is no resin matrix confining the fibres [51], making it less stiffer. The absence of a resin system within the material reduces the chances of resin build-up in regions of the material, which can result in variability in the mechanical properties of the final part [27]. However, this absence of a resin system can cause fibre fluff Dry fibre tows can be manufactured through different processing each affecting the final tow characteristics. One common method is the slitting process, where the binder-stabilized material sheet is slit into tapes. Although this minimizes tape width variability, it often results in loose fibres along the edges. These loose fibres can leave residues on the surface of the tape. Another process of manufacturing dry fibre material is the tow-based process where the raw carbon tow is converted to a tape that is further stabilised with the help of a binder material [52]. The different commercially available dry fibre tows are shown in Figure 2.5.

Material ID	Supplier	Product name	Nominal fiber density, g/cm^3	Nominal areal weight, g/m^2	Nominal tape width, mm	Binder type	Binder application	Tape type
A	Cytec Solvay Group, US	TX1100 IMS65	1.78	196	6.35	EP	CF veil + EP powder	Slit tape
B	Toho Tenax Europe GmbH, Japan	TENAX-E HTS40 X030	1.76	126	6.35	EP	EP powder	Tow based
C	Porcher Industries, France	TP bindered yarn	1.77	126	6.35	TP	TP powder	Tow based
D	Hexcel Corporation, US	HiTape®	1.79	210	6.35	TP	TP veil	Tow based
E	Porcher Industries, France	TP bindered yarn	1.78	261	6.35	TP	EP powder	Tow based

CF = carbon fiber; EP = epoxy based; TP = thermoplastic based.

(a) Types of commercially available dry fibre material [52]

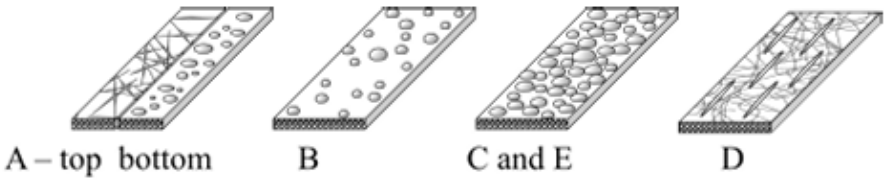

(b) Sketches of the material architecture of commercially available dry fibre material [53]

Figure 2.5: Overview of commercially available dry fibre materials and their surface topographies. (a) Types of commercially available dry fibre materials. (b) Sketches of the material architecture of these dry fibre materials.

From the investigations done by Veldenz et al [52], different commercially available dry fibre tapes were studied. The surface topographies of these dry fibre tapes are illustrated in Figure 2.5.

The dry fibre materials follow a similar architecture, with binder material on the surface of the tows. Material A has a carbon fibre mesh with a binder on one side and only epoxy binder particles on the other side. The carbon veil/mesh is present to improve the tack between the

Material	Material Composition	TOP Architecture	BOTTOM Architecture
A-Solvay TX1100 IMS65	CF veil + Epoxy powder	Carbon fibre Mesh + Epoxy Binder	Epoxy Binder particles
B-TENAX-E HTS40 X030	Epoxy Binder	Epoxy binder	Epoxy binder
C-Porcher TP Bindered yarn (126 gsm)	Thermoplastic binder	Thermoplastic binder	Thermoplastic binder
D-Hexcel HiTape®	Thermoplastic veil + perforations throughout fibre	Thermoplastic veil + perforations throughout fibre	Thermoplastic veil + perforations throughout fibre
E-Porcher TP bindered Yarn (261 gsm)	Thermoplastic Binder	Thermoplastic binder	Thermoplastic binder

Table 2.2: Material Compositions and Architectures

plies during layup by increasing the surface area and as a method of interlaminar toughening as the veil will ensure uniform uptake of the resin and the binder acting as a flow channel.

Materials B, C and E have the binder system on both sides of the tapes. Material B shows a lower density of binder than materials C and E. Material D contains a thermoplastic-based binder veil on both sides. There are perforations on the tapes that are manufactured to enhance the permeability of the tapes through the thickness direction during resin infusion and to increase the strength of adhesion through the thickness. B and C ,which are the materials with the lowest areal weight) exhibited a high amount of defects, the reason for this was that the thin tapes were not as stiff as the other materials and was prone to folding and twisting. Tapes manufactured using the slit tow process show the least variability in width, however, some edges had loose fibres that caused an increase in fibre residue on the substrate. The effect of these topographies on tack properties of the materials, to ultimately decrease the fault count of the final preform are yet to be investigated Dry fibre materials with a thermoplastic binder system have a shorter temperature range than thermoplastic prepreg material.

2.2 Automated Dry fibre Placement (ADFP)

ADFP or Automated Dry fibre Placement is fundamentally similar to AFP in terms of deposition hardware, but differs primarily in the material used. ADFP utilises bindered dry fibre materials rather than prepreg tapes. The melting of the binder of dry fibre material using the heating element on the ADFP head helps achieve the tackiness required during fibre deposition. Achieving tack requires carefully controlled heating to melt the binder at the point where the fibre meets the substrate, known as the nip point. Both the substrate and incoming tow must be heated at the nip point to create sufficient tack between the layers, allowing for effective layer-wise adhesion and creating a stable preform.

Compared to ADP, ADFP offers cost reduction due to its reliance on lower-cost raw materials, liquid resin and the post-processing of the preforms using Out of Autoclave process (0oA). Ooa processes like Resin Transfer Moulding(RTM), Vacuum Assisted Resin transfer moulding (VARTM), Vacuum Bag only (VBO) methods counter the high costs related to when using autoclave equipment and high energy consumption. Using vacuum pressure and moderate heating instead of the high temperatures and pressures cut operational costs significantly. Additionally, dry fibres and liquid resins contribute to lower logistical costs as well. Large aerospace-grade parts that wouldn't fit into autoclaves or need custom autoclave can be manufactured using ADFP followed by OoA processes.

Laminates that are manufactured using ADFP with vacuum resin infusion demonstrate improvements over the manual layup method with vacuum infusion, including a 9% increase in fibre volume fraction from 47.80% to 56.30%. [54].Liu et.al [50] demonstrate that using the AFP-processed preform lowers porosity from 2.00% to 0.6% and reduces the coefficient of thickness variation from 8.11% to 3.75% [50]

Dry fibres used in ADFP also bring notable improvement in resin flow during the infusion step after the production of preforms. As the dry fibre is devoid of pre-impregnated resin, it reduces the chances of resin pooling and void formation, leading to higher part uniformity and fewer defects in the final composite part. This allows manufacturers to tailor resin distribution precisely, resulting in more permeable structures and enhancing consistency in mechanical properties. This is important as these parts must perform consistently under stress conditions.

A summary of the AFP and ADFP processes is tabulated in table 2.3

Category	**Thermoset AFP**	**Thermoplastic AFP**	**ADFP**
Heating Requirement	Low temperature: typically under 70°C [55], [56]	High temperature: around 400°C for PEEK [57]	Moderate temperature: around 200°C for Solvay TX1100 tapes [50], [52]
Pressure Range	Low pressure: usually below 0.3 MPa [55], [58]	0.3 to 0.9 MPa [57]	Approximately 0.25 to 0.87 MPa [54], [52]
Post-Processing	Autoclave curing for optimal quality	Autoclave consolidation for best results	Resin infusion followed by OoA curing
Primary Advantage	Well-established; requires low heat and pressure	Environmentally sustainable; potential for in-situ consolidation	Cost-effective with OoA curing, reducing equipment and operational costs
Disadvantages	Long autoclave curing times increase production costs and limit flexibility	High processing temperature and pressure increase energy demands	Requires resin infusion, adding complexity to the process; lower interlayer bonding strength compared to autoclave processes

Table 2.3: Summary of AFP and ADFP Processes

In the Aerospace industry, the goals of AFP and ADFP processes are not only to reduce defects but also to meet strict quality standards defined by individual manufacturers for their components. By developing a reliable process that achieves consistent tack and precise fibre placement, ADFP can minimize the need for rework and achieve high quality aerospace grade parts [1].

2.3 Tack and its influence

Tack, is the ability of a material, to adhere to itself or other materials when processed [17] or the property possessed by a material that helps it to form a bond immediately on contact with another surface, which can be a layer of adhesive [6].

Why understand tack?

During the deposition of the tapes on tools with complex geometry or during fibre steering, the material is stretched and compressed in different ways. The fibre is very stiff (no longitudinal extension) along the length, which suggests a significant amount of stress build-up in the material with longitudinal extension. This stress state can lead to a loss of stability in the finished part as the preform is imbalanced and has insufficient transverse and normal support, causing internal stresses. These internal stresses are relieved through deformations in the material. For example, when fibres have to be laid up on a concave tool, there exists a longitudinal tensile force that exists long the fibre direction that can cause the tape to unravel perpendicular to the fibre direction. When this longitudinal force exceeds the tack strength, it can cause the fibres to partially lift, creating a shear failure known as bridging .Bridging shear compromises the intended placement, leading to partial detachment of the fibre from the tool surface, as can be seen in figure 2.6.

The fibres that are deposited have an amount of tack between the plies, with the tack force being the force holding the different plies together. In the case of a convex tool, insufficient tack can cause the fibre to lift off the tool which can also be exaggerated with the bending stiffness of the fibre is high causing a force to act normally to the end of the tape causing fibre pull-up that can be seen in figure 2.6.

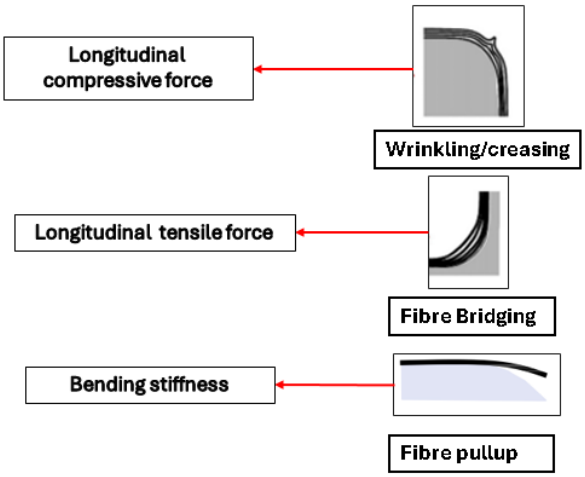

Figure 2.6: Examples of Material damage mechanisms influenced by tack strength of material post AFP deposition

During fibre steering, the fibres experience compressive force on the inner side along the fibre direction (Longitudinal compressive force) which causes bumps and fibre creasing. A

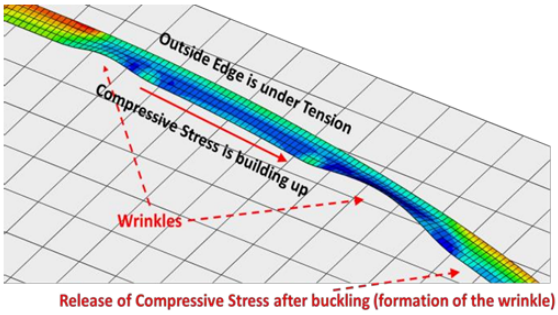

Figure 2.7: Stress distribution of resulting fibre wrinkling [5]

sufficiently high tack strength between the plies is necessary to avoid the formation of these types of damages because the tack counteracts the internal stresses. Obtaining high enough tacks requires an understanding of the effect of process parameters like layup speed, nip point temperature and compaction pressure. [59] [60].

Formation of tack and tack models

In the analytical studies initially conducted by Matveev et al. [29], the tack model was derived from an experimental analysis using thermoplastic prepregs [29].

In the development of the tack model for the Solvay TX1100 dry fibre material, Saar [4] used this thermoplastic prepreg model as a baseline for modelling the tack behaviour of the Solvay TX1100 dry fibre material. The Solvay TX1100 dry fibre epoxy binder was formulated to have thermoplastic properties and behave similarly to thermoplastic binder material. Therefore the model proposed by Saar [4] was based on the assumption that this material would behave similarly to thermoplastic prepreg material. The most important difference between these two materials is that in the process modelling of thermoplastic prepreg material, the material

has a resin matrix impregnated homogeneously resulting in complete consolidation across the entire material. However for dry fibre material, the binder is applied as a veil or sprayed on binder particles. From the figure 2.8, the difference in the matrix distribution of the prepreg and dry fibre material can be observed.

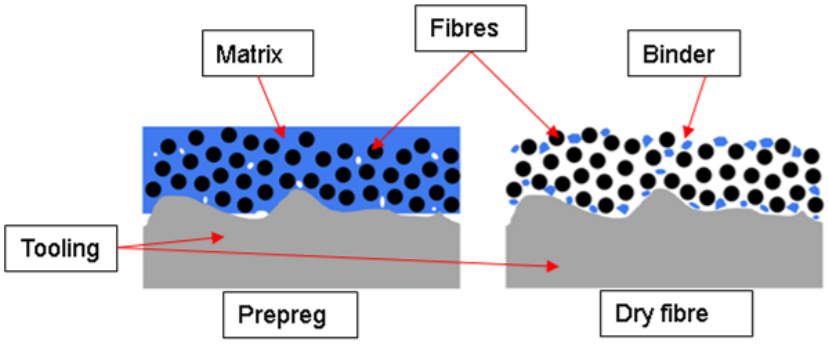

Figure 2.8: Prepreg vs dry fibre architecture [6]

Figure 2.8 shows the resin matrix in prepreg material is seen to be distributed throughout the thickness of the material, whereas in dry fibre material, the binder particles are coated on the surface of the material.

In the contact surface between the two thermoplastic interfaces, the bond is mainly formed through fusion bonding [7]. In addition to fusion bonding (binder to binder), interfacial bonds exist as well between the binder and the sizing of the fibres. Therefore, the following processes can occur during the bonding of dry fibre thermoplastic material:

- binder to binder specific cohesion (chemical, thermodynamic, fusion bonding) [4]
- Mechanical adhesion between binder and fibre (mechanical interlocking) [61]

Fusion bonding model

The typical manufacturing cycle for composites involves heating the material above the polymer's melting temperature, applying a specified pressure for a set duration to ensure proper consolidation, and cooling the material while maintaining that pressure. The consolidation phase is particularly crucial, as it influences the final material properties and the effectiveness of the bond formed between layers. This cycle is common across different heating methods, including infrared, hot air, thermal conduction, laser, electromagnetic radiation, microwave, radio frequency, and friction [7].Fusion bonding is the common physical model used to explain the cohesion between the plies. The fundamental mechanisms in fusion bonding process include: Heating, Intimate contact development, Polymer Chain Diffusion(Autohesion), Consolidation and cooling.

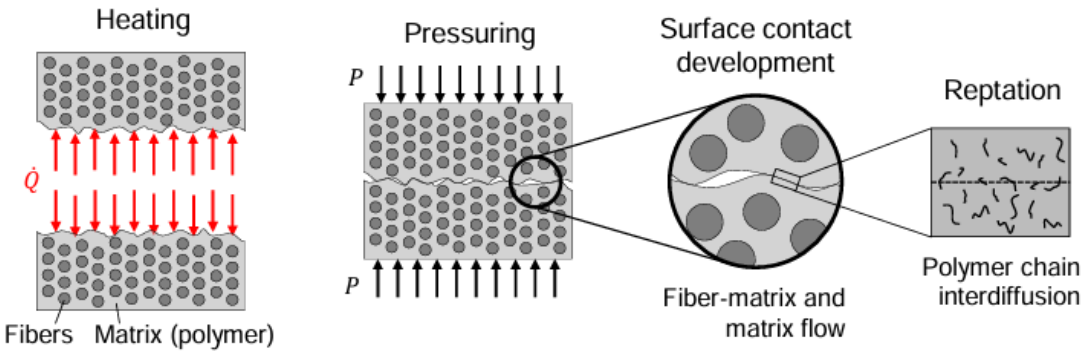

Figure 2.9: Fusion bonding mechanism [7]

Heating: Heating of the incoming material and sub is important as it determines the quality of the bond between the ply interface. The temperature at the nip point must exceed the T_m of the thermoplastic binder which ensures better intimate contact and prevents the formation of voids that cause part defects. There are a plethora of heating systems employed in ADFP, including LASER, IR lamps, hot gas torches, and Flashlamp heating systems like humm3® flashlamp that heats up the material using pulsed light. A summary of heating systems used in AFP is shown in table 2.1.

Intimate Contact Development: As the material is heated up, the binder becomes soft and pliable. Heating up the material causes the binder molecules to gain kinetic energy that overcomes the intermolecular forces. These weakened interactions reduce the resistance to flow, further lowering the viscosity [62].

Pressure is applied simultaneously using the compaction roller to bring the plies in intimate contact. Initially, the surfaces of the plies may be rough and not fully in contact. There are gaps between the layers owing to the surface roughness as can be seen in figure 2.10. The heat and the pressure work together to flatten these rough surfaces, allowing them to come into intimate contact, this step ensures the stage for a strong bond. At the micro level, bond formation occurs only in areas of intimate contact [63].

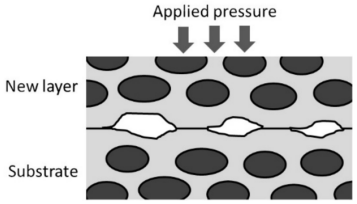

Figure 2.10: Gaps between the two plies due to surface roughness in prepreg material [8]

The effective surface contact depends on the surface roughness of the surfaces to be joined. In the intimate contact model proposed by Dara and Loos [64] to study the influence of process parameters of contact time, temperature, and compaction pressure, D_{ic}(Degree of Intimate contact) is used to describe the effective contact area. The $D_{ic}$is the ratio of the area in contact to the total interface area. The viscoelastic behaviour of the thermoplastic is modelled as the flow of a homogeneous fluid being pressed between two plates.

$$D_{\text{ic}} = \frac{\text{Area in contact}}{\text{Total area of the interface}} \tag{2.1}$$

[4] When D_{ic}=1,complete intimate contact is achieved. The degree of bonding D_B between

the surfaces can be explained as a coupling of Degree of Intimate Contact(D_ic) and Degree of healing (D_h) [4]

$$D_{\mathrm{B}} = D_{\mathrm{ic}} \cdot D_{\mathrm{h}} \tag{2.2}$$

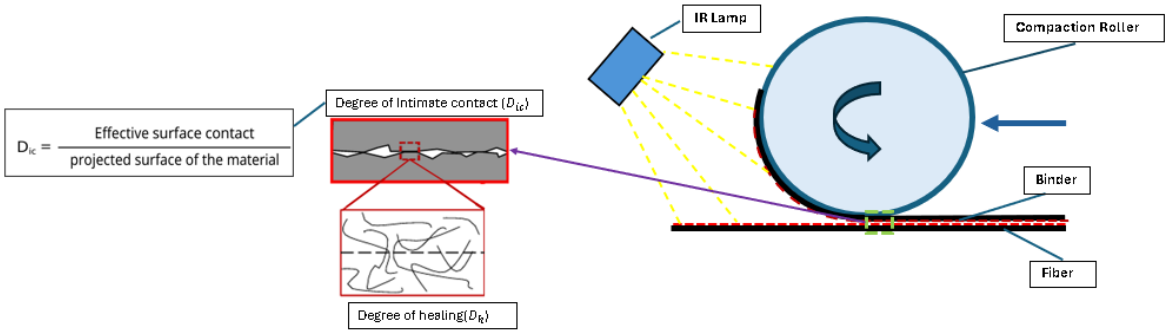

Figure 2.11: Fusion bonding mechanism

Polymer Chain Diffusion(Autohesion): Once intimate contact is achieved, the bonding process begins at the contact points. The polymer chains in the thermoplastic material start to diffuse across the interface between the layers. This process is called autohesion. As the chains are mobile and inter diffuse, they effectively "heal" the bond between the two surfaces.

Autohesion starts when the temperature applied exceeds the T_g(glass transition temperature) of the matrix material. The longer the surfaces are held in contact at the right temperature, the more and more chains get to move and diffuse, leading to a stronger bond.

The thermal movement of the long linear ,entangled macromolecules can be explained by De Gennes' reptation theory [65], According to this theory, the dense entanglement of polymers restricts their motion to a confined "tube" formed by neighbouring chains. Within this tube-like region, the chains can only move forward and backward in a manner resembling the slithering of a snake within a narrow corridor—a process referred to as reptation.At larger time scales, the polymer chains elongate, and the ends of the chains can extend beyond the confines of the tube, forming minor chains. Eventually, the polymer chain relocates to a new position outside the initial tube. The time required for a polymer to reach this new configuration is known as the reptation time (t_r) [65].

Based on this theory Yang and Pitchumani proposed a model to describe autohesion under non-isothermal conditions [66]. In their model, the bonding process at the interface is influenced by the critical entanglement molecular weight (M_C), which is dependent on several factors, including the number of monomers, polymer chain length, monomer weight, the number of C-C bonds per monomer and bond length [67]. For thermoplastic polymers where the molecular weight M exceeds eight times the critical molecular weight (M>8M_C), the maximum bond strength is typically reached at the welding time (t_w), with t_w<t_r. This relationship is valid for most engineering thermoplastic polymers. The degree of healing $D_h(t)$ is given by equation 2.3

$$D_h(t) = \left[\int_0^t \frac{1}{t_w(\vartheta)}\, dt\right]^{\frac{1}{4}} \tag{2.3}$$

[66]

where t_w is weld time, ϑ is process temperature,

For polymers with a molecular weight less than 8 times the critical entanglement molecular weight (M<8M_C), the welding time equals the reptation time (t_w=t_r).This shows that the welding time t_w is temperature-dependent following an Arrhenius relationship. As the temperature increases, the polymer chains are able to diffuse more easily, resulting in a shorter t_w. According to Saar [4], the arrhenius relationship that describes welding time with the process parameters of temperature, pressure, and speed is as follows:

$$D_h(t) = \left[\frac{t}{A \exp\left[\frac{E_a}{R}\left(\frac{1}{\vartheta} - \frac{1}{\vartheta_{ref}}\right)\right]}\right]^{\frac{1}{4}} \tag{2.4}$$

- $D_h(t)$: Degree of autohesion with time t
- t: Time of the process
- A: Pre-exponential factor (constant based on material and process)
- E_a: Activation energy (material-specific energy required for tack behaviour to initiate)
- R: Universal gas constant (8.314 J/mol · K)
- ϑ: Process temperature (in Kelvin)
- ϑ_{ref}: Melting temperature (T_m)(in Kelvin)

equation 2.4 models the evolution of tack behaviour, factoring in time, temperature, and activation energy. Tack increases with time, but higher process speeds (inversely proportional to time) reduce tack formation. The Arrhenius relation shows that higher temperatures enhance tack by reducing the activation energy barrier, enabling more molecules to reach the necessary activation energy.

Consolidation: After the polymer chains have diffused and the bond is formed, the material needs to be consolidated. This step happens as the material cools down. Pressure is maintained during cooling to ensure that the bond remains strong and that no gaps or voids form between the layers. Proper consolidation prevents defects like delamination (where layers separate) or porosity (where air pockets form), which can weaken the composite material.

Cooling:In the final step, the material is allowed to cool below the glass transition or melting temperature as the compaction roller is passed over the material.As it cools, the polymer chains become less mobile, and the material regains its stiffness. The bond that was formed during the previous steps is now locked in place, resulting in a solid bond.

2.3.1 Physical model Proposed for tack prediction

To quantify the effects of the parameters,a physical model based on the fusion bonding model and equation 2.4 was developed by Saar in his investigation of tack behaviour of the Solvay TX1100 dry fibre material. This model, predicts tack force as a function of temperature, force and velocity. The general form of the physical equation is :

$$f_P(T, F, v) = \frac{cF^{0.2}}{a \exp\left(\frac{b}{5T}\right) v^{0.5}}$$

[4]

- f_p represents the predicted tack force
- T is the nip point temperature (in degrees Celsius)
- F is the compaction force
- v is the layup velocity (in m/s)
- a,b and c are the empirical parameters that capture the material-specific effects

The equation incorporates both temperature dependence, with the exponential term and mechanical force effects(as a power function of F). This approach is designed to capture the non-linear interactions between the parameters, which are essential in predicting the tack behaviour in different operational settings.

2.4 Measurement of Tack

Historically in the realm of AFP processing, tack is often used to refer to prepreg adhesion and the literature present to date has significant studies on prepreg tack. However, there is research yet to be done on dry fibre material to quantify the tack properties. Usually, the manufacturers of materials used for AFP processes give very little information on the precise tack properties of the prepreg material/binder material on the dry fibre. Datasheets are usually limited to general data such as 'low', 'medium' or 'high' tack, and for prepregs [17], Practically, the quality of part is dependent on experience working with the material and the AFP process all the while running the risk of using unusable material or disposing of expensive material after the tack life expiry (only in the case of prepregs). This lack of knowledge can cause defects like fibre bridging or fibre buckling as seen in figure 2.6. This calls for an understanding of the interaction of the tack behaviour of the material and the process parameters. Measurement of tack is thought to be a straightforward property, however it depends on multiple factors and their interactions.

Probe tack testing

The most common method in literature to quantify tack, typically for prepregs, is the probe tack test. In this method, the sample is introduced between two plates and compacted using the lower punch plate moving upwards for a defined time under a specific pressure. After compaction, the sample is unloaded at a controlled speed in the normal direction to the surface. During this unloading, the axial displacement and detachment force are simultaneously tracked. The tack is calculated in the form of tensile force as a function of strain [13]. However, Wohl et al. [68], used a rheometer to find out prepreg tack by probe tack testing. The advantage of probe tack testing is that it is a quick and relatively simple method of testing tack. There is precision in the control of the parameters used and in assessing the reproducibility of the results [69].

However, the probe test only provides the value for the initial tackiness and not the long-term adhesive properties of the material. The matrix in the joint zone is reduced between the stamp plate and the sample when the thermoplastic matrix begins to flow owing to its lower viscosity at a higher temperature and pressure. Therefore, lower tack is observed at high temperatures [70].The debonding rates tested are relatively low compared to those seen in a real AFP process [71]. This is explained by Crossley [72], who states that the measured values of the probe test do not align with the tack during the AFP process as failure can occur here in which the fibres of the relatively short sample are torn out. This failure is a rare sight in AFP laid-up samples with long continuous fibre-reinforced tapes.

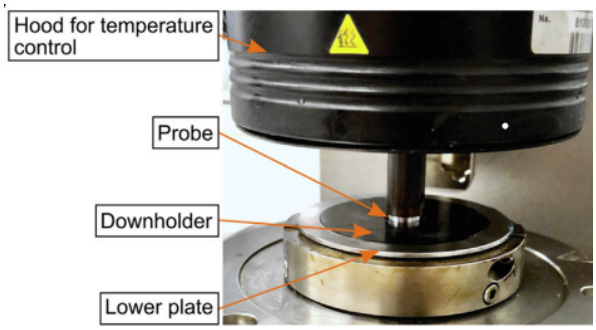

Figure 2.12: Probe tack test setup [9]

Peel testing

Peel tests are another method employed in tack testing of materials and is the standard method for characterizing tack of prepreg material as described in ASTM D8336-21 [73].A sample of the material is deposited using AFP or hand layup onto a plate.Next, this sample is detached from the plate by peeling it off with an applied force as shown in Figure 2.13. The angle of peel has to be consistent throughout the peel test. One end of the sample is attached to the tensile machine with different peel angles depending on the type of peel testing used.

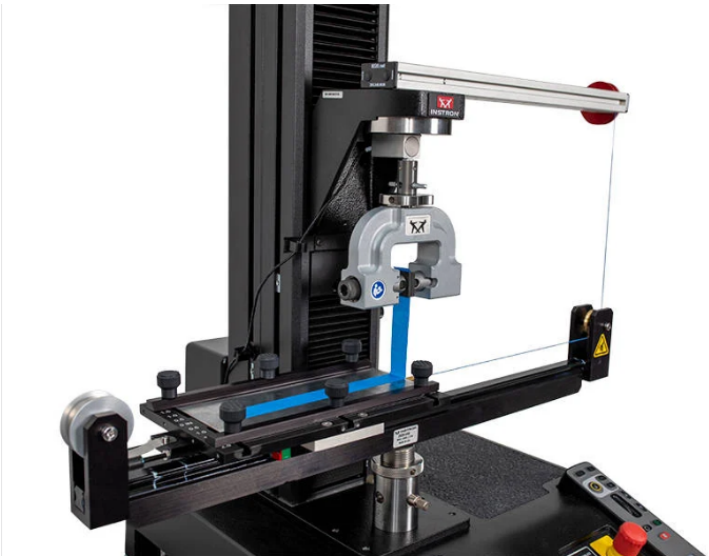

Figure 2.13: 90 degree Peel test setup [10]

Peel testing is found to be more accurate than the probe tack testing. This is because it accounts for a larger length of the sample, while the probe test accounts for only a small area of the specimen. The contact area for probe testing is very small, just a few millimetres in diameter, where the probe contacts the surface to measure the tack force [74].

Peel testing has been used in various configurations based on the angle of the peel. Common configurations of peel testing include the 90° peel test, the floating roller peel test, and the T-peel test.This is illustrated in figure 2.14.

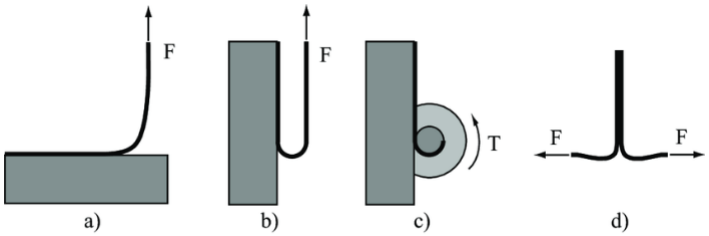

Figure 2.14: Types of peel tests a) 90 °peel test b) 180 °peel test c)Floating roller peel test d) T-peel test [11]

Readings from peel tests typically include the peel force F and in some cases the work of adhesion W_{adh} [13]. To ensure comparability, the results from the peel tests are usually normalized over the width of the specimen. The described peel tests are based on the standards of pressure-sensitive adhesive(PSA) but are sensitive to factors such as the specimen application method and specimen stiffness, which is considerably higher in the case of dry fibre.

Crossley et al. [12] introduced a prototype peel testing system to test for compliance and determine the tack behaviour of prepreg material. This experimental setup as seen in figure 2.15 allowed the simultaneous measurement of the peel force at the moment of deposition, providing insight into the influence of layup parameters like compaction force.

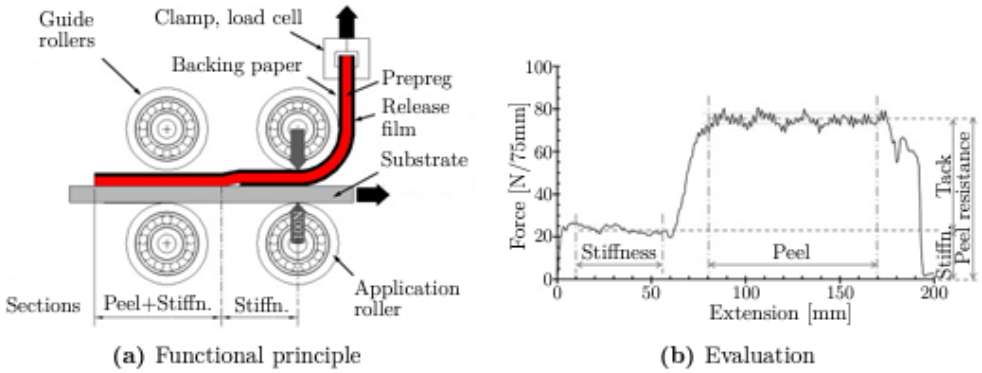

Figure 2.15: single stage peel test adapted from Crossley [12] [13]

The experiment investigated the normal and shear forces experienced by the prepreg undergoing detachment from the sample plate. The results found from this peel test were found to be very consistent showing a 16% standard deviation. He conducted tack testing using the probe tack method as well. However, the results revealed major inconsistencies.

Wedge peel test

Wedge peel testing is used to test the interlaminar strength of fibre-reinforced composites. In this test, a wedge is inserted between the layers of a laminate to induce delamination by driving the wedge along the length of the sample, typically under Mode I (opening) loading conditions. The test is straightforward and can be performed relatively quickly, providing insights into the bond strength between layers. The force required to propagate the delamination is recorded, and the wedge peel strength is calculated based on the force normalized over the width of the specimen [75].

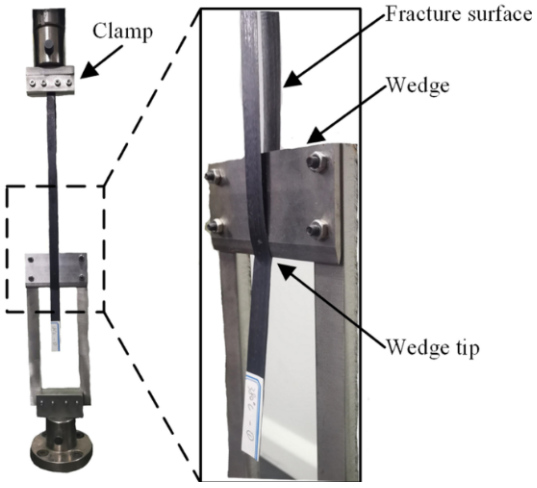

Figure 2.16: Wedge Peel test setup [14]

Although the wedge test offers quick results and is often used for initial assessments, it is not standardized and suffers from several limitations. For example, the wedge peel test is highly sensitive to frictional effects between the wedge and the material, which can lead to variability in results. Additionally, the test induces multiple failure mechanisms such as fibre breakage

and inter-fibre breakage, making it challenging to isolate the effects of the interfacial forces alone. [75].

Comparatively, the 90-degree peel test is standardized under the ASTM standard ASTM D8336-21 [73] and is particularly advantageous to AFP laid tow force measurement as it can provide a more consistent and repeatable measurement of the peel force required to separate the plies. The design of the test ensures that it is less influenced by extraneous factors like friction or complex stress states, making it more reliable to characterize the tack behaviour.

Some other tests for tack measurement

In addition to probe, peel and wedge tack tests, there are other measurement techniques that have been developed to assess the tack of prepreg materials. Nguyen and Krombholtz [76] manufactured single lap shear specimens using AFP and evaluated them on a custom-built test bench. Subsequently, Nguyen and Delisle [77] designed a tack measuring system that measures the shear force required to pull the AFP-manufactured specimen from the substrate providing insights into the adhesion between laid-up prepreg tow and substrate.

Böckl et al. [78] proposed a tack test based on friction, where the material is passed through a pair of rollers under load, and the resulting transverse frictional force was used to indicate tack. As this is a continuous measurement technique, it holds potential for integration into the material feed of an AFP unit, allowing the real-time monitoring and measurement of tack during AFP manufacturing.

2.5 Parameters and Tack Dependence

The effect of process parameters on the tack behaviour of prepregs has been extensively studied as shown in the following subsections. According to [60]and [59] the three most important parameters to investigate the tack behaviour for prepreg materials are processing temperature, compaction force and Lay up speed. The tack behaviour of dry fibre materials can also modelled by understanding the interactions and influence of these parameters. Following the peel test prototype developed by Crossley et al. [12], Endruweit et al. [79] highlighted the need to investigate a range of test parameters to explore the complex tack properties.

2.5.1 Nip Point Temperature

Through the control of nip point temperature, the AFP processes can be tailored for different prepreg materials. According to Bakshi et al [15], with increased values of temperature, the tack values reach a maximum peak and then decrease, as seen in Figure 2.17. Heating up any resin system results in the bonding of the material with the substrate, this bonding is the result of heating the binder in incoming tows up to it's glass transition T_g temperature. Thermoplastics have a higher T_g , around 200 °C, even reaching up to 600 °C, resulting in higher processing temperatures [80] For resin systems such as the ones present in prepregs, the temperatures affect the viscosity of the resin. With higher temperatures, there is lower viscosity of the resin giving it the ability to efficiently wet the surface of the fibres, leading to better intimate contact between the bonding surfaces [15].

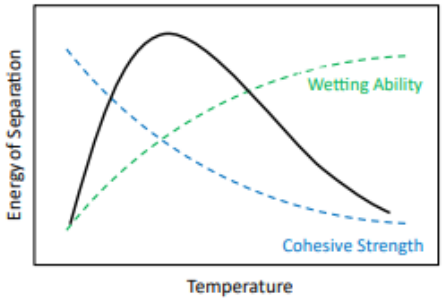

Figure 2.17: schematic representation of the evolution of tack energy of separation with varying temperature [15]

The findings of Saar [4] while investigating the tack behaviour of the Solvay TX1100 dry fibre material found that the tows consolidated at higher nip point temperatures showed larger peel force values implicating higher tack strength, which could be because the increased wetting ability of the binder at higher temperatures, resulting in a higher intimate contact between the ply interface resulting in strong cohesive bonding after consolidation of the material.

Bakshi et al. [15], view the dependence of nip point temperature on tack as a tradeoff between having sufficient adhesive interactions at the interface of the material and substrate and the cohesive strength. He also states that maximum tack performance is obtained at the transition region from cohesive to adhesive failure. Lower temperatures result in adhesive failures, while cohesive failures occur at higher temperatures, due to the failure of the resin itself. Crossley et al. [72] observed the same type of failure in their samples, and Budelmann et al. [17] observed the same behaviour in their study. It can be observed that nip point temperature is a significant parameter in the layup process, and it is also highly dependent on the material used. The trends of thermoplastic and thermoset prepregs at varying temperatures can be seen in Figure 2.18. However, the processing temperatures for dry fibre materials vary with the manufacturer's specification.The trends of dry fibre materials for different ranges of temperatures have yet to be studied.

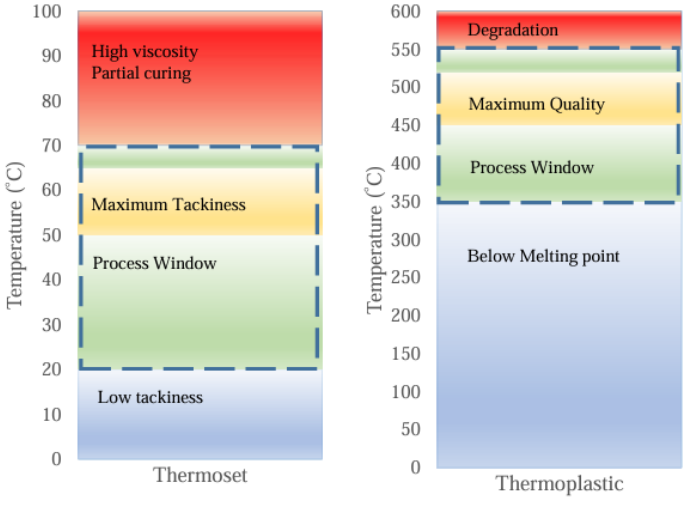

Figure 2.18: Trends in the effects of temperature on thermoset and thermoplastic prepreg materials [16]

As can be seen in figure 2.18, processing temperatures higher than the specifications mentioned

by the manufacturer results in degradation of the resin matrix in the case of prepreg. This can be translated to binder in the case of dry fibre material.

2.5.2 Layup Speed

Obtaining a deposition rate that ensures the quality and consistency of the final parts of the final laminate is a challenge. The deposition rate determines the window of exposure of the fibres to the heat source, thereby dictating the amount of heat absorbed by the tows during the layup process, affecting the nip point temperature.

In the experiments conducted by Francesco et al. [47], the nip point temperature as a function of deposition rate was investigated for PEEK thermoplastic composite and dry fibre material. The deposition rates of the dry fibre were 6,12,24 and 48 m/min and the thermoplastic material had an incremental speed of 2.88 m/min. The temperature at the nip point of the layup as a function of heater power at different deposition rates were recorded. The experiments showed that increasing the deposition rate, resulted in the need for a higher heater power to obtain the same temperature for both materials.

Budelmann et al. [17] investigated the influence of varying debonding speeds represented by changing the rate of displacement during measurement of results.The higher the rate of debonding, the weaker the tack force.It is stated that the rate of debonding will be very low magnitude than for a case in which the prepreg is debonded right after layup.

It can be seen in figure 2.19 that the maximum tack stress σ_{max} is seen to increase steadily as a function of the rate of displacement V_d.

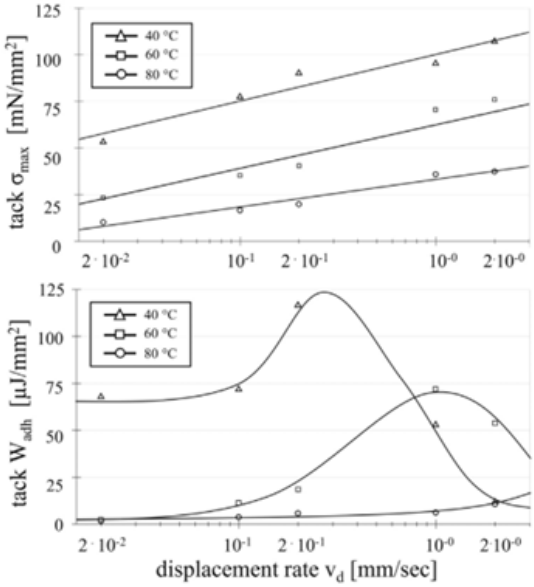

Figure 2.19: Prepreg tack σ_{max} and W_{adh} measured for varying rates of displacement and temperature [17]

At lower debonding rates, σ_{max} experiences a notable increase. This behaviour is best described logarithmically across the different temperatures investigated. With an increasing debonding rate, the rate of increase in σ_{max} slows down. Previous work done by Dubois et

al. [70] also observed a steady increase in σ_{max} with the displacement rate. However, he did not account for different temperatures in his study.

The effect of temperature was accounted for in the work of Budelmann et al [17], that showed increasing temperature, decreases tack performance after a certain threshold. W_{adh} which is "work of adhesion," which is a measure of the energy required to separate the two plies as seen in Figure 2.19, for the temperatures of 40 °C and 60 °C showed maxima. Increasing temperature led to a decrease in the extent of W_{adh} maxima and a shift towards higher temperatures, suggesting that maximum W_{adh} at 80 °C may exist beyond the range of investigated rates of displacement. At lower displacement rates, there is enough time for the stress relaxation of the matrix, resulting in lower stress over the displacement and consequently lower values of W_{adh}.

Conversely, high stress within limited displacement, at high displacement rates leads to lower W_{adh} values. However, the experiments were done using probe testing, and probe testing samples are smaller in size, also the method in which the force and heating are applied on the sample is much different than the typical AFP process, therefore these results have to be verified using AFP samples and peel testing.

Endruweit et al. [79] found out that higher adhesive strength in the unidirectional prepreg tape is seen with reducing layup speed, since the formation of stronger bonds occurs by increasing the dwell time (time of compaction). Cohesive strength increases with increasing layup speed (determined by peel rate). The same findings obtained by Saar [4] in his investigation of tack behaviour in Solvay TX1100 dry fibre material.

2.5.3 Compaction Force

Compaction force is an important parameter in the AFP process. The tows laid up are compacted using compaction rollers, as the tapes are deposited onto the surface of the tool. Sufficient force has to be applied to compact the material and ensure that the layers are properly adhered together after the layup process. Compaction force helps increase the contact area between the layers of plies, which enables a larger number of bonds to form(increase intimate contact), leading to higher tack. According to Endruweit et al. [79], at a high compaction pressure, the true contact area remains the same as complete contact of the substrate is made, and increasing the pressure does not change the area of intimate contact any further. The tack force converges to a value of $F_{t\infty}$, which is dependent on the resin system/binder used. Budelmann et al. [17] found out that increasing compaction force with increasing temperature up to the maximum processing temperature of the binder increased the overall tack behaviour as seen in Figure 2.19.

Bakshi et al. [56], found out that the type of compaction roller used affects the final quality of the product. They used 5 different types of compaction rollers. They were made of different hardness and structures. It was found that solid compaction rollers were better than perforated rollers as perforated rollers were found to cause force fluctuations of up to 50%.

2.5.4 Interaction of Parameters

From the above subsections, the single parameter influence on the tack properties were discussed, however, to be able to completely understand the tack behaviour of the material, the interactions between these parameters have to be studied, these parameters are dependent on

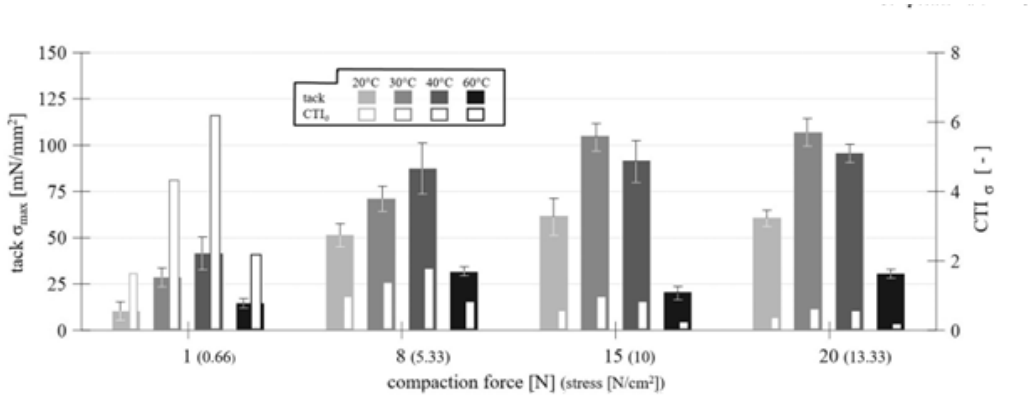

Figure 2.20: Tack σ_{max} as a function of compaction force and prepreg temperature [17]

each other and each parameter will contribute to the tack behaviour that will affect the final layup quality, ultimately affecting the final part produced. Wohl et al. [81] used Design of Experiments to investigate the influence of the different parameters and used probe tests to test the tack levels. It was found that a decrease in compaction force and temperature, along with the increase in relative humidity resulted in an increase in tackiness. This contradicts the previous findings that predicted that a higher compaction force and a higher temperature results in higher tack properties.

Rao et al. [18] used the OOA(Out of Autoclave) thermoset towpreg CYCOM® 5320-1 material to conduct peel tests to test for the tack behaviour of the AFP deposited material. The design of experiments accounted for the three parameters of Compaction load L, lay-up speed S, and Processing temperature T. The main factor effects were plotted on each side of the global average to investigate the contribution of each parameter to the tack properties of the material as seen in Figure 2.21

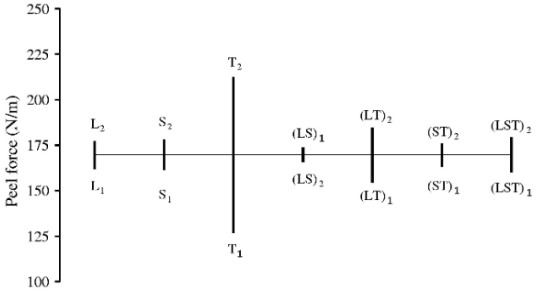

Figure 2.21: Interaction factors influencing peel force L-Compaction load, S-Lay-up Speed, T-Processing Temperature, LS-interaction between Compaction load and Lay-up speed, LT- Interaction between compaction load and Processing temperature, ST-Interaction between Layup speed and Processing Temperature, LST-Interaction between Compaction load, Layup speed and Processing temperature [18]

In figure 2.21, it can be seen that the parameter that affects the peel force the most is the processing temperature. Aized and Shimzadeh [60]tried to identify the parameters that influenced the final quality of the layup by using response surfaces and it showed that nip

point temperature was the most important factor as well. This is followed by the interaction between compaction load and temperature. Interaction plots were made to determine whether the processing parameters influenced each other or not. If plotted lines are parallel to each other, it shows that there is no interaction between the two parameters being accounted for, meaning that the change in response from one level to another is not influenced by the other factor. The higher the deviation from being parallel, the higher the interaction between the two parameters. These are the interaction plots found by S.Rao et al. [18]

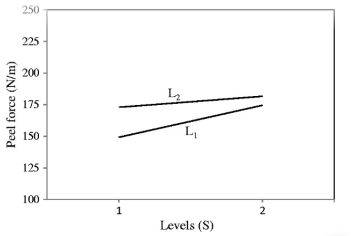

Figure 2.22: LS interaction effect plot $L_2 = 1$ kN, $L_1 = 0.5$ kN, $S_1 = 20$ mm/min, $S_2 = 120$ mm/min

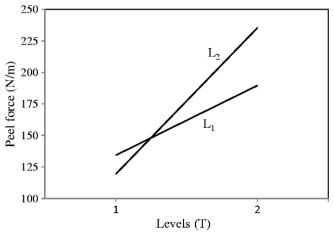

Figure 2.23: LT interaction effect plot $L_2 = 1$ kN, $L_1 = 0.5$ kN, $T_1 = 25°$C, $T_2 = 65°$C

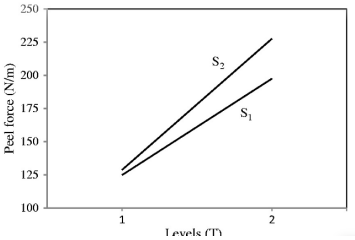

Figure 2.24: ST interaction effect plot $S_1 = 20$ mm/min, $S_2 = 120$ mm/min, $T_1 = 25°$C, $T_2 = 65°$C

Figure 2.25: Interaction plots of LT, LS, and ST interactions. [18]

LS interaction effect: Figure 2.22 shows the LS interaction plot, the plot shows a negative interaction between the compaction force and the Layup speed. At the higher layup speed, the increase in compaction forces from 0.5 kN to 1 kN has little to no effect on the peel force, however at a lower layup speed, higher compaction load yields higher peel force values. This interaction produced a negative effect of 8 N/m on the peel force when the levels were changed from L_1S_1 to L_2S_2

LT interaction effect: Figure 2.23 shows the intersection of the two interaction plots, showing significant interaction between the compaction load and temperature.A higher nip point temperature results in larger peel force values, regardless of the compaction force (0.5 kN or 1 kN). However, If a lower temperature layup is required, a lower compaction load (L1) favours a higher peel force. The temperatures when rising from T1 to T2, an increment of 0.5 k N causes a significant increase in peel forces. This can be because the viscosity of the resin is lower at high temperatures, and the wetting of the fibres is achieved better at higher compaction forces. There is a 30 N/m increase in the peel force when the compaction load and nip point temperature are taken from L_1S_1 to L_2S_2.

ST interaction effect: Figure 2.24 shows the ST interaction effect. It can be seen that there is a positive effect with peel force with increasing the temperature from T_1 to T_2. This indicates that,for a high layup speed , the nip point temperature has to be increased. The interaction between S and T is not as strong as the interaction between L and T and this interaction causes a 13N/m increase in the peel force when taken from a lower level to a higher level. From this data, a half normal plot representing the importance of each factor was plotted as shown in Figure 2.26

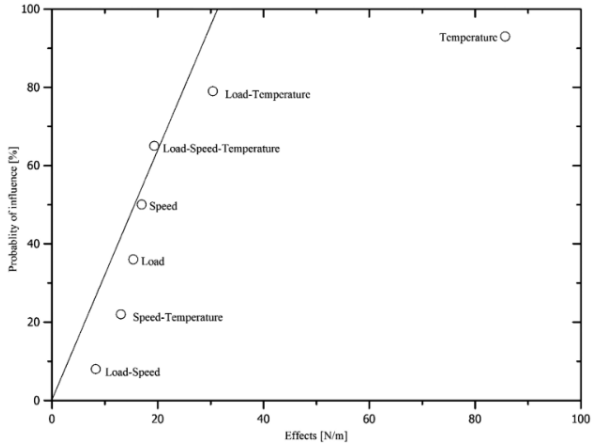

Figure 2.26: Half-normal plot showing the importance of all the factors. [18]

It can be seen in Figure 2.26 that the most influencing factor for high peel force is temperature. This is followed by the ST and the LS interaction factors. The three-way interactions and the load and speed that is clustering around the 11 normally do not have a significant contribution to the peel force. However, for the prediction of peel force, the layup speed S has to be taken into account because it is present in the contributing interaction effects of ST and LS. however, this study was done for prepreg material.

Saar [4] investigated the effect of interactions on the Solvay TX1100 dry fibre material in the prediction of the tack model of dry fibre material.

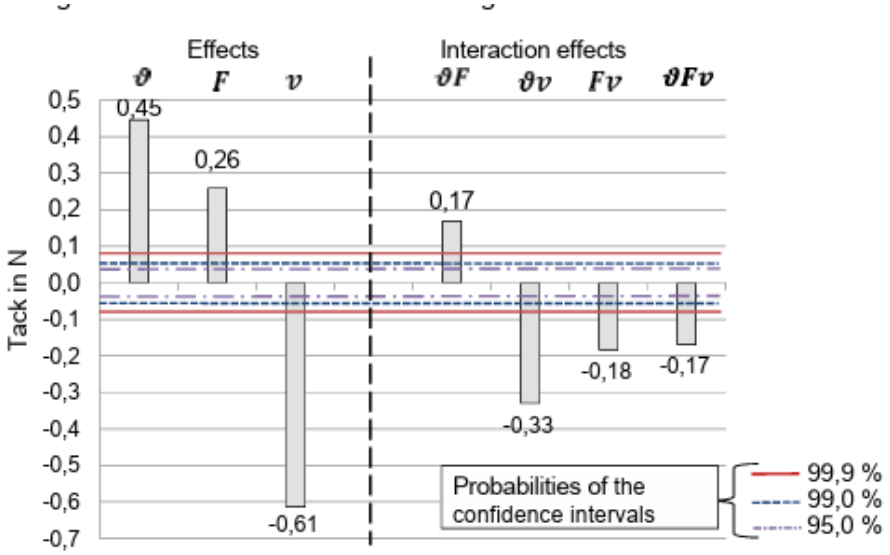

Figure 2.27: Effects and interaction effects on tack behaviour T-nip point temperature, F-Compaction Force, v-Layup Speed [4]

Figure 2.27 depicts the interaction between the Exposure time, nip point temperature, and compaction force influencing tack behaviour. The exposure time is taken with direct reference to the dry fibre placement process from the reciprocal value of the feed speed of the tape deposition head. It is found that the strongest effect on tack is obtained by changing the

layup speed of the head. An increase from 0.04 m/s to 0.2 m/s decreases tack by an average of 0.61 N /6.15 mm material width. Therefore, increasing the exposure time (decreasing the deposition speed) from 5 s/m to 25 s/m during deposition is shown to increase tack by 0.61 N/6.15 mm material width. The second-strongest effect is shown to be increase of temperature in the contact zone from 160 °C to 200 °C. This is shown to increase tack by 0.45 N/6.15 mm material width. The least effect is shown by the compaction force, when compaction force was changed from 300 N to 500 N, tack increased by 0.26 N/6.15 mm material width. The strongest interaction between two parameters is between exposure time (layup speed) and nip point temperature, similar to the findings by Rao et al. [18]. The tack was increased by 0.33 N/6.15 mm. The other interaction effects of Layup speed-compaction force, Compaction force-Layup speed, and nip point temperature-Compaction force-Layup speed are weaker interactions

Chapter 3

Research Definition

3.1 Research gap

The literature review reveals a substantial body of research addressing the material behaviour of prepreg and dry fibre material. While the behaviour of prepreg materials is well-documented, understanding the tack behaviour of dry fibre materials remains underexplored due to their relatively recent introduction into high-volume manufacturing and comprehensive characterization studies are needed as it directly influence defect concentration and, consequently, final part quality.

Tack is a critical property that directly affects the quality and integrity of the final composite part [81]. Insufficient tack can lead to defects such as delamination, fibre bridging, or wrinkles, especially when complex geometries are involved [79]. The unique challenge posed by dry fibre materials is that their binder is applied in discrete regions, varying in the type of dry fibre material leading to localised binder-to-binder bonds in some areas and binder-to-fibre bonding in other areas resulting in more complex tack behaviour compared to fully impregnated prepreg materials, that have the resin matrix homogeneous throughout the fibre.

The numerical model developed by Saar [4] was pivotal in understanding the tack behaviour of Solvay TX1100 dry fibre material, representing an attempt to quantify dry fibre tack behaviour. However, validation is required to ascertain its applicability to other dry fibre materials possessing different material architectures and whether similar material behaviour can be observed. To address this, it is important to understand the tack formation of the selected Hexcel HiTape® dry fibre material, which would allow characterising its material behaviour and provide the base for understanding the tack behaviour of dry fibre materials as a whole.

3.2 Research Objectives

- To systematically investigate the influence of nip point temperature, compaction force, and layup speed on the tack behaviour of Hexcel HiTape® dry fibre material
- To compare the tack behaviour of Hexcel HiTape® with Solvay TX1100, a dry fibre material previously studied by Saar (2021), to assess whether similar material behaviour can be generalised across different dry fibre architectures.
- To evaluate whether the current tack model for Solvay TX1100, can be adapted for Hexcel HiTape® or if new models must be developed to account for unique binder distribution and fibre architecture.

3.3 Research questions and Hypotheses

Building on the identified research gap and objectives, this section outlines the primary research question, sub-questions and hypotheses, focusing on understanding the tack behaviour of the Hexcel HiTape® dry fibre material during layup.

Research question 1: What is the influence of nip point temperature, compaction force, and layup speed on the tack behaviour of Hexcel HiTape® dry fibre material in the Automated Dry fibre Placement process?

Sub question 1.1:How does the variation in nip point temperature affect the tack behaviour of Hexcel HiTape® dry fibre Material?

Hypothesis: Increasing nip point temperature will increase the tack behaviour of Hexcel HiTape® dry fibre material. This is due to the reduction of the binder viscosity at higher temperatures. This behaviour enables better flow of the binder and improves wetting of the fibre surface. As the temperature rises, the polymer chains within the thermoplastic binder gain mobility, lowering the viscosity and allowing the binder to spread across the surface, strengthening the bonding between the plies. As seen in section 2.3, according to De Gennes' reptation theory, polymer chains interdiffuse across the interface while sufficiently mobile, as glass transition temperature is exceeded. The increased mobility facilitates stronger adhesion between the plies due to better intimate contact and fusion bonding. The reduced viscosity at higher temperatures plays a role in improving the bond surface area as well.

However, exceeding a critical temperature or the operating temperature range threshold can cause binder degradation. Exceeding the temperature causes the polymer chains to break down, weakening the tack strength [17]. Wohl et. al [81] also highlighted the risk of thermal damage of the matrix system at excessive temperatures, causing adhesive properties to weaken.

For Hexcel HiTape ®, which features a perforated structure and localised binder distribution, controlling the viscosity of the binder through optimization of temperature is crucial. As the manufacturer of the material has not specified the activation temperature of the binder,it is important to find the operating range for future investigations as well. The operating

temperature must be high enough to melt the binder without degradation. Therefore nip point temperature is expected to be the most dominant factor influencing tack behaviour.

Sub question 2 : How does the layup speed influence the tack behaviour of the Hexcel HiTape® dry fibre material?

Hypothesis: It is hypothesized that decreasing the layup speed will improve tack behaviour, as slower speeds allow more time for the binder to melt and spread across the fibre surface, thereby increasing the strength of adhesive bonds between layers.

In Hexcel HiTape ® dry fibre material, the continuous thermoplastic veil ensures that the binder is distributed over the fibres.Lower speeds would allow the binder to melt uniformly, increasing the surface area for adhesion.

Conversely, at higher layup speeds, the reduced dwell time or the heat exposure time results in insufficient heating of the thermoplastic veil, limiting its ability to soften and spread efficiently. This would lead to incomplete bonding between the interface of the plies, reducing tack strength. Endruweit et. al [79] support this and state that higher speeds limit thermal exposure, leading to weaker adhesion between the layers. For Hexcel HiTape ®, maintaining adequate heat exposure is crucial for good tack performance. Saar [4] has also found out that slower speeds improved tack strength for the Solvay TX1100 dry fibre material. The perforations in the Hexcel HiTape ® material would also contribute to the tack strength, where the binder veil needs to be able to melt and fill the perforations, enhancing the mechanical interlocking between the plies, thereby increasing the tack force.

Sub question 3:How does the compaction pressure influence the tack behaviour of the Hexcel HiTape® dry fibre material?

Hypothesis: It is hypothesized that increasing compaction force will improve tack behaviour by increasing the contact area between the fibre layers, but only up to an optimal point. As compaction force increases, it forces the binder to flow and creates more intimate contact between the fibres. However, beyond this optimal pressure, further increases may cause binder thinning, excessive binder flow, or fibre distortion, which could weaken the adhesive bond [15]. Endruweit et. al [79] demonstrated that higher compaction pressures lead to an increased contact area between the fibre layers, facilitating more extensive bonding between the binder and the fibre. For Hexcel HiTape ®, possessing a thermoplastic binder veil, and a perforated fibre architecture, compaction pressure plays a dual role.

Firstly, it ensures that there is sufficient fibre to binder contact. Secondly, it helps fill the perforations, enhancing, the mechanical locking between the plies.

Sub question 4: Does the interaction between the parameters show significance in understanding the tack behaviour of Hexcel HiTape ® dry fibre material?

Hypothesis: It is hypothesized that the interaction between nip point temperature, compaction force, and layup speed significantly affects the tack behaviour of Hexcel HiTape® dry fibre material, with tack performance being highly dependent on achieving a balance between these parameters. Due to the thermoplastic veil and perforated structure of Hexcel HiTape®, the parameters interact in unique ways that influence both adhesive bonding and mechanical interlocking.

nip point temperature plays a critical role in reducing the viscosity of the thermoplastic binder. At higher temperatures, the binder flows more easily, improving wetting of the fibres and increasing intimate contact between the fibre layers. This is especially important for Hexcel HiTape®, where the binder must flow into the perforations to form mechanical interlocking. However, Endruweit et al. [79] noted that when high temperatures are combined with excessive compaction force, the binder may thin out excessively or even squeeze out of the material, leading to reduced bonding strength due to binder depletion or fibre distortion. This effect is to be kept in mind for Hexcel HiTape® due to the risk of binder flow through the perforations, reducing the adhesive surface area. At lower temperatures, the binder remains more viscous, requiring higher compaction pressures to ensure sufficient tack. Once the fibre layers achieve full intimate contact, further pressure increases do not improve tack strength and may lead to material deformation or excessive binder flow.

Layup speed also closely interacts with temperature and compaction force. Higher layup speeds reduce the time the material spends under the heating element, potentially leading to incomplete melting of the binder, as noted by Francesco et al. [47]. In the case of Hexcel HiTape®, this can result in poor binder flow into the perforations, reducing both adhesive bonding and mechanical interlocking between layers. To compensate for higher speeds, higher temperatures are necessary to ensure proper binder flow, but this requires balancing compaction pressure to avoid over-thinning the binder. Conversely, at slower speeds, the material has more time to melt and flow, allowing better penetration of the binder into the perforations. However, if the speed is too fast, even increased compaction force may not compensate for the lack of heat transfer, leading to inconsistent bonding and weaker tack.

Reasearch Question 2: Will the perforations in the Hexcel HiTape® dry fibre material show differences to the results of the Solvay TX1100 dry fibre material possessing a completely different binder type and material architecture?

Hypothesis: The tack behaviour between the Hexcel HiTape® and Solvay TX1100 dry fibre material will be different as difference owing to their distinct binder distribution and material architecture as can be seen in table 2.2.

The Solvay TX1100 has binder particles distributed across the dry fibre. In contrast, the Hexcel HiTape® features a thermoplastic binder veil and also perforations throughout the material. This could mean that the TX1100 material which could lead to tack behaviour due to less binder-to-binder and more binder-to-fibre interactions. Conversely, due to the presence of a thermoplastic veil, there would exist more binder-to-binder interaction than binder-to-fibre interactions, resulting in higher tack. Endruweit et al. emphasized that material architecture (specifically matrix distribution) plays a critical role in determining the interfacial adhesion properties of prepreg materials [79], which could be translated to dry fibre materials and the presence of perforations and the thermoplastic binder veil in Hexcel HiTape® is likely to enhance bonding. The fusion bonding process in both materials will not be different.

Research Question 3: Will the dry fibre tack model for the Solvay TX1100 material fit the tack behaviour of the Hexcel HiTape ® material?

Hypothesis: The tack model developed for Solvay TX1100 will also fit the tack behaviour of Hexcel HiTape® due to their similarities as dry fibre materials with thermoplastic binder systems. Although Solvay TX1100 uses a modified epoxy binder present as binder spots across

the material. The modified epoxy binder system performs like a thermoplastic material and Hexcel HiTape® employs a thermoplastic veil, both materials rely on binder flow under heat and pressure to achieve tack. The Solvay TX1100 model accounts for temperature, layup speed and compaction force, key factors influencing binder softening, wetting, and adhesion, which are equally important for Hexcel HiTape®. The fusion bonding mechanism should be the same for the Solvay TX1100 and Hexcel HiTape material. The main difference is Hexcel HiTape®'s perforated structure, which may enhance mechanical interlocking, but this is not expected to significantly deviate from the overall tack behaviour captured by the Solvay TX1100 model. Therefore, the same tack model should apply to Hexcel HiTape®, with any minor differences in performance resulting from binder distribution and perforation effects.

Chapter 4

Methodology

This chapter presents the methodology followed to carry out the investigation into the influence of process parameters on tack behaviour during the ADFP process. Section 4.1 outlines the design of the experiments chosen. Section 4.2 describes the experimental setup, detailing the ADFP system, dry fibre materials, and the parameter settings. Section 4.3 discusses the preliminary tests conducted for calibration and setup validation. The manufacturing of specimens is covered in Section 4.4 while Section 4.5 explains the peel testing procedure. Finally, Section 4.6 focuses on data acquisition from the peel test and section 4.7 explains the evaluation of the data obtained.

4.1 Design of Experiments

The design of Experiments is a critical part of any scientific investigation as it provides a structured and systematic approach to obtain as much information as possible from the experiments while minimizing the number of experimental combinations. The DOE for this project sought to capture both linear and non-linear relationships between the key influencing parameters :

- nip point temperature of the bonding zone T
- Speed of the compaction roller v
- Compaction Force of the compaction roller F

as mentioned in section.2.5.The process parameters of the ADFP robot are adjustable. The experimental design is based on a design cube. In this setup, multiple factors are adjusted simultaneously relative to the centre point of the experimental design in the second stage enabling the reuse of experimental outcomes. DOE is conducted in two phases as follows:

- 2^k Full factorial design -To understand the main interactions of each factor on tack and to understand the pairwise interactions between the factors.

- Face Centred central composite Design- To identify potential nonlinear relationships between the variables as well as assess linearity

4.1.1 2^k factorial Design

The 2^k factorial experimental design captures the main effects and interactions between the process parameters. corresponding to a coordinate system with three factors, they are tested at two levels: A high (+1)level and a low (-1)level. In figure 4.1, each green dot represents a factor-level combination

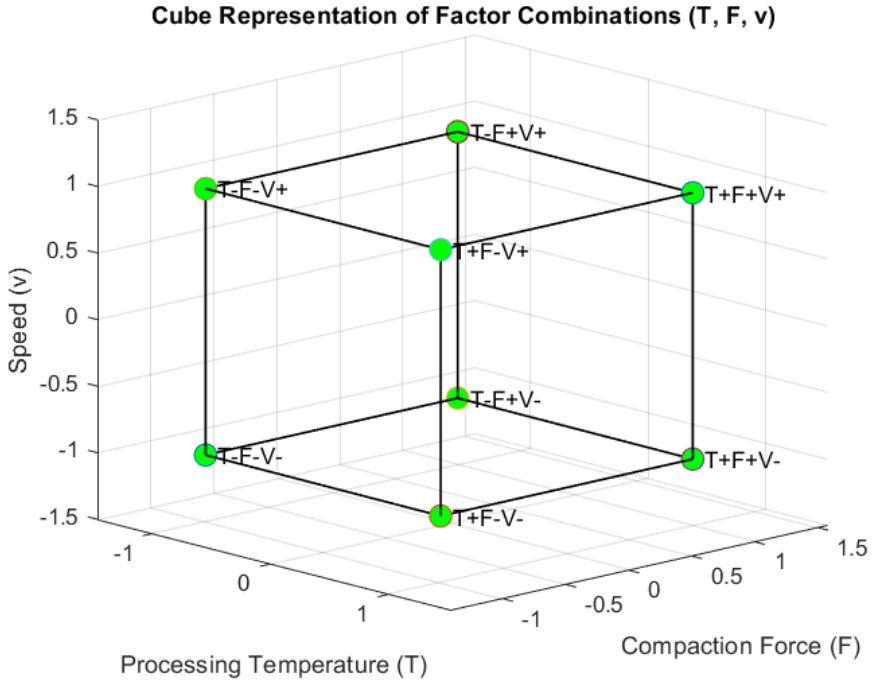

Figure 4.1: Visual representation of the factor level combinations of the 2^k experimental design

The objective is to identify how temperature, speed, and force parameters individually and collectively influence tack behaviour. The number of experiments(N) in a 2^k factorial design is :

$$N = 2^k \tag{4.1}$$

[82] where N is the total number of combinations of parameters of the experiments, k is the number of factors (process parameters in our case) for this experiment k=3 ,yielding:

$$N = 2^3 = 8 \tag{4.2}$$

There are 8 possible factor level combinations, where the result of each factor level is a value for the tack force. The factor combinations are shown in table 4.1

Table 4.1: Factor level combinations of the $2^k factorial$,experimental design

No.	Processing Temperature(T)	Compaction Force F	Speed v	Tack Measurement
1	−	−	−	y1
2	+	−	−	y2
3	−	+	−	y3
4	+	+	−	y4
5	−	−	+	y5
6	+	−	+	y6
7	−	+	+	y7
8	+	+	+	y8

The effect of a factor explains the effect of a factor level increase in the tack, the difference between the two mean values of tack level for the mean values at the high level(+1) and the mean values at the low level(-1) gives the effect. Using temperature as an example, the mean values of the high and low-level combinations are calculated as follows :

$$\bar{Y}_{T+} = \frac{Y_2 + Y_4 + Y_6 + Y_8}{4} \tag{4.3}$$

$$\bar{Y}_{T-} = \frac{Y_1 + Y_3 + Y_5 + Y_7}{4} \tag{4.4}$$

[83]

Effect of temperature on Tack is calculated from equations 4.3 and 4.4

$$\text{Effect T} = \bar{Y}_{T+} - \bar{Y}_{T-} = \frac{Y_2 + Y_4 + Y_6 + Y_8}{4} - \frac{Y_1 + Y_3 + Y_5 + Y_7}{4} \tag{4.5}$$

[83] Analogous to this method, the effects for F and V can be found. An interaction effect exists between two factors when the effect of one factor depends on the setting of the other factor. Here, the effect of one factor can be strengthened or weakened, if this factor is increased in the level at the same time as the other factor.

$$\text{Effect } T_{F+} = \frac{\bar{Y}_{T+F+} - \bar{Y}_{T-F+}}{2} = \frac{Y_4 + Y_8 - Y_3 - Y_7}{2} \tag{4.6}$$

[4]

$$\text{Effect } T_{F-} = \frac{\bar{Y}_{T+F-} - \bar{Y}_{T-F-}}{2} = \frac{Y_2 + Y_6 - Y_1 - Y_5}{2} \tag{4.7}$$

$$Effect(TF) = \frac{\text{Effect } (TF_+) - \text{Effect } (T_{F_-})}{2} = \frac{Y_1 + Y_4 + Y_5 + Y_8 - Y_2 - Y_3 - Y_6 - Y_7}{4} \tag{4.8}$$

Similarly, the effects VF and TV can be found. Due to the orthogonality of the experimental design according to [83]. An interaction between all 3 effects are found out using the following equation.

$$TFV = \frac{Y_2 + Y_3 + Y_5 + Y_8 - Y_1 - Y_4 - Y_6 - Y_7}{4} \tag{4.9}$$

Other possible effects influencing tack, which are not investigated have to be kept at a constant so that the effects of the three factors are reliable. The experiments of each factor level are carried out 3 times to obtain statistically significant results. By comparing the 3 repetitions, the variations can be identified. In addition, the experiments are conducted in a randomized order of parameter combinations to avoid unrecognized changes in the experimental conditions that would cause a trend that can falsify the resultant effects. However, the tests of replicates of each combination would be carried out one after the other.

To capture any non-linear behaviour, the two-level factorial experimental design is extended to a three-level factorial design.

4.1.2 Face Centred central composite design

The face-centred composite design expands on the full factorial design, where additional centre points (midpoints of the factor levels) result in 3-factor levels added to account for any non-linearity. This is shown in figure 4.2

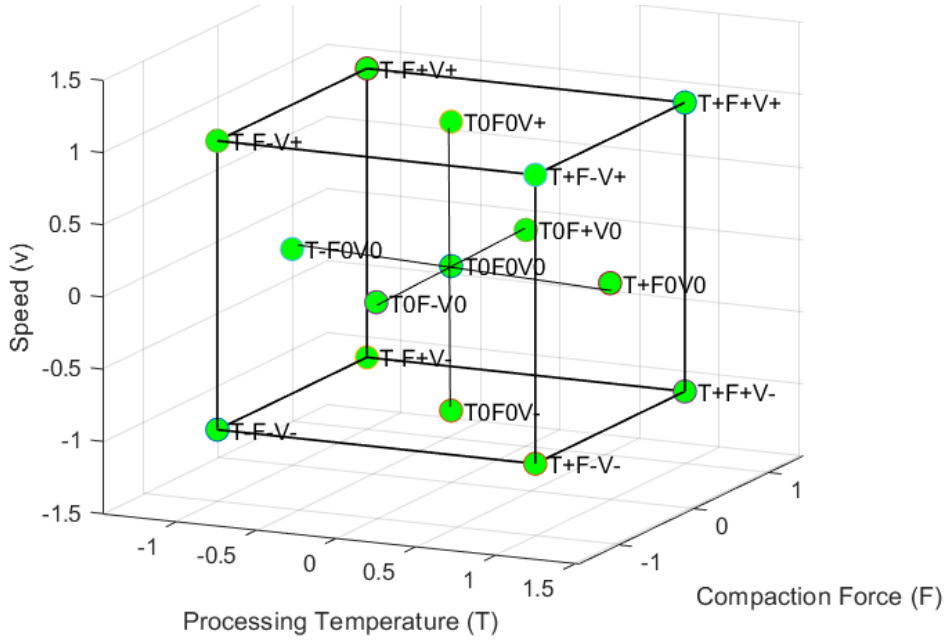

Figure 4.2: Visual representation of the factor level combinations of the face centred central composite experimental design

The total number of experimental runs in the Face centred composite design is:

$$N = 2^k + 2k + 1 = 2^3 + 2 * 3 + 1 = 15 \tag{4.10}$$

[82] The total configuration includes:

- **8 factorial points** from the inital two-level design of experiment

- **6 axial points**,which is the midpoint of the factor levels
- **1 centre point**,the mid level of all the factors(T0F0V0)

Each combination will be replicated three times, resulting in a total of 45 experimental runs. This approach allows for better statistical significance of the results. The combination of these 15-factor levels can be seen in Appendix A table A.1.

The additional factor level combinations are the midpoints of the high and the low settings. The midpoint(T0 F0 V0) is the midpoint of all the factors. The experimental effort only increases moderately with the addition of these extra points as only one factor is changed at a time enabling the assessment of the nonlinear behaviour of the parameters. The face-entered central composite design is chosen as the values selected stay within the cube, unlike the central composite design of experiments that possess values outside the cube. Depending on boundary conditions, it may be necessary for factor-level combinations to deviate from the initial experimental design. It is often challenging to set these factors precisely in real-world conditions due to technical or environmental constraints. However, such deviations are accepted in the context of a three-level experimental design. This flexibility is permissible because the experiment's goal is to observe and describe any nonlinear correlations between variables, which do not require exact, fixed changes in influencing factors to obtain meaningful results. The nonlinear behaviour can still be captured effectively, even with minor variations in the experimental setup [4].

4.2 Experimental Setup

The experimental investigation is limited to the dry fibre material Hexcel HiTape® with a thermoplastic binder from one manufacturer. An industrial-scale Coriolis C1 ADFP layup unit is used as the deposition unit, enabling industrial characterization, and a custom-made state-of-the-art post-layup peel test rig both provided by the DLR was used to perform the peel tests.

4.2.1 Dry fibre Analysis

In order to understand the visual differences and have a closer look at the dry fibre material, the Hexcel HiTape® and the Solvay TX1100 were studied under the Keyence VHX-5000 digital microscope to understand the binder distribution and difference in fibre architecture of both the dry fibre materials.

Hexcel HiTape ®

- The Hexcel HiTape® is a proprietary dry fibre material from Hexcel. It is manufactured using the tow-based method.
- **Binder distribution**: Both sides of the dry fibre possess the thermoplastic binder veil.
- **Binder composition**:It has a thermoplastic binder system. The exact composition of the binder system is not known.

- **Material architecture**: There are characteristic perforations to aid in the through-thickness permeability during the resin infusion stage following the manufacturing of the preform.

The material can be seen in figure 4.3.

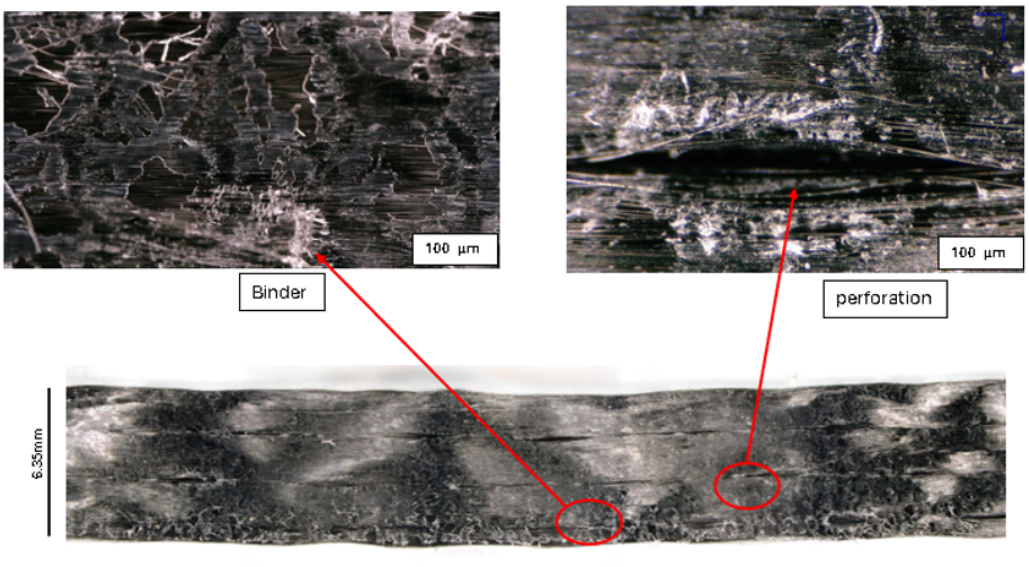

Figure 4.3: Hexcel HiTape® binder and perforations under microscope

Solvay TX1100: This is a commercially available dry fibre material from Solvay.It has a tow width of 6.35mm 2.5. It is manufactured using the slit-based method as mentioned in section 2.1.2. This material is seen in figure 4.4.

- **Binder distribution**: One side of dry fibre contains binder particles only and the other side contains a carbon fibre mesh, this is to add in the resin flow during the post-preform resin infusion process.

- **binder composition**: It has a modified epoxy binder system, engineered to behave like a thermoplastic binder system with an operating temperature range of 160 °C to 200 °C [4]

- **Material architecture**: Does not have perforations like Hexcel HiTape®.

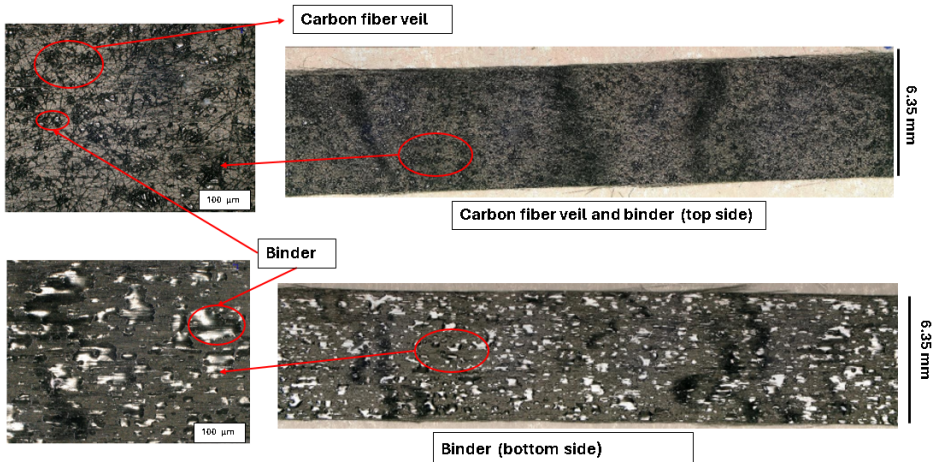

Figure 4.4: Solvay TX1100 top and bottom side microscopy

Key Observations

The binder is present in the form of binder particles at the surface of the Solvay TX1100 fibre, whereas in the HiTape® material, the binder is more spread out along the entirety of the fibre on both sides as a veil. It can be seen that there is an accumulation of binder around the perforations in the Hexcel HiTape® material. The distribution of the binder in both the materials is different with the Hexcel HiTape® having more of the binder across the surface of the material. Additionally, the perforations can be a source of mechanical interlocking between the plies along with the binder accumulation around the perforations. The question is, will this significantly affect the fibre tack behaviour while in use during the ADFP process?

4.2.2 ADFP setup

The manufacturing of the specimens for the experiment is done using the Coriolis C1 fibre deposition robot from Coriolis composite, this machine complies with all the aerospace standards. Up to 16 tapes of 6.35 mm can be simultaneously deposited using this layup unit. The tapes are deposited with no gaps. The maximum feed rate of the layup head is 1 m/s and the maximum compaction pressure exerted by the compaction roller is 1KN. [84]. During the fibre deposition, the fibres are fed through an environmentally controlled creel system through individual channels to the layup head. [47] as shown in figure 4.5.At the start of fibre deposition using the AFP unit, the dry fibre material is conveyed through the deposition head onto the sample plate. As the AFP head accelerates towards the table, the approach height of the head is carefully adjusted to prevent the compaction roller from colliding with the table surface. Once the head reaches the designated starting position, the material is deposited at a constant speed. At the end of the deposition, the material is cut using blades located inside the AFP head, and the robot is slowed down.

Figure 4.5: Creel system of the Coriolis C1 ADFP unit

The incoming dry fibre tape is heated using 3 independent IR heating lamps of power 1430 W each. The setup is shown in figure 4.7. The compaction roller is covered with a Teflon heat-protective layer to prevent the compaction roller from overheating and to prevent the Hexcel material from sticking to the compaction roller during deposition due to the presence of binder on both sides. It should be noted that the use of the Teflon protective layer on the compaction roller was retrofitted for this experimental testing and is typically not used in the real manufacturing process.

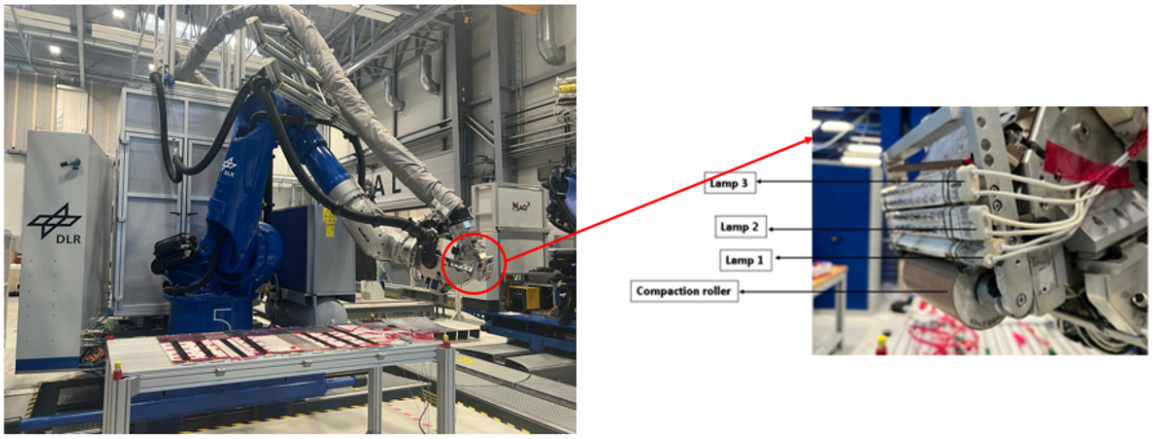

Figure 4.6: left-Coriolis ADFP unit, right-ADP Deposition head

The highest feed speed for a specific process temperature at the nip point is dependent on the heating power output of the lamps. The factors that influence the resultant nip point temperature are: the power output of the lamps, inclination of the lamps, air pressure of the compaction roller cooling system, and lamp cooling system [4].

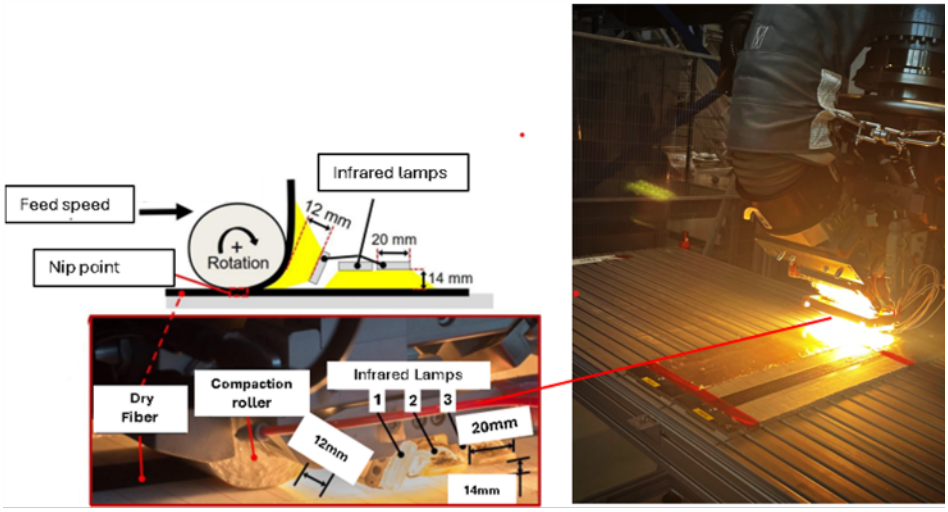

Figure 4.7: Coriolis ADFP robot with sketch of the deposition head

Before manufacturing the sample, a custom CAM file was created specifically for this experiment to ensure precise deposition. This CAM file was designed to instruct the layup unit on the exact spatial points within the manufacturing plant's global coordinate system where material should be deposited.

The first step involved referencing the table on which the specimen would be manufactured. This was achieved using the 4-point referencing method with a probe attached to the Automated Fiber Placement (AFP) head. By probing four reference points on the table, the coordinates of the table in relation to the manufacturing plant's coordinate system were determined. This step established a clear alignment between the physical table and the digital model.

Next, a CAD model of the table, including the specimen plates, was created and imported into the Coriolis C1 unit's CAM software (offline programming software). This CAM file outlined the deposition areas, tool contours, and measurement points required for accurate positioning on the table. When this file was uploaded into the system, the software calculated the relative position of each deposition area and tool(specimen plates and table) measurement points with respect to the global coordinate system.

Additionally, It had to be ensured that the sample plates were positioned accurately on the table. This was done because, after each production cycle of one parameter group of specimen plates, the plates had to be removed to manufacture the next set of 3 replicate plates for the next group. A reference plate was attached to the left edge of the table to ensure that the specimen plates were accurately positioned to the calibrated positions. This plate, fixed securely to the table, provided a consistent point of reference for plate alignment. Magnetic holders for sphere reflectors were also positioned on the four reference points to assist with the calibration process as seen in figure 4.8.

Finally, the gathered measurement data was processed through Coriolis Composites software to develop a precise deposition program for the robot.

Additionally, the referencing of the layup unit is crucial for ensuring the precise alignment of the compaction roller with the specimen plates, ensuring that the roller's midpoint aligns

with the plate's midpoint. Misalignment can lead to uneven tack across the substrate, with some material deposited outside the intended area or near the edges, adversely affecting peel test results due to edge effects. When a portion of the ply extends off the substrate, the tack values differ, leading to inconsistent performance.

Additionally, proper referencing ensures that the approach of the Automated fibre Placement (AFP) head aligns accurately with the specimen plate and substrate. Faulty alignment of the compaction roller during deposition can cause variations in compaction force, as different sections of the roller may be at varying heights relative to the substrate.

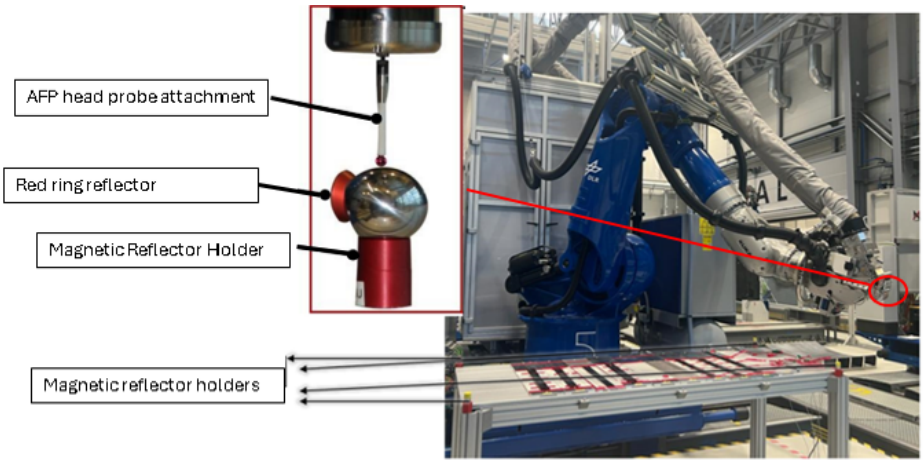

Figure 4.8: Probe measuring system

4.2.3 Parameter Settings

For most prepreg materials, the process parameters are documented, however, the references for dry fibre materials like the Hexcel HiTape ® are scarce. Additionally, these parameters vary on the specific AFP machine used. The process parameters selected for the tests are provided in the table 4.2.

Temperature(°C)	64	95	125
Feed Speed (m/s)	0.04	0.12	0.2
Force (N)	300	400	500

Table 4.2: Parameters used for the experiment

The lack of a datasheet of the material necessitated a trial and error and discussion with the engineers at the DLR who worked with similar materials to identify the effective machine settings of the process parameters. The range of operating temperatures were estimated. The operating temperature range of 160-200 °C of the Solvay TX1100 material was used as an assumed baseline for the activating temperature of Hexcel HiTape ® material. These temperatures proved to be too high for the Hexcel HiTape ® material as there was the presence of smoke during temperature trials at around 200 °C which indicated the burning of the binder of the Hexcel HiTape ®.

From the experience of the trials and the insights from the engineers who worked with similar material as well, the initial target temperatures for the Automated fibre Placement (AFP) process were set at 100 °C, 140 °C, and 180 °C. Through heating trials that will be seen in

section 4.3, the activation temperature of the binder had to be determined. The nip point temperatures for the deposition process were obtained by modifying the power outputs on the 3 lamps. However, in the table 4.2, the temperatures 65 °C,5 °C and 125 °C were selected. The reasons for this will be seen in subsection 4.3.3. Deposition speeds of 0.04 m/s, 0.12 m/s, and 0.2 m/s were selected for the experiments. Since the nip point temperature depends on the power output of the lamps, higher power outputs were necessary to achieve higher temperatures at higher deposition speeds. At the maximum power setting for all three lamps, a nip point temperature of 180°C was reached at a deposition speed of 0.2 m/s. The speeds of 0.12 m/s and 0.04 m/s were used as progressively lower settings. The compaction forces of 300 N,400 N and 500 N were chosen based on discussions with engineers with experience in similar materials.

4.3 Preliminary testing

From the design of experiments, the factor value stages were determined, and a selection of high, medium, and low values for the nip point temperature, Layup speed, and compaction force were selected in section 4.2.3.

4.3.1 Preliminary Heating trials

As mentioned in subsection 4.2.2, the power outputs of the IR lamps have to be individually set to obtain the required nip point temperatures. This is influenced by the layup speed, as higher layup speeds result in lower dwell times, meaning the lamps have to be set to a higher power output, and, at lower speeds, the power output can be reduced accordingly. Compaction force is not affected by the other 2 factors and is controlled independently by input of required value to the AFP unit. The temperature between the interface of the 2 plies of Hexcel HiTape® material is measured using 4 type K thermocouples of 0.25 mm diameter attached at 4 points along the length of the first deposited ply as shown in figure 4.9.

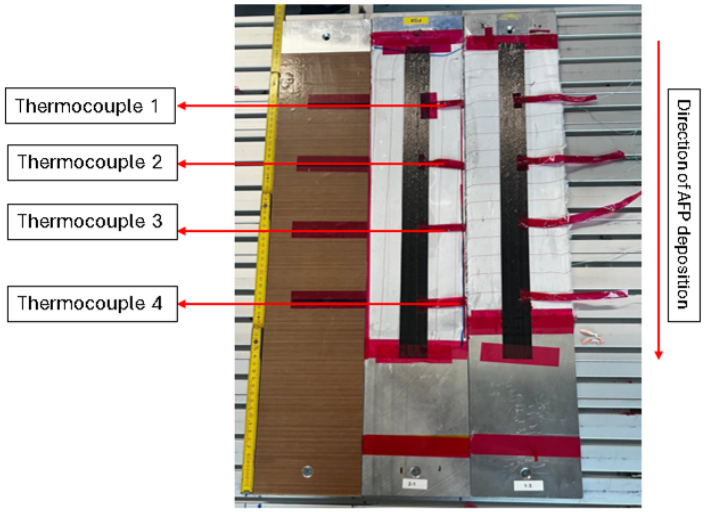

Figure 4.9: thermocouple placement for temperature setting

The thermocouples are attached by extension to the channels of the Graphtec Midi Datalogger GL840. The resolution is set at 200 ms or 5Hz. First, the temperature was measured by

running the deposition head along the length of the plate with the compaction roller turning on lamps and not laying up any material to observe the power curve. The data obtained for the Solvay TX1100 material [4] was used as a baseline for the power settings of the AFP robot for the Hexcel HiTape® Material. These tests are done to observe how consistent the temperatures are along the ply during deposition.

4.3.2 Obtaining the power curves

Each of the three independently adjustable IR Lamp 1, Lamp 2, and Lamp 3 are used in parameter setting to obtain a constant temperature at the nip point. The parameter setting was done in 2 stages:

1. **W**ithout material deposition
2. **W**ith material deposition

First Stage: First, the experiments were carried out with lamp 2 only, to observe how the temperature fluctuated under varying power outputs. As the thermocouples are at 4 different locations along the length of the material, This step also provided a baseline temperature curve. The graph obtained is shown in figure 4.10 The resulting temperature log exhibits

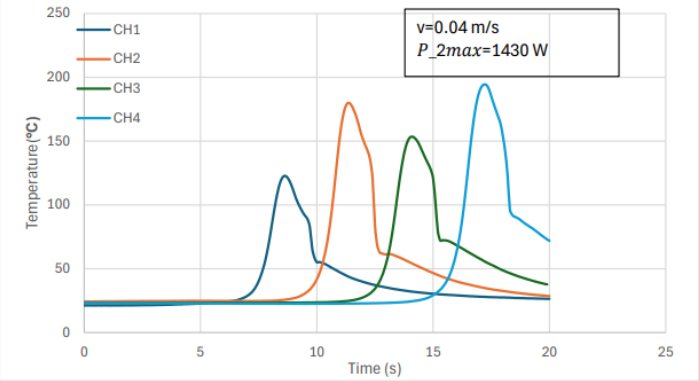

Figure 4.10: Temperature profiles obtained with lamp 2 activated

a parabolic and asymmetric shape. After a steep rise, the maximum temperature (peak) is reached, followed by a more gradual decline. The temperature falls sharply as the compaction roller passes over the thermocouple. The heat capacities and thermal conductivities of the specimen setup like the aluminium plate, the peel ply, the compaction roller, and the dry fibre material also influence this behaviour. It can be seen that the temperature increases towards the end of the length of the material, this could suggest that lamp 2 is not heated enough and requires a preheating step to ensure consistent power output. For the following trials, Lamps 2 and 3 were set at 75% of maximum power output (1072.5 W) and a preheating of 10 runs across the sample plate was carried out without any material deposition. This step was done to ensure that the heat radiation of the lamps did not vary across the runs. Lamp 1 was not activated in the preheating trials as the power output at 75% could risk the melting of the compaction roller After establishing the baseline temperature profile, the next phase of the experiment involved activating all three lamps to observe their combined influence on the temperature profile during material deposition. As seen in figure 4.11, lamp 3 is first to pass over the material, followed by lamps 2 and 1.

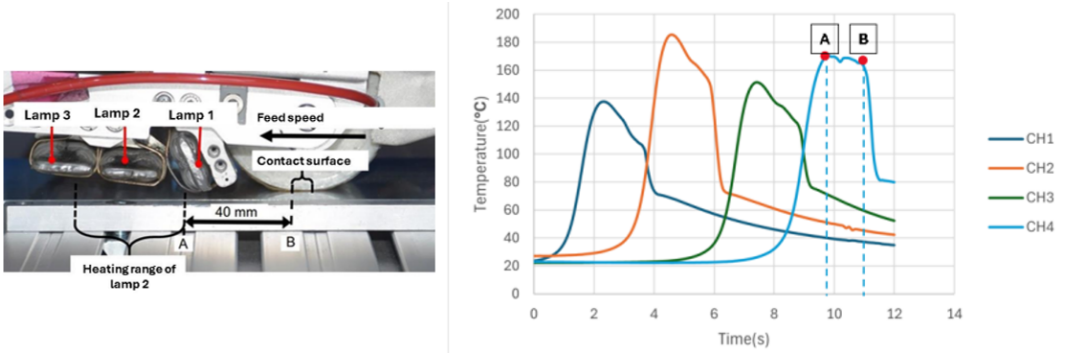

Figure 4.11: left-Lamp and compaction roller setup. **Right**- Temperature profiles obtained with all lamps activated for a speed of 0.04 m/s CH1, CH2, CH3 and CH4 are thermocouples 1, 2, 3 and 4 respectively

The functions of 3 lamps are as follows according to the trend shown in the figure 4.11.

Lamp 3: During the deposition process, Lamp 3 is the first to pass over the material. This lamp is responsible for preheating the substrate, gradually increasing the material's temperature to prevent thermal shock when it encounters the more intense heating of Lamp 2. Preheating also helps to slightly activate the binder.

Lamp 2: Following Lamp 3, Lamp 2 creates a sharp peak in temperature. This lamp also helps heat up the substrate further. It provides the primary heat at the nip point, which is critical for the fusion bonding process. Lamp 2 is the most significant of the three, as it ensures the material reaches the required processing temperature of the material to facilitate bonding.

Lamp 1: Lamp 1 heats up the incoming tow .It is necessary to have the incoming tow and the substrate obtain the same temperature at the nip point. This is of importance in the case of thicker preforms where more heat is required to obtain the target temperature than the thin incoming tape. Therefore the power settings have to be adjusted in a way that lamp 1 does not cause the incoming to tow to overheat. This lamp also helps to reduce the abrupt temperature drop caused by the compaction roller by sustaining the temperature reached by Lamp 2, thus increasing the dwell time. This stabilization allows the binder to activate uniformly and supports polymer diffusion. The flattened region AB in figure 4.11 shows this sustained temperature, where point A represents the rear limit of Lamp 2's radiation and point B is the nip point. However, the power of Lamp 1 must be carefully controlled to avoid material degradation or damage to the compaction roller. If the power output is too high, the binder risks burning, which could lead to smoke formation. The effect of Lamp 1 is particularly pronounced at lower speeds, due to the extended dwell time.

Following the initial trials, the nip point temperatures were calibrated with material deposition. The nip point was assumed to be the peak of the parabolic graph obtained. It can be seen that the 4 peaks across the deposition show variation. It should be noted that at 0.04 m/s, the data was logged every 8 mm, and at a higher speed of 0.2 m/s, every 40 mm. Given the importance of the nip point in heat transfer, the resolution may have caused some temperature measurements to miss this critical area, especially during high-speed placement. The actual nip point could also occur before the thermocouple reading as well.The temperature

values were calculated by averaging the peak readings from the four thermocouples attached to the system. To ensure consistency and reliability, the calibration tests were replicated three times. Initially, after each temperature calibration run, the setup required changing the plates. This process caused the heating lamps to cool down between runs, affecting the stability of the nip point temperatures.

A more efficient method was employed to mitigate this issue. Instead of changing the plates after each run, three plates were laid up sequentially, each equipped with four thermocouples that can be seen in figure 4.12. This approach not only saved time but also prevented the lamps from cooling down, ensuring consistent heating throughout the tests. Importantly, Lamp 1 was not used during the preheating rounds, as its proximity to the compaction roller posed a risk of overheating and potentially melting the roller. It can be noted that, at high

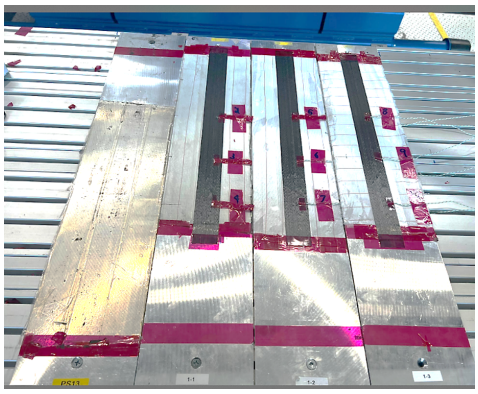

Figure 4.12: use of 3 plates for temperature calibration

speeds like 0.2m/s, a clear distinction between points A and B like in figure 4.11 is no longer possible as the temperature curve only has one extreme point shown in Figure 4.13 due to the increased speed and the constant measurement frequency. It can be assumed that the peak is the point in the order of magnitude of the maximum nip point temperature. The individual heating power settings of all three lamps for the respective temperature and feed speed are summarised in Appendix A table A.4.

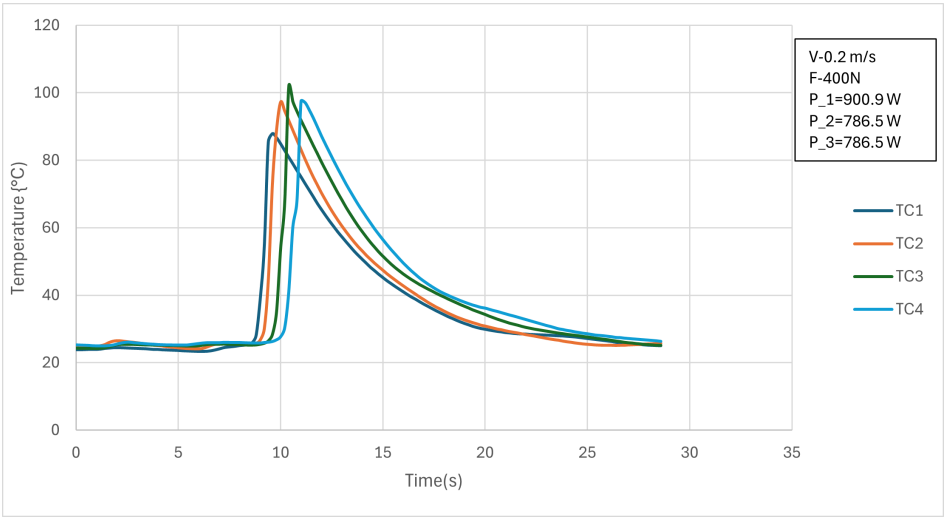

Figure 4.13: Temperature vs time graph for speed 0.2 m/s for 100 °temperature setting

4.3.3 Evaluation of thermocouple readings during temperature setting of the lamps

The thermocouple temperature measurements of the nip point temperatures were measured again after setting the power outputs for the parameter settings of the lamps as some temperature data was missing during the parameter settings, which was found out after the manufacturing of the specimens with the set power outputs for each parameter. The retesting of the parameters showed lower nip point temperatures than the original values. By the time this change was identified, the specimens had already been manufactured using the power settings calibrated for 100 °C, 140 °C, and 180°C, the same settings that resulted in the lower temperatures. Re-manufacturing the specimens with higher power settings for the lamps to reach the initially planned temperatures would have required more time, which was not feasible within the window available for the experiments at the facility. Therefore, the recorded temperatures of 64 °C, 95°C, and 125°C were deemed reliable representations of the actual conditions during AFP and were used in the study. The lamp power settings were obtained from these measurements of the nip point temperatures as determined in subsection 4.3.1. The resulting nip point temperatures for all the combinations after retesting are shown in figure 4.14 Figure 4.14 represents the mean, minimum and maximum temperatures

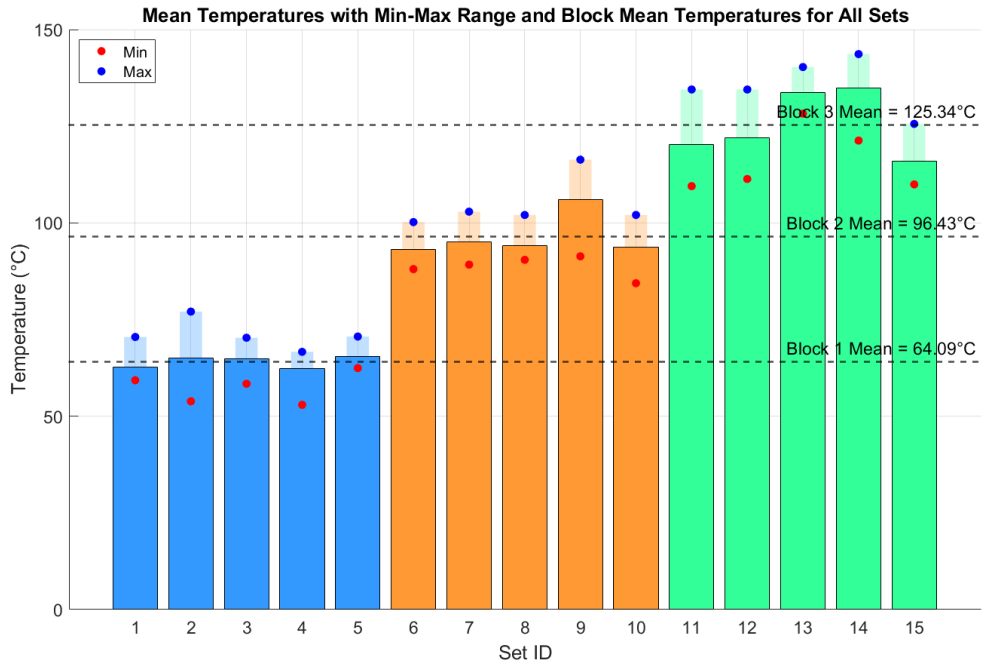

Figure 4.14: Nip point temperature values and obtained nip point temperature from thermocouple testing for power output settings of lamp

recorded for each of the 15 experimental sets across the three temperature blocks of 64°C (Block 1), 95°C (Block 2) and 125 °C (Block 3).

Block 1 (groups 1-5) has an average nip point temperature of 64°C, the mean temperatures for these sets are tightly clustered around this temperature ranging from 59 °C to 66 °C, and all sets in the block stay clearly below 70 °C.

Block 2 (groups 6-10) has a mean nip point temperature of 95°C and the temperatures of the sets range from 89 °to 103 °C. The sets in block 2 are distinctly above the temperature range of block 1. However, there is a slight elevation in temperature for group 9.

Block 3 (groups 11-15) has a mean temperature of 125°C and the temperatures recorded range from 116 °C to 94 °C. This block shows the most variation in temperature measured from all the other block

The bar chart indicates that the temperature distributions for the blocks 1 and 3 are non-overlapping. The maxima of set 9 overlaps with the minima of group 11 and group 12. This does not affect the study of main interactions as the statistical analysis of the main effects is done using groups 1 to 4 and groups 11 to 14 belonging to the 64 °C and 125 °C block respectively. The maximum temperatures of block 1 (66 °C) do not cross over into the minimum temperatures of block 2 (89 °C). This clear separation of temperatures across the 2 blocks demonstrates the intended temperature control of the experiments was successful with the intended significant temperature differences in the blocks owed to the heating of the lamps.

Observations during the parameter settings

During the temperature setting, for higher temperatures, fraying of the fibre was observed, as seen in figure 4.15. This fraying was exacerbated by the presence of binder on both sides of the Hexcel dry fibre material, making it more sensitive to heat during the AFP process. To address this, a Teflon protective sheet was initially applied to the compaction roller to prevent binder adhesion, but this was not sufficient to mitigate the issue. The fraying was ultimately reduced by using pressurised air to locally cool the compaction roller at the point of deposition of the fibres, preventing the fibres from sticking to the roller and fraying.

While recalibrating the parameters, it was observed that during the layup runs, if the compaction roller gets heated to more than approximately 80 °C, the fibre sticks to the roller causing fraying of the substrate and the material laid up. The heating of the compaction roller was measured using a handheld FLIR TG167 thermal camera.

Figure 4.15: (a) fibre fraying **(b)**Temperature measurement of compaction roller **(c)**fibres sticking to the compaction roller

The thermocouple data was logged using a 200 ms resolution, which introduced potential inaccuracies in capturing the nip point temperature, particularly at higher speeds. At 0.04 m/s, the data was logged every 8 mm, and at a higher speed of 0.2 m/s, every 40 mm. Given the importance of the nip point in heat transfer, the resolution may have caused some temperature measurements to miss this critical area, especially during high-speed placement. Although the readings were consistent, the actual recorded average temperatures were approximately 64 °C, 95C, and 125°C, which were lower than the originally planned values.

It is also observed that a difference in the diameter of the k-type thermocouple used also contributes to differences in the readings of temperature. A thermocouple with a smaller diameter of 0.20 mm was shown to be more sensitive and give a higher reading of temperature. K-type thermocouples of 0.25 mm diameter were used for nip point temperature measurement that showed realistic values of the temperature calculated. It should be noted that the thermocouples used for parameter setting were of the same diameter.

It is to be noted that the measured temperature may not be the exact temperature experienced by the material and is subject to the sensitivities of the thermocouples and the testing resolution.

4.4 Manufacturing of Specimen

4.4.1 Preparation of sample plate

The 45 specimens are to be manufactured on aluminium plates. Due to the availability of only 16 plates, each temperature set of 15 samples was manufactured at a time for each temperature set and then peel-tested. The plate used for the preheating runs were covered with a layer of release film material secured using AIRTECH double-sided Tape.

The specimen plates are first cleaned using ethanol and are covered with peel-ply material in the area of deposition for the first ply. The peel ply is secured with AIRTECH double-sided tape. 3 layers of Marbocote release agent are applied in the area of no tack as seen in figure 4.16 to ensure no tack in that region during the peel testing. Peel ply is applied to the area of the tack. This reduces the heat dissipation of the aluminium plate.

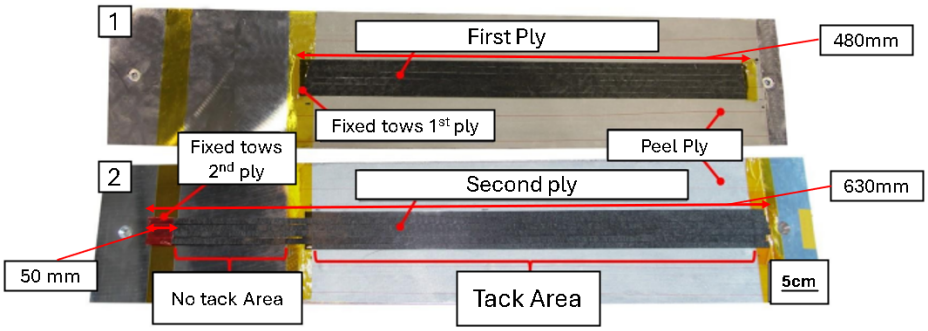

Figure 4.16: Prepared Sample plated for peel testing

Following this, the first and the second ply are deposited using the ADFP Coriolis unit and

the end of the first ply and the loose ends of the second ply are secured with tape.The first ply becomes the substrate and the second ply is peeled off.

4.5 Peel testing

To characterize the tack behaviour of the Hexcel HiTape® dry fibre material and the influence of the varying parameters and also verify its applicability to the previously proposed model, an experimental investigation is required. Based on the findings mentioned in the literature review in subsection 2.4, a 90-degree peel test was selected as a primary method for evaluating the tack behaviour of the Hexcel material after ADFP layup.

4.5.1 Peel test

The advantages of the modified peel test include:

- It offers a broad assessment of the tack behaviour over a large surface, as opposed to more localized tests like the probe tack test.
- This test measures tack along the entire length, accommodating forany variation in binder distribution that influences tack.
- The 90-degree peel angle is closely aligned with the detachment forces that are present during the ADFP process, making it an ideal choice for assessing peel strength
- Availability of peel test rig [4]t the DLR Center for lightweight systems for peel testing ADFP manufactured specimens.
- allows for the measurement of the influence of tack on deposition rate, independent of the peel rate. [13]
- provides the ability to evaluate tack at various intervals after material deposition, offering greater flexibility in testing
- The procedure is standardized [73], ensuring consistent and reliable results
- The test bench can be positioned next to the placement machine, enabling efficient preparation and testing of specimens.

The peel test rig used for the peel testing is shown in figure 4.17 and the schematic representation in figure 4.18

The specimen plate containing the sample deposited using AFP forms two layers one on top of the other. the top ply is peeled off along its length. As can be seen in figure 4.18, the end of the top ply of the prepared specimen is attached via a clamp attached to a force sensor. The clamp is used to pull the sample via a linear axis at a constant speed to ensure uniform conditions. This vertical upward movement of the clamp pulls the support of the sample plate in a horizontal direction. The sample table therefore moves in synchronisation with the vertical movement of the testing apparatus. This synchronised motion prevents the effect of external forces, such as the rolling resistance of the horizontal sledge, from interfering with

Figure 4.17: Setup of the peel test machine

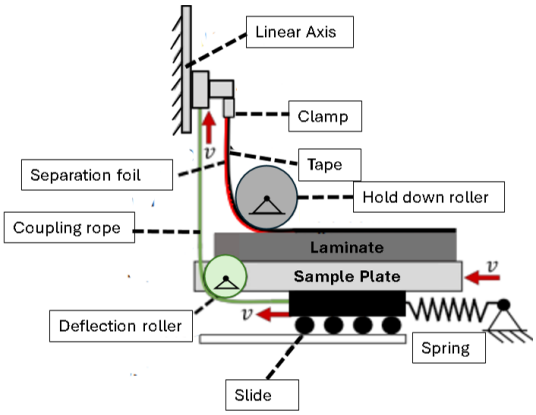

Figure 4.18: Schematic diagram of peel test setup

the measured peel force. At the same time, the sample is peeled off the sample table via the deflection roller. The rig has been designed to purely record the peel force.

The initial length of the top ply of the prepared specimen will not be in contact with the bottom ply to provide length to clamp the specimen in place and to provide a reference point to where tack starts to aid in data analysis. When the material is pulled off initially, the bending radius of the fibre changes as it's being fed through the roller. In line with the ISO/FDIS 29862 international standard that governs the determination of the peel adhesion properties of materials, the peel force F_S is measured continuously along the length of the sample.

During the peel test, the detachment point of the fibre from the substrate may change. A noticeable change in detachment point can cause the cracking of the matrix that produces inaccurate tack values. Therefore, the detachment point of the specimen during the peel test should be kept constant. The hold-down roller limits the area in which the detachment point changes. The distance between the hold-down roller and the ply to be peeled should be kept at a minimum. However, it should be kept in mind that the ply should not be in direct contact with the hold-down roller to avoid frictional forces being recorded with the peel forces. The hold-down roller can be compared to a mandrel test. An important phenomenon that is observed during mandrel peel tests, especially with fibre materials, is the stick and slip behaviour [19].

Stick and slip behaviour refers to the alternating phases of temporary sticking (energy stored) and sudden detachment (energy released) that occur as the fibre interacts with the substrate during the peeling process. This behaviour results in the fluctuation of peel force. These fluctuations can be seen in the force-displacement curve, where the forces arise during the "stick" phase and then drop abruptly during the "slip" phase. The pattern of the force fluctuations can be seen in figure 4.19.

From figure 4.19 C-A can be seen as the area in which the detachment point changes limited by the hold-down roller(stick to slip), As the load continues to increase, the ply to be peeled off is pulled under tension until it reaches a peak force, which is a resultant of the increasing internal stresses due to the increasing extension. This peak force is high enough to break

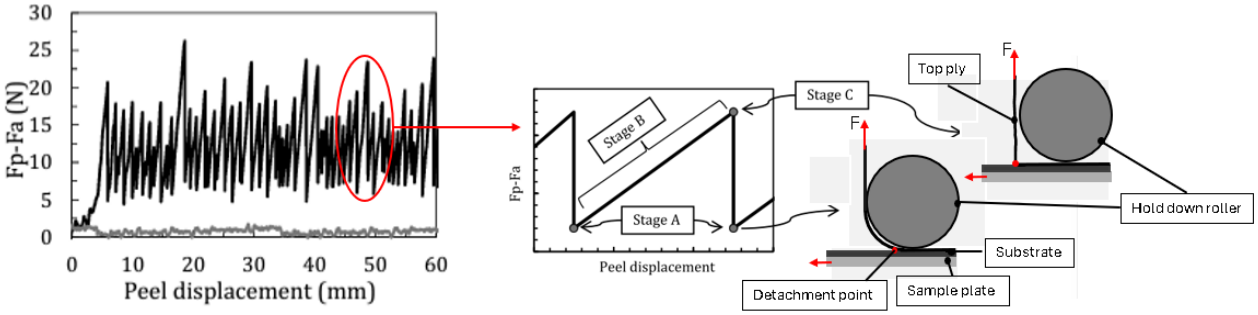

Figure 4.19: Left-Force vs Displacement curve of mandrel peel test Right-Schematic representation of stick and slip phenomenon [19]

off against the bending stiffness causing the material to rapidly detach from the detachment point causing a sharp drop in force from point C. After this abrupt drop, the system resets with the ply under tension, repeating the cycle once again. The detachment point is kept slightly ahead of the hold-down roller and the addition of foam pieces at the edge of the plates enables the synchronicity of the plate and hold-down roller while the peel test takes place. This helps reduce the variation in the detachment point throughout the peel test, preventing erroneous peel force measurements.

The average peel force is typically calculated over several cycles of the stick and slip events. The peel force F_S includes not just the tack force (reflecting the adhesive bonding between the plies) but also the bending force of the material, F_B as the sample resists being deformed during the peel process.

To isolate the tack force, the force required to bend the material is subtracted from the total peel, yielding the actual tack force responsible for ply separation. This is particularly important, as the bending force can introduce significant resistance, especially for stiff or thick materials, and could lead to the overestimation of tack strength.

The tack force F_T is derived as the difference between the average peel force F_S in adhesive regions (presence of tack) and the average bending force of the material F_B (where no tack is present). This approach follows the methodology outlined by Crossley et al. [12] and Heller [85] and an example of the resulting peel force measurement is given in figure 4.20

$$F_T = F_S - F_B \tag{4.11}$$

Accounting for the peel test unit, the sample plate is set up as seen in figure 4.20

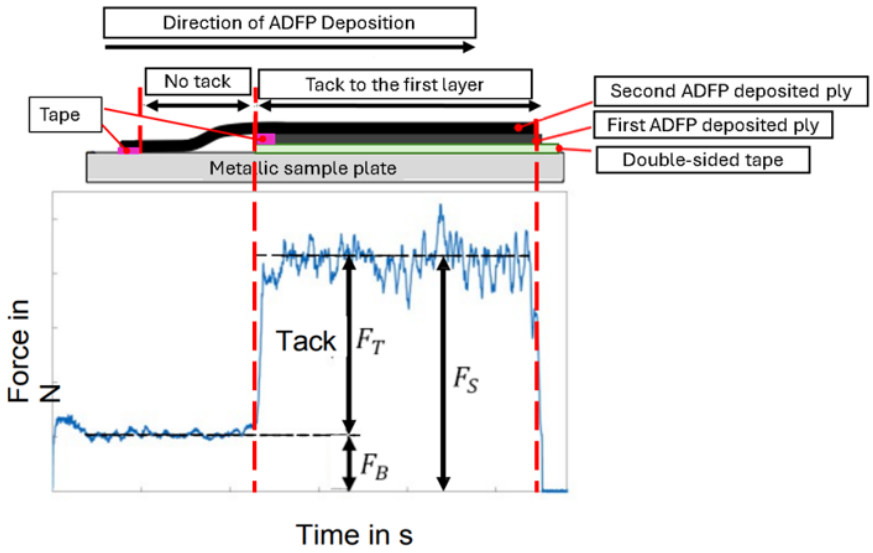

Figure 4.20: design of specimen plate

The first layer of the tape is to be deposited using ADFP and is attached to the specimen plate using double-sided tape. This layer is to be applied partially over the length of the specimen. The second layer is deposited over the entire length using ADFP. The region of no tack is present to account for the beginning of tack during the peel test and the extra length ensures that the specimen can be clamped and bent with the bend point at 90 degrees.

The first ply in the Automated fibre Placement (AFP) process consists of 6 tows of Hexcel HiTape® material, while the second ply consists of 4 tows as seen in figure 4.21. This specific tow configuration was chosen to ensure that the peel test results are not affected by the edges of the fibres.

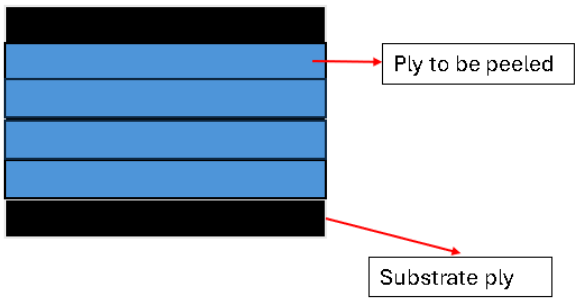

Figure 4.21: representation of the ply placement on the substrate ply

By reducing the number of tows in the second ply, the edges of the fibre are the boundary of the critical bonding area that is subjected to testing. This reduces potential inconsistencies caused by edge effects, such as uneven bonding or tension concentrations, which could skew the peel test results. It should also be noted that the edges of the tow of the first ply should be aligned with the second ply.

A total of 45 specimens were manufactured and tested to systematically carry out the experiments. The 15 parameter sets were divided into three temperature blocks: Block 1 corresponding to 60 °C, Block 2 to 90 °C, and Block 3 to 120 °C. Each block contained five

distinct parameter sets based on different combinations of speed (V) and force (F), as outlined in Appendix A table A.2.

To streamline identification and tracking during testing, a systematic three-digit coding system was used for each specimen. The first digit of the code represents the temperature block, the second digit corresponds to the set number within that block, and the third digit indicates the replicate number for that set. For example, the code "123" refers to Block 1 (60 °C), Set 2, Replicate 3 as shown in figure 4.22.

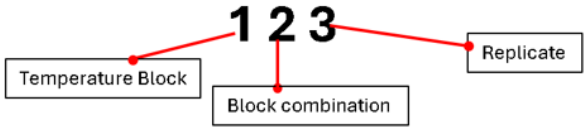

Figure 4.22: Specimen Identification number

This approach ensured that the experimental process was carried out in an organised and traceable manner, with each specimen identified by its unique code and experimental setup.

4.6 Peel test Data Acquisition

As seen in section 4.5.1, the tack is calculated as the difference between the average peel force and the bending force of the material. The peel test is designed to calculate the tack over the tack region of the manufactured specimen plate as seen in fig 4.16. The initial no-tack region has no tack in between the layers and the metallic surface coated with a release agent. Therefore, purely the bending force of the material is measured in that region. After the preparation of the plates of one temperature block, the peel tests are carried out. The peel test rig is shown in figure 4.23.

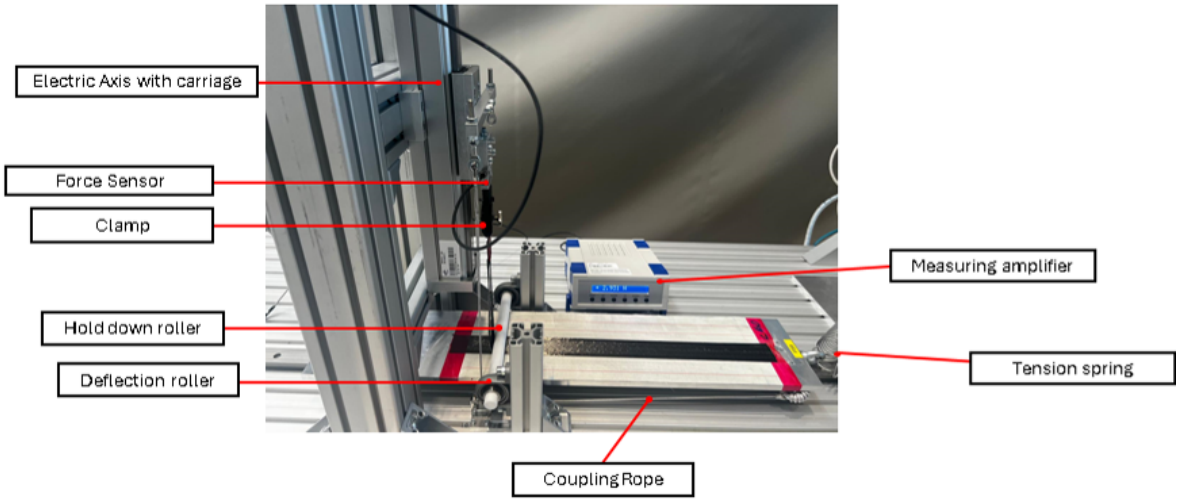

Figure 4.23: Peel test rig setup

Test Setup and key components of peel rig

- **Force Sensor**: The KD40s S-shaped force sensors of maximum load capacity of 10 N and 20 N and an accuracy class of 0.1% were used to capture the peel force throughout the test. The 10 N force sensor was used for the lower temperature block and the 20 N sensor was used for the higher temperature blocks. The sensor is connected directly to the clamp holding the tape-clad end of the second ply of the manufactured specimen, measuring the exact force required to peel the tape from the substrate. Before starting the tests, the system was calibrated using standardized calibration weights (10g, 100g and 200g) to ensure the accuracy of the force sensor. During the peel tests, the measured force sensor values were recorded and processed by the GSVmulti measurement software.

- **Measuring Amplifier**: The sensor is paired to the GSV-2TSD-DI measuring amplifier, which gives a resolution of 24 bits and an accuracy class of 0.05%. The amplifier converts the force sensor's analog signals into digital data, which is processed by the connected data acquisition system that generates real-time data of the bending force of the material and the peel forces of the tack region.

- **Coupling rope**: The SK78 Dyneema® coupling rope is used to maintain the synchronized motion of the specimen plate with the linear axis. It has a working elongation of less than 1% which is important as the rope should not stretch during the peel test. This rope is under constant tension using a spring system of two steel springs, this prevents the rope from going slack which could result in the specimen plate shifting or getting misaligned. By maintaining the tension, it is ensured that the force required to move the plate is transferred consistently, without interference with the rope elasticity.

- **Hold down roller**: The hold-down roller which is made of PTFE (polytetrafluoroethylene) serves a dual function during the peel test. Firstly, it prevents the variation of the detachment point of the ply that is peeled off. Secondly, it minimises friction between the fibre and the roller by keeping a small distance between the ply to be peeled and the hold-down roller, all the while guiding the ply, ensuring that the peeling occurs without excessive resistance that could distort the force readings. The ply is positioned slightly ahead of the clamp but not directly underneath it, which ensures there is no continuous contact between the tape and the roller. This is seen in figure 4.24. This setup is essential to prevent the roller from introducing additional forces (such as friction or tension) that could interfere with the peel force measurement.

Positioning of the clamped second ply and control of the bending radius

To ensure the accuracy of the peel test, it is essential to position the second ply to the clamp precisely. The clamping length is set at 50 mm The detachment point of the second ply must be positioned directly below the line of clamping. This alignment ensures that the peel occurs without a large bend radius (large variation in detachment point) which can be seen in figure 4.24.

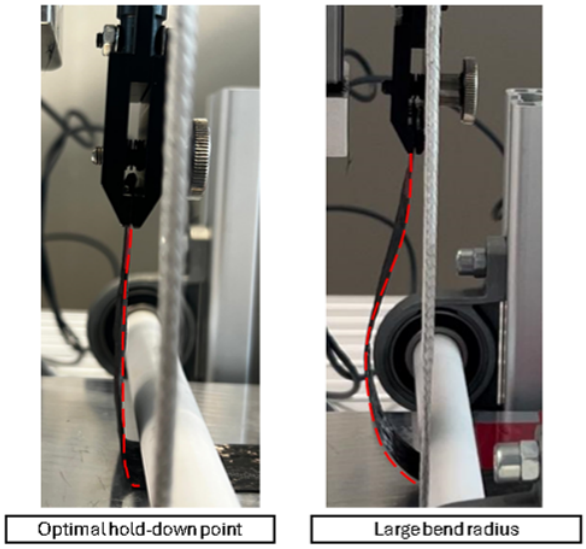

Figure 4.24: **left**-Optimal hold down point **Right**-Large bend radius

If the detachment point is far away from the clamping line, the bend radius becomes larger and can lead to crack propagation in the matrix. This can cause the premature failure of the specimen compromising the accuracy of the force measurements. Cracking of the matrix would result in force readings that would reflect the material failure rather than the peel tack, distorting the results.

4.6.1 Execution of the peel Test

Once the specimen plate is properly mounted and the clamping and bending points are aligned, the peel test is executed. It has to be made sure that the clamped end is positioned in the centre of the clamp to have an even force distribution to prevent uneven peel forces. This also ensures that the material does not twist, and the bending radius remains consistent. The evaluation areas of the specimen are assigned as follows:

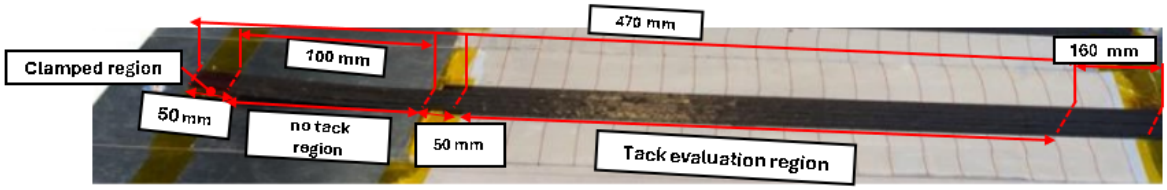

Figure 4.25: Evaluation areas of the specimen plate

The clamped region corresponds to the clamped part of the tow which is secured with tape. The whole width of the taped section is clamped, which is 50mm. Following this region is a 100 mm no-tack region, used for measuring the material's bending force. The tack measurement region begins 50 mm from the end of the no-tack region. Due to the tape securing the first ply at the end of the no-tack region, its tackiness can contribute to the overall tack value. Therefore, the tack measurement region starts immediately beyond the 50mm length of the securing tape and extends for 470 mm.

Referencing of the specimen plate is done to ensure the tension of the coupling rope and the

spring system. The test rig is now initialised, and the electric axis is programmed to maintain a constant peel speed of 0.5 mm/s for a travel distance of 470 mm. The analogue output of the force sensor can be set to zero before the measurement to calibrate it for the measurement.

The linear axis moves vertically upwards while the sample plate moves horizontally to the left over a total distance of 470 mm, with the real-time peel force recorded in the software at 200 ms resolution. The initial 150 mm of travel measures the bending force of the material, capturing the mechanical resistance without contributing to the adhesive (tack) evaluation. The actual peel force assessment begins at 200 mm, as the region between 150 mm and 200 mm contains force contributions from peeling off the tape placed on the first ply. This tape does not represent the material's tack behaviour and causes a force spike in the graph that is unrelated to the adhesive properties being tested. Therefore, the 50 mm section (between 150 mm and 200 mm) is excluded from the final peel force evaluation. The peel forces are calculated from 200 mm to 470 mm to ensure that only the true adhesive properties are measured. The last 160 mm of the sample is not evaluated, as the total test length is limited to 470 mm.

4.7 Evaluation of results

The force-time data was extracted from the GSV multi-software and exported to Excel for initial processing. For more detailed analysis and graph generation, a custom MATLAB script was created. This script facilitated the identification of key time intervals, including the start and end points of the no-tack and tack regions, as shown in Figure 4.26.

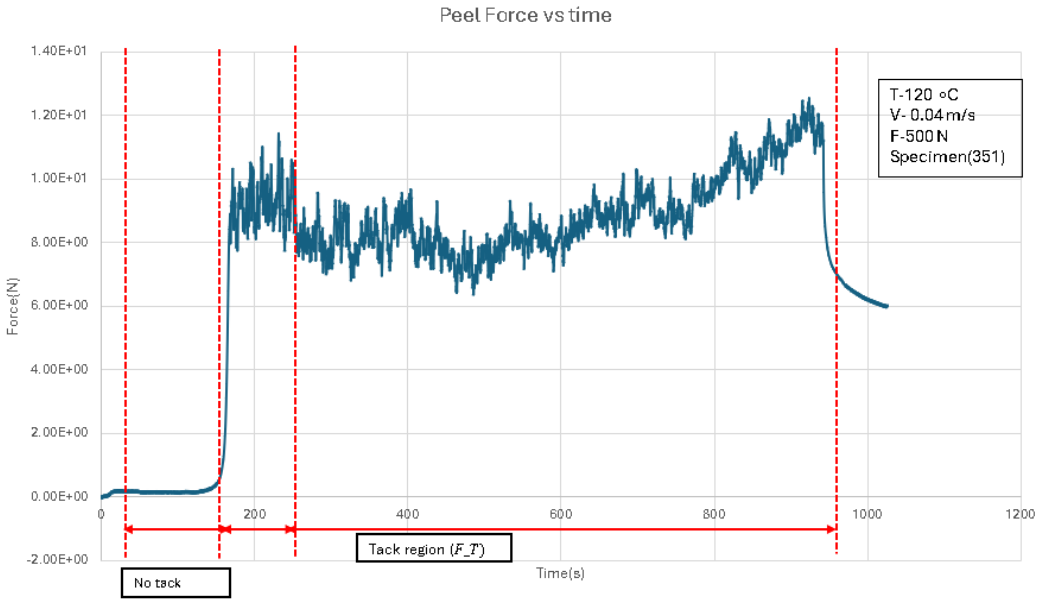

Figure 4.26: Force time measurement diagram of the peel test for specimen 351(group 15,first replicate) with the marked measuring areas

During the peel test, the second dry fibre ply forms a bent shape in the no-tack region until

the ply is taut, the average of these forces represents the fibre bending force. The region of 50mm (100s) from the end no tack region represents the tack formed due to the tape used to attach the first ply. This area is not considered in the tack evaluation. The actual tack measured in the tack evaluation region is seen in figure 4.25.

According to Crossley and Heller [86], [85] that the peel test setup is based on mentions that the pure measurement of bending forces due to the bending stiffness is presumably not completely accurate in the measurement region, this is because the frictional forces on the hold down roller and the increasing self-weight of the tapes are measured. But in our case, it is made sure that the development of frictional forces is avoided by preventing contact of ply with hold down roller and synchronising the movement of the roller with the linear motion of the plate. In addition, lateral forces also may be present if the tape is not clamped parallel to the clamp.

In the tack region, the Tack forces F_S are calculated which includes the bending forces. Following the assumption of Crossley et al. and Heller et al., it is assumed that the fibre bending forces and the pull-off forces and force distortions from both regions are reliable.

The stick and slip behaviour of the tape can be seen in figure 4.26, the increase in the force value to the peak represents the temporary adhesion(stick) behaviour and the abrupt drop in force value represents the slip behaviour.

Accounting for fibre Fraying The peel region of the plies accounts for the second ply coming clean off of the first ply. This can be seen in figure 4.27 where the white spots on the ply are the activated binder particles

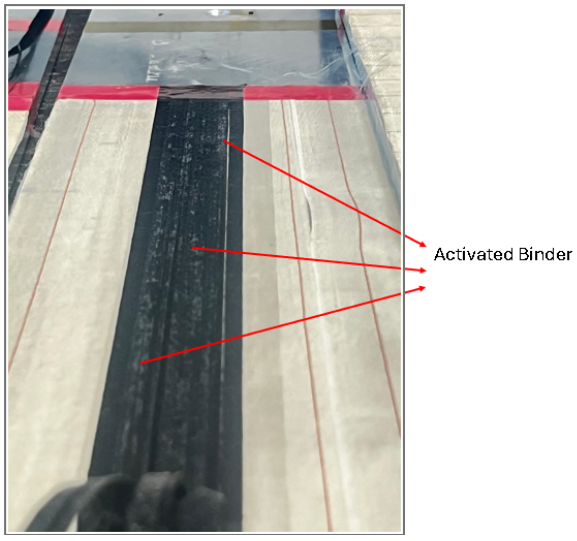

Figure 4.27: Activated binder spots

During the peel tests, it was observed that, for the higher temperature sets(95°C and 125°C) fraying of the fibre took place, it is observable in the figure 4.26 as the abrupt increase in the slope of the graph.

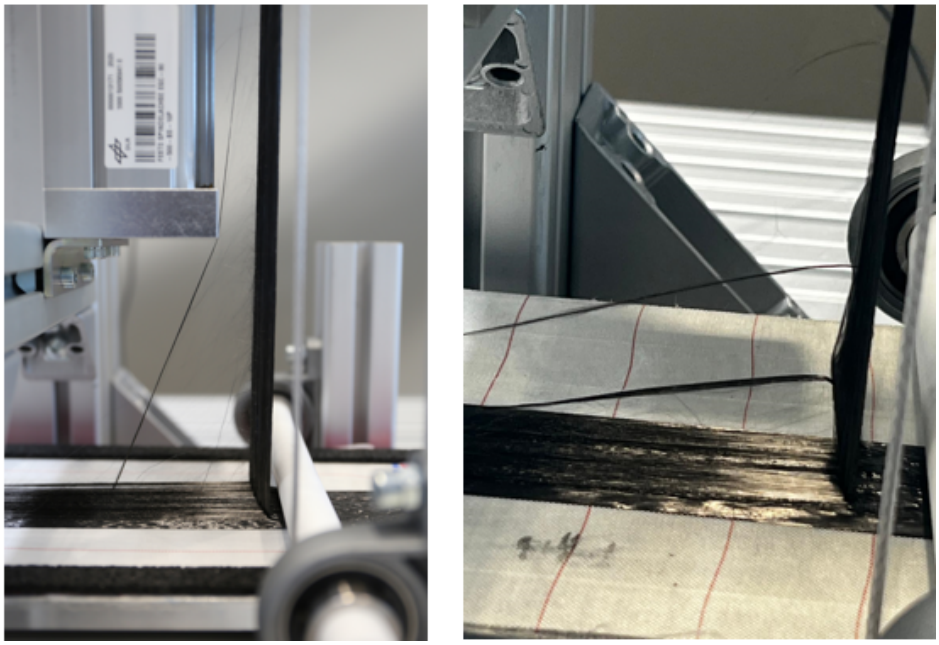

Figure 4.28: fibre fraying observed during peel test

To mitigate the impact of fibre fraying, an alternative test method—the wedge peel test—was considered. This method was designed to address the instability caused by fibre fraying by introducing a wedge to peel the material at a controlled angle. However, this approach presented new challenges, as the forces recorded were too low to be analysed accurately. Additionally, the frictional forces of the wedge interfered with the peel force measurement, compromising the reliability of the results. Due to these limitations, the wedge peel test was deemed unsuitable for accurate tack force evaluation.

To extract meaningful peel force data from the peel force versus time graphs, the graphs were segmented into regions based on the presence or absence of fibre fraying. Specifically, the graphs were divided into non-frayed and frayed regions, as illustrated in Figure 4.29. The frayed region begins at the abrupt increase in the slope of the peel force vs time graph. the transition between the non-frayed and frayed regions was not consistent across the different sample groups, with some groups with earlier onset of fraying and some sets with the onset of fraying towards the end of the peel test.

The frayed region introduces irregularities due to the unstable detachment of fibres, which often results in fluctuating force readings that are not representative of the adhesive bond. Fraying can cause sudden force drops or peaks, as the detachment process transitions from a cohesive peel (dominated by adhesion) to a more chaotic fibre sliding or breakage. By isolating the non-frayed region, the analysis could focus on the segment of the peel force vs. time graph where the detachment process was uniform and repeatable. This approach allows for more reliable comparisons between samples, as it eliminates the variability caused by fraying.

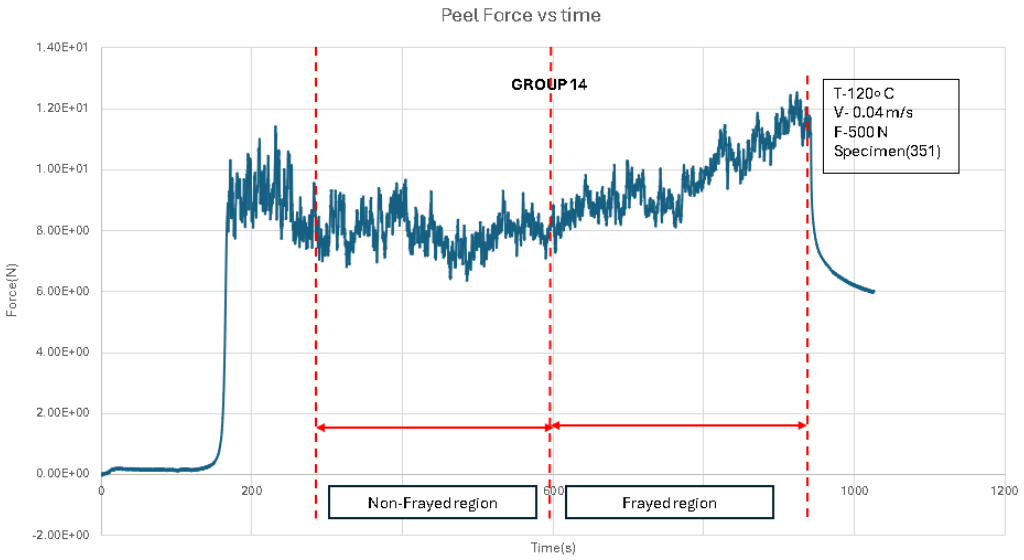

Figure 4.29: Non-frayed region used for tack and bending force calculation

Ultimately, the portion of the non-frayed tack region was used in the final analysis of the peel force. This was done to prevent the variation of peel forces due to the fraying. The statistical evaluation for this work is based on Design of experiments as mentioned in 4.1.

4.7.1 Statistical evaluation of Data

Following the extraction of the peel force, according to the three-level face-centred central composite design with the combination of sets in table A.1. An example of the graphs of a set obtained is as follows:

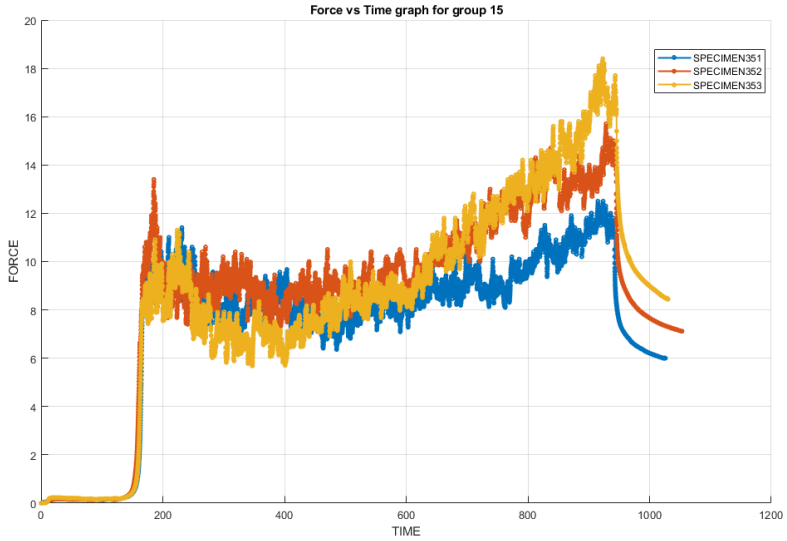

Figure 4.30: Peel force vs time graph obtained for the Group 15

The peel force and the bending force data were averaged across the three replicates for each of the 15 parameter sets. Rather than averaging the means of each replicate individually, the entire dataset for each test was averaged together. This averaging method ensured the accurate representation of the overall variability in the data and provided a reliable standard deviation of the results.

The averages of the F_S(Peel force) was found using the following formula:

$$F_S = \frac{1}{N}\sum_{i=1}^{N} F_{S_i} \tag{4.12}$$

where N is the size of the experiment.

Similarly, the averages of the bend forces F_B were calculated. Using equation 4.11 the tack forces were calculated. The averages of the tack forces for each of the 15 parameter sets F_T were calculated.

The statistical evaluation for the main effects is based on the 2^k experimental design where all the (2^3) or 8 possible combinations of factors are examined. According to the figure 4.31, the green points on the cube represent the 8 factors considered. This is done to study the main effect of the described factors.

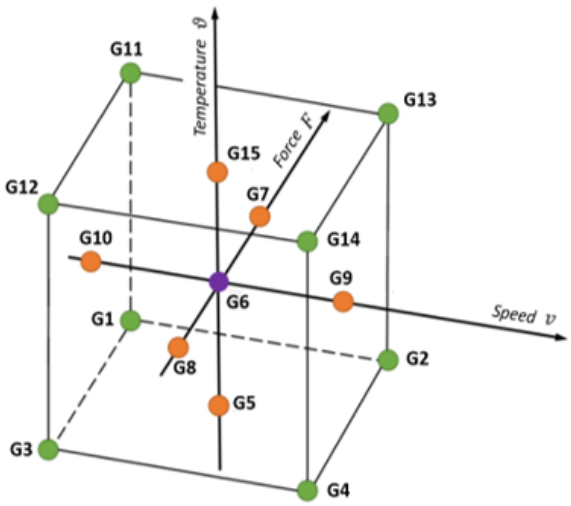

Figure 4.31: Face-centered central composite design cube representing the 15 combinations of parameters

From the table A.3, the mean of the variance S^2 was calculated to account for the variance in the 8 sets. The standard deviation of the data sets chosen was calculated from this variance using the formula found in the literature:

$$S_d = \sqrt{\frac{4}{N}S^2}$$

[4]

- S_d is the standard deviation,

- N is the size of the experiment

  N= n*m where n is the number of replicates and m is the number of factor level combinations tested for. In this study, n is 3 and m is 8, therefore N is 24

- S^2 is the calculated variance

The calculated standard deviation and mean of variances for F_B and F_T can be found in A,table A.7.

Before conducting the statistical evaluation, the distribution of the measured average tack values was assessed to ensure the validity of the statistical analysis of the main effects. The analysis of the significance for parametric studies assumes that the data is to be normally distributed. [87] The face-centred central composite design of experiments was employed to verify the data. Q-Q plots allow for the straightforward visual assessment of normality. Deviations from the normality can lead to inaccurate p-values and misleading confidence intervals, that would affect the reliability of the assessed main effects and interactions.P-values are a measure that helps decide if the results we see are meaningful or just due to random chance. A p-value less than 0.05 usually means that the results are statistically significant. A Q-Q plot was constructed, where the measured values were plotted against the quantiles of a normal distribution.

The quantiles were calculated using the following formula:

$$\mathrm{Q} = \frac{i - 0.5}{N} \times 100\% \tag{4.13}$$

[88] where,

- Q is the quantile
- i is the order of the measured value
- N is the total number of observations

with a normal distribution, the measured values should lie approximately on a straight line. If the lowest or highest values lie far away from the straight line, they are probably outliers due to a measurement error. If all values lay on a curved line, they may not originate from a normally distributed population and should be transformed (logarithmised). [88] The estimation of the significance of the effects of interactions is obtained by the comparison with two-sided confidence intervals. In our case, the t-distribution is used because of the limited sample size n and the unknown variance is calculated via the 15 samples. The empirical variance s^2 is estimated first from the number of replicates n, the individual y_i and the mean $\bar{y}$ of the factor level combination is measured using the following formula:

$$s_i^2 = \frac{1}{n-1} \sum_{i=1}^{n} (y_i - \bar{y})^2$$

The standard deviation of the 8 combinations for interaction of effects is calculated using the

experimental sample size N and the mean value s^2 of the individual variants of the m factor level combinations

$$N = n * m$$

$$s^2 = \frac{1}{m}\sum_{i=1}^{m} s_i^2$$

$$s_{\bar{d}} = \sqrt{\frac{4}{N}s^2}$$

Following the quantile test, the interaction effects between the three parameters were analysed to assess how these factors jointly affect the tack. The 2^k factorial design allowed the investigation of the individual effects as well as the interaction effects. The effects V, T, F, VF, TF and VT were calculated using the formulas 4.3, 4.1.1, 4.5, 4.6, 4.8 based on the independent factor t-test. To confirm that the result was statistically significant, thereby rejecting the null hypothesis (that the parameters don't have any effect on tack force) requires the assessment of the significance of each factor's effect on the tack force.

The t-test is part of the analysis of variance (ANOVA) framework and provides a t-value that indicates whether the observed differences between the groups are statistically significant. t-test is used in this case as the size of the experiment is 24. The t-value is calculated from the student's t-distribution table which can be found in Appendix A table A.17.

To determine the t-values of a probability, the number of degrees of freedom f is calculated as follows:

$$f = N - m \tag{4.14}$$

where N is 24 and m is 8, therefore f=16, this According to the p-value table as seen in Appendix. Figure A.17, the confidence intervals are calculated using the f value and converted into the p values for the confidence intervals of 95%,99% and 99.9% corresponding to 0.05,0.01 and 0.001 columns in p distribution table for two-sided confidence interval respectively. the formula:

$$\text{Confidence Interval} = \pm t \times s_{\bar{d}}$$

where s_d is the standard deviation calculated.

Chapter 5

Results and Discussion

This chapter presents and analyzes the results of this study, focusing on how temperature, layup speed, and compaction force impact the tack behavior of Hexcel HiTape® in Automated Dry Fibre Placement (ADFP). Section5.1 details the peel test results, outlining tack force trends across various parameter settings. Section 4.3.3 examines the temperature stability of the IR lamps during parameter and its implications for tack performance. Statistical insights into data distribution and parameter effects are provided in Section 5.2. The non-linear behaviour of the parameters on tack force is analysed in Section 5.3. Section 5.4 compares observed data with the Solvay TX1100 tack model, assessing its applicability to Hexcel HiTape®. This is followed by the discussion in Section 5.5 that analyses the results. A summary of the findings is provided in Section 6.1. Section 5.6 highlights attempts to quantify material-specific behaviours, such as binder seepage, while Section 5.7 addresses fibre fraying. Finally, Section 5.8 addresses the limitations of the study.

5.1 Evaluation of peel test results

The raw data of peel force vs time measurements were collected from the 15 parameter sets of 45 peel tests. The combinations of the nip point temperature, layup speed and compaction parameters used is shown in table 5.1

Group	T (°C)	V (m/s)	F (N)
Group 1	64	0.04	500
Group 2	64	0.2	500
Group 3	64	0.04	300
Group 4	64	0.2	300
Group 5	64	0.12	400
Group 6	95	0.12	400
Group 7	95	0.12	500
Group 8	95	0.12	300
Group 9	95	0.2	400
Group 10	95	0.04	400
Group 11	125	0.04	500
Group 12	125	0.04	300
Group 13	125	0.2	500
Group 14	125	0.2	300
Group 15	125	0.12	400

Table 5.1: Parameter Combinations for Each Group

The data was filtered from the force vs time graphs and the section representing the non-frayed section of material was used in the calculation of tack behaviour. An example of the area taken for calculation is shown in figure 4.29

The final tack force and bending force values with their standard deviations and variances are shown in A, tableA.3. This data is converted into a bar chart. The bar chart displays the tack and the bending force measured across the 15 groups of the chosen parameter combinations.

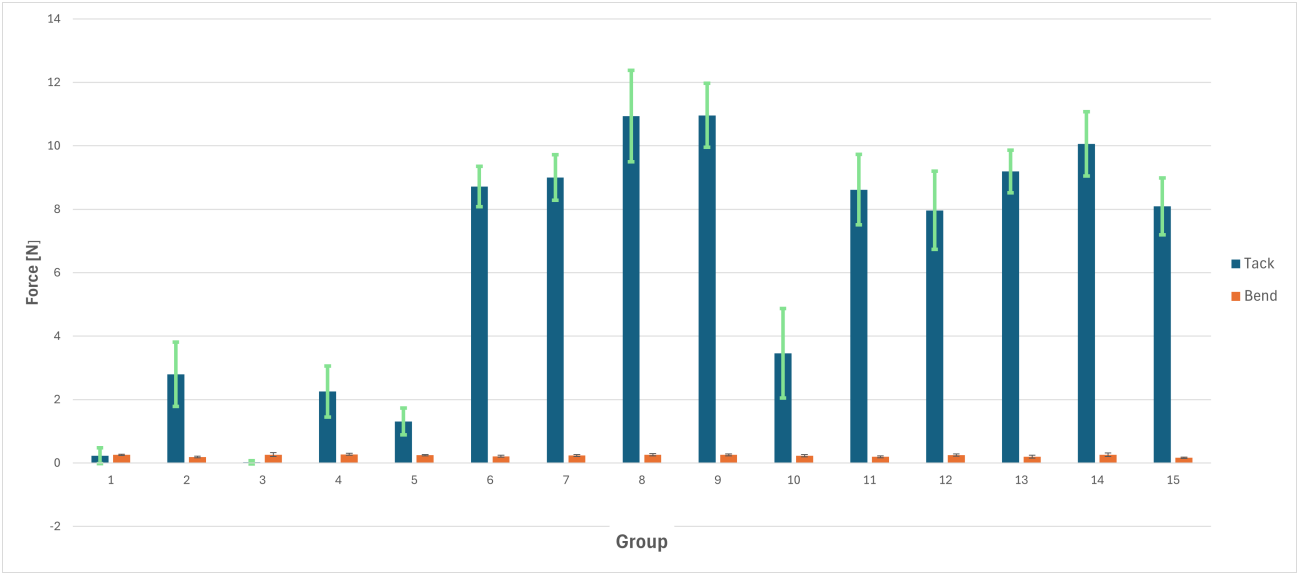

Figure 5.1: Mean values and standard deviation for the tack forces and bend forces

The blue bar represents the tack force measured during the peel test and the orange bar represents the fibre bend force.

Tack force F_T : The tack forces for groups 1 to 5 belonging to the 65 °C exhibit relatively

low values compared to all the other sets. The values can be seen ranging between 0.022 N in group 3 to 2.79 N in group 4. Where the lowest value is seen for the low-speed and low-compaction force combination and the maximum tack is seen for groups 2 and 4 with high speeds. Groups 2, 4 and 5 show some tack, while groups 1 and 3 have almost no tack.

The tack forces for groups 6-10 of temperature 95 °C show a significantly higher tack ranging from 3.96 N for group 10 to Groups 8 and 9 showing an average tack force of 10.93 N and 10.96 N respectively. These values of tack forces obtained are the highest of all the 15 combinations. The lowest tack is again exhibited by the group with the lower speed setting. The higher average tack force is seen for the material with the higher speed settings.

Groups 11-15 of temperature block 125°C show tack forces that do not have drastic differences in tack values as seen in the other two sets. The tack values range from 3.46 N for group 10 to 10.06 N for group 14. With higher tack is shown for the higher layup speed of 0.2 m/s and the lower tack for the lower layup speed of 0.04 m/s.

Fibre bend force F_B: As seen in figure 5.1 and table A.3, the fibre bend force across all 15 sets exhibits minor variations, suggesting that the metric remains fairly the same despite changes in parameter combinations. Across the experimental sets, the mean fibre bend force values range from 0.1666 N in group 15 to 0.2731 N in group 4, with most sets averaging between 0.2 and 0.26 N. Overall, the fibre bend forces show a uniform trend across the different sets, with only minor fluctuations in mean values and variability.

5.2 Statistical Analysis

This section shows the statistical analysis of the results obtained from the peel tests. This analysis ensures the reliability of the data and the validity of the experimental procedure.

5.2.1 Q-Q plot to assess normal distribution of measured data

To check if the average tack force values obtained from the peel test data follow a normal distribution, a Q-Q plot was generated for the average tack and the corresponding 15 parameter combinations as outlined in section 4.7.1. The tack force were divided into quantiles, as detailed in Appendix A, tables A.5 and A.6. The resulting distributions of the mean values of tack force for the 15 combinations are plotted in figure 5.2.

The Q-Q plot shows that while most data points follow a linear trend, there are slight deviations for the points at higher values. The numbers shown indicate the respective group IDs.Groups 12, 13, 11 and 15 of the parameter combinations according to table A.2 show slight deviation from the line of normality. These deviations mean that while these groups have tack force values that are somewhat higher than expected under perfect normality, the overall trend remains close enough to the line that we can reasonably assume a normal distribution for most of the data.

For the study of the interaction effects, the extreme points of the design cube are crucial. These points correspond to groups 1, 2, 3, 4, 11, 12, 13, and 14, as shown in Table A.2. They are represented in the Q-Q plots and play a significant role in capturing the boundary

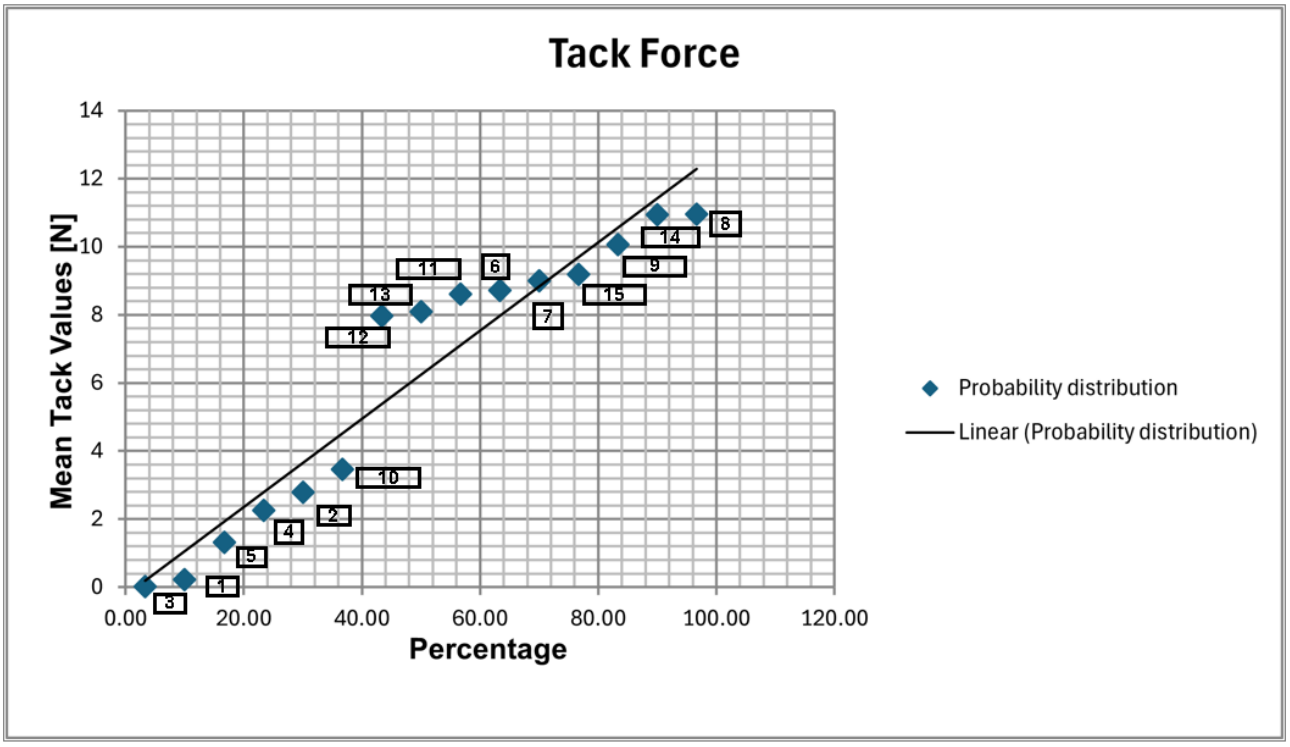

Figure 5.2: Q-Q plot to check for normal distribution of tack force

conditions of the 2^k factorial experimental design. This design was implemented to study the main effects of nip point temperature, layup speed, and compaction force on tack behaviour. It can be seen that the values of these groups exhibit an increase in mean tack force when moving through the quantiles. Group 1 has a mean tack force of 0.228 N while group 14 quantile has a tack force of 10.96 N. This means that there is no need for transformation of the obtained data making this dataset reliable for statistical analysis. Although group 12 in the combination of parameters shows noticeable skewness, it does not invalidate its use in interaction analysis.

5.2.2 Main effects and Interaction effects

Following the verification of normality for the tack forces, the main interaction effects between nip point temperature, layup speed and compaction forces are analysed using the 8 combinations of the 2^k factorial design using the extreme points of the experimental design . The main effects and interaction effects for tack forces and bend forces were calculated for the following :

- nip point temperature (T)
- Layup speed (v)
- Compaction force (F)
- interaction between Layup speed and nip point temperature(VT)
- interaction between Layup speed and compaction force (VF)

- interaction between nip point temperature and compaction force (TF)

The values of the main effects and interaction effects are calculated from the equations 4.3, 4.1.1, 4.5, 4.6, 4.7 and 4.8 and is shown in figure 5.2. Following this, the confidence intervals

Effect	Tack
V	1.87
T	7.63
F	0.13
VT	-0.53
VF	-0.30
TF	-0.24

Table 5.2: Main and interaction effects of Velocity (V), Temperature (T), and Force (F) on Tack Forces.

were chosen based on the student t-distribution table in Appendix A, table A.17 for the degree of freedom for the confidences of 95%, 99% and 99.9% as seen in section 4.7.1. The values chosen are then multiplied with the standard deviation calculated for the dataset shown in table 5.3.

Confidence Interval	95.0%	99.0%	99.9%
$\pm t * S_{\bar{a}}$	0.748	1.031	1.417

Table 5.3: Confidence intervals for the tack force at 95%, 99%, and 99.9% levels.

These confidence intervals were used to determine the significance of each factor and interaction. If an interaction's effect exceeded the 99.9% confidence interval, it was considered highly significant; if it fell below the 95% interval, it was deemed insignificant. If it falls between 95% and 99%, it is indifferent meaning that more trials need to be done. The interaction effects along with the confidence intervals were plotted to identify the significance of the individual factors and interaction effects for the tack forces.

Effect of Temperature

It can be observed in figure 5.3 that nip point temperature exhibits the largest effect on the tack force with an effective magnitude of 7.63 N. This means that for an increase in temperature from 64 °C to 125 °C there will be an increase of 7.63 N in tack force. This is further illustrated in figure 5.4, where the effect of nip point temperature on tack force is seen to go from 1.32 N for the T- (64 °C) level to 8.96 N for the T+ (125 °C) level. It is significantly higher than any of the other factors or interactions calculated. The calculations of the main effects and standard deviations are tabulated in Appendix A, table A.8 and A.9.The effect of nip point temperature exceeds the 99.9% confidence interval, indicating that the influence of temperature on the tack behaviour of Hexcel HiTape® dry fibre material is highly statistically significant.

Velocity

Velocity has a positive effect on tack with a value of 1.87 N. This shows that with an increase in layup speed from 0.04 m/s to 0/2 m/s, there will be an effective 1.87 N increase in tack force. The effect of this parameter is further illustrated in figure 5.4. The effect of layup

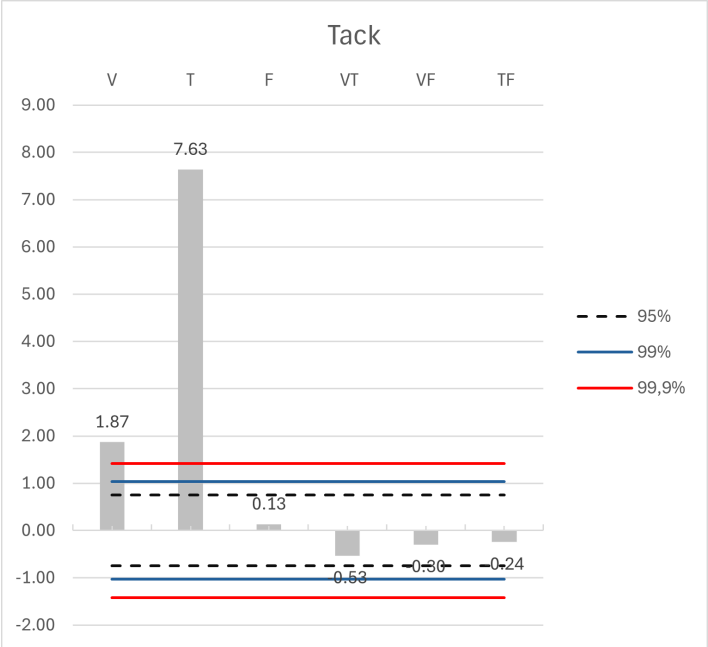

Figure 5.3: Chart capturing significance of the tack forces for different parameters and their combinations

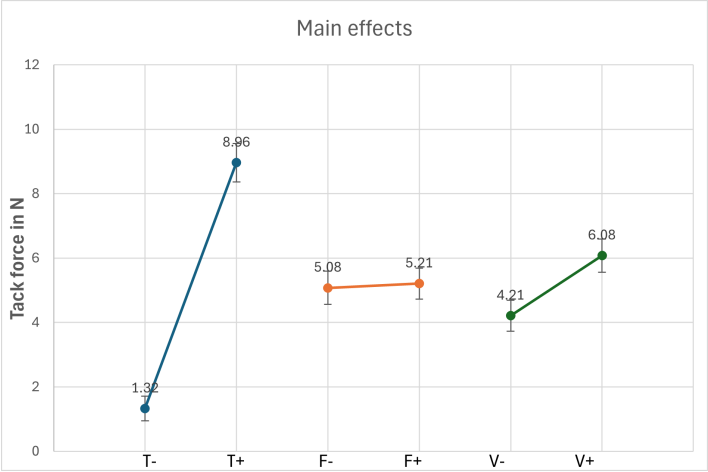

Figure 5.4: Line graph of the main effects of the parameters:nip point temperature (T), layup speed (V), and compaction force (F)

speed is seen to increase from 4.06 N at the V- (0.04 m/s) level to 7.05 N at the V+ (0.2 m/s) level. The calculations of the effects and standard deviations are tabulated in Appendix A, table A.8 and A.9 The interaction computed exceeds 99.9% confidence intervals indicating high statistical significance.

Compaction force

Compaction force has the lowest contribution to tack behaviour with a minor positive effect contribution of 0.13 N. However, it can be observed that the value for the compaction force

effect lies below the range for the confidence intervals of 95%. This indicates that, while the changes in compaction forces may influence the tack behaviour, the effect observed is not strong enough or consistent enough to be statistically accurate within the realm of this study.

Interaction Effects between Temperature and Velocity(VT)

The interaction between the velocity and temperature on the tack behaviour shows a negative effect of -0.53. This is indicative of an inverse behaviour of nip point temperature and layup speed. With a reduction in tack of 0.53 N with increasing temperatures and increasing speeds or reduced dwell times. The effect does not cross the 95% confidence range, suggesting that the effect is not statistically significant

Interaction between Layup speed and compaction force(VF)

The interaction between the layup speed and the compaction force shows a negative effect of -0.3 N on the tack force, however, this effect is not statistically significant as it does not cross the 95% confidence range. This could suggest that the interaction between compaction force and layup speed does not have a meaningful effect on the tack force.

Interaction between nip point temperature and compaction force (TF)

The interaction between the nip point temperature and the tack force exhibits a negative effect of - 0.24 N on the tack force. However, this effect also lies below the range of the 95% confidence interval.This suggests that the interaction is not statistically significant.

The above observations show that temperature has the highest effect on the tack force as it surpasses all three confidence intervals, followed by the effect of increasing velocity. The interaction effect of TV lies below 95% statistical significance, suggesting that the effect of temperature on tack is not independent of the velocity and vice versa.

The effect of compaction force and interaction of VF and TF, show limited or no significance, suggesting that these interactions do not influence tack force.

5.3 Check for Non-linearity

The face-centred central composite design of experiments was employed to analyse if there exists non-linear behaviour of the main parameters. The interaction effects were calculated for 15 groups that account for the high, low and mid-level of the parameters. The calculated effects are tabulated in Appendix A, table A.8. An interaction line graph is plotted as follows:

The graph 5.5 illustrates how the tack force varies with temperature, force and velocity at three levels: low(-), medium (0) and high (+) levels. The difference in tack between the levels gives the effect of the parameter.

- **Temperature**: Temperature shows a steep increase in tack force from the low level(T-) to medium level(T0), where the tack force jumps from approximately 1.72 N to 8.52 N. This sharp increase may suggest that the binder is insufficiently activated at the lower

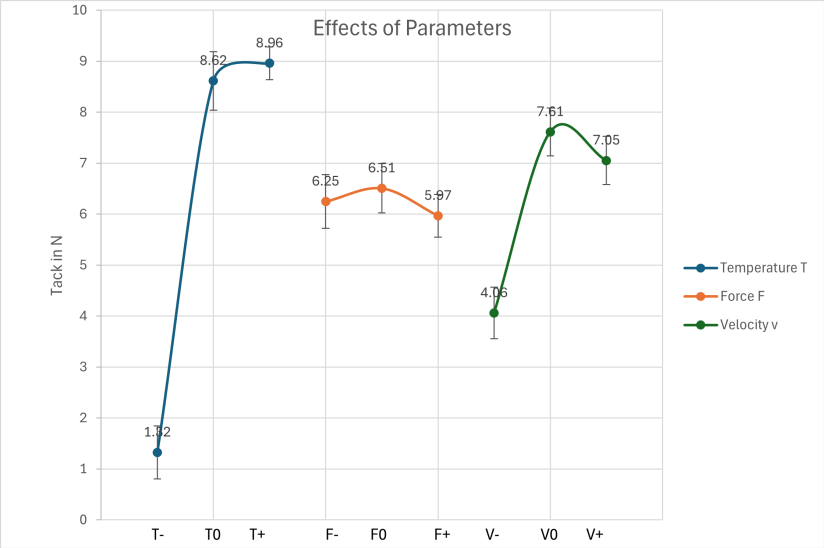

Figure 5.5: Main effects of parameters plot to check non-linearity

temperature (T-) level, leading to low adhesion. At this stage, the binder probably has a higher viscosity, due to incomplete melting which hinders proper bonding.

However, as the temperature reaches the medium (T0) level, the binder becomes completely activated, transitioning into a more adhesive state that significantly enhances the tack force. This activation continues as the temperature increases to a high level (T+,125 °C), where the tack force reaches 8.96 N.Notably this change in tack force between medium (T0) and high(T+) levels is much lesser than the low to medium transition.

- **Force**: Force shows very low variation in tack force across the three levels. Tack force ranges only slightly from 6.25 N at low (F-) to 6.51 N at mid-level (F0) and decreases to 5.97 N at high (F+) level. This flat trend confirms that the force has negligible impact on the tack force within the tested range. The low variation in tack force across force levels aligns with the statistical findings that the force is not a significant factor that meaningfully influences the tack force.

- **Velocity**: Velocity shows a non-linear relationship, directly proportional to the tack force. At the low velocity(V-), tack force is approximately 4.06N . Moving to the medium level (V0), tack force increases sharply to 7.61 N, suggesting that the velocity influences the tack force positively. It can be seen that between the medium velocity level(V0) and high-velocity level(V+), the tack force is seen to decrease from 7.61 N to 7.05 N. The standard deviations calculated may indicate that the observed value from V0 to V+ are not significantly different and may overlap. This overlap implies that the decrease could be linked to the normal variation than the actual reduction in tack force at higher velocities.

This non-linearity effect of the parameters should be accounted for while estimating the tack model.

5.4 Evaluation of the Fit between the experimental values and proposed Physical model equation

The physical equation derived by Saar from the thermoplastic prepreg model to model the tack behaviour of Solvay TX1100 dry fibre material as seen in chapter 2, section 2.3.1, the equation is as follows:

$$f_P(T, F, v) = \frac{cF^{0.2}}{a \exp\left(\frac{b}{5T}\right) v^{0.5}}$$

This equation incorporates three parameters a, b and c which are estimated to best fit the experimental data obtained from the peel tests of the Hexcel HiTape ® dry fibre material. Owing to the differences in binder type and fibre architecture, this fit check is performed to see if this model applies to this material as well.

To determine the best fit for the parameters a, b and c, a non-linear regression analysis was conducted. Non-linear regression is chosen, as the model equation has 3 different parameters and exponential and power functions within the formula that suggest non-linearity as can be seen in the section 5.3. The regression process iteratively adjusts the parameters to minimise the residuals, which are the differences between the predicted values of tack force and the observed values of tack force.

The following metrics were used to evaluate the goodness of fit

- **R-squared (**R^2- This statistical value indicates the proportion of variance in the data explained by the model. An R^2 value close to 1 suggests a good fit of the model equation, while values near or below 0 indicate that the model does not explain the data. It is calculated as :

$$R^2 = 1 - \frac{\text{SSE}}{\text{SST}}$$

[89]

  where:

  - SSE is the Sum of Squared Errors, calculated as the sum of squared residuals,
  - SST is the Total Sum of Squares, representing the total variance in the observed data.

- **Mean Absolute Error (MAE)**:This value measures the average absolute difference between the observed and predicted values. This reflects the accuracy of the model predictions

$$\text{MAE} = \frac{1}{n} \sum_{i=1}^{n} |y_i - \hat{y}_i|$$

  where:

  - y_i are the observed values,

  - $\hat{y}_i$ are the predicted values,
  - n is the number of data points.

- **Root Mean Squared Error (RMSE)**: It is similar to the MAE but gives more weight to larger errors, calculated as:

$$\text{RMSE} = \sqrt{\frac{1}{n}\sum_{i=1}^{n}(y_i - \hat{y}_i)^2}$$

  RMSE provides insight, on average, into the predictions that deviate from the observed data, it penalizes the higher errors, as the squares for the errors are calculated. The averages for higher differences between observed and predicted values will result in a higher RMSE compared to the MAE.

Model fit check using MATLAB

To perform the non-linear regression and fit the model to the experimental data, a MATLAB script was developed, as detailed in Appendix B B.1. The model works by defining a function tackmodel, that represents the physical equation 2.3.1 taking T, F and V as inputs, along with the initial parameter guesses. The function then computes the predicted tack force for given values of nip point temperature, compaction force and Velocity based on the initial parameter estimate. The parameter estimate was set to 0.3, 1488, and 0.24 as a baseline for a,b and c respectively as these were estimated for the Solvay TX1100 material.

The initial estimates serve as starting parameters for the optimisation process. The lsqcurvefit function in MATLAB then iteratively adjusts a, b and c to minimise the sum of squared residuals between observed and predicted values. The model returns the optimised parameters for the closest fit to the model and returns the optimised values along with the residuals. The goodness of fit is also calculated using the R-squared, MAE and RMSE values.

The regression analysis yielded the following parameter estimates and statistical values

Parameter/Metric	**Value**
Parameter a	0.4845
Parameter b	1672.9874
Parameter c	5.4685
Residual Norm (SSE)	284.2725
R-squared (R^2)	-0.2464
Mean Absolute Error (MAE)	3.5831
Root Mean Squared Error (RMSE)	4.3533

Table 5.4: Summary of Updated Model Fit Results

The table 5.4 shows an R^2 value that is negative. This shows that the model does not perform well with the data and this equation cannot capture the data pattern and has to be modified. The parameters a,b and c estimated are the values that result in the least difference between the predicted and the observed values of tack force. The RMSE value is also on the high

side showing the spread of errors and suggesting that, on average, the predictions are about 4 units away from the observed values.

The mean absolute error (MAE) of 3.5331 suggests that, on average, the model's predictions deviate from the actual tack values by about 3.5 N. This error is relatively high in the given range of tack values, indicating that the prediction of the model is not close to the observed values.

The plot for the predicted values of tack force after regression and the actual values are plotted below

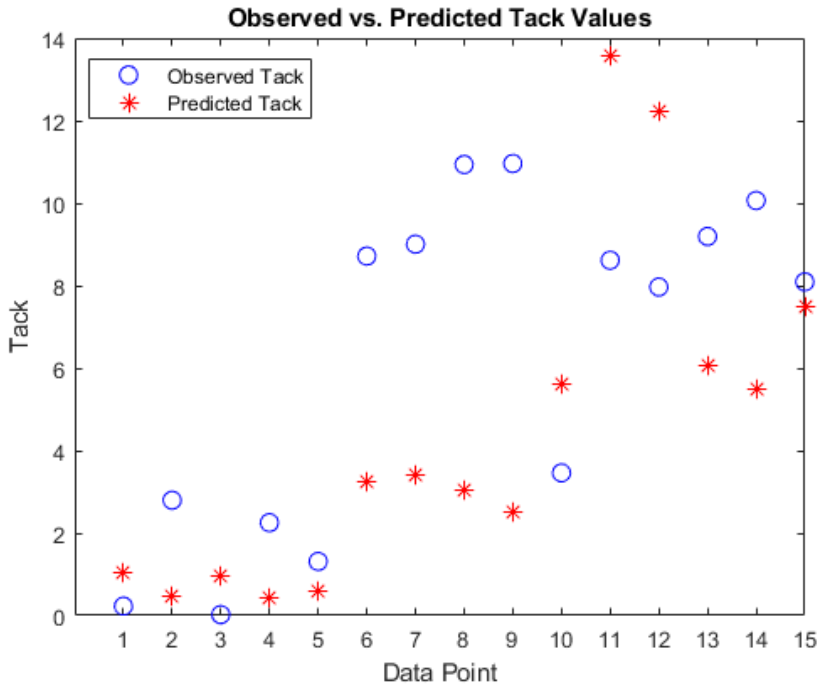

Figure 5.6: observed vs predicted values from regression analysis

The plot 5.6 shows the predicted values of the regression analysis to the observed values of tack from the peel tests. For a good fit of the model, the actual tack measurement(blue points) would closely follow the predicted tack (red points) for each data point, indicating that the model's predictions are in alignment with the actual tack values. In this plot, there are several areas where significant discrepancies occur: For data points 1 and 3, the observed values fluctuate close to zero, but the predicted values are higher, indicating an overestimation by the model. However, for groups 2 and 4, the predicted values are lower, indicating an underestimation of the model.

Between points 6 and 10, there is a sharp increase in observed tack values, reaching up to around 10–12 N. The model, however, fails to capture this rise accurately and produces lower predictions, particularly around data points 8 and 9.

At data points 11 and 12, the model overestimates the tack significantly, while the observed values show a decrease.

Towards the end, at point 15, although the observed and predicted values align somewhat better, in points 13 and 14 discrepancies remain.

This lack of alignment between observed and predicted values further illustrates that the model does not adequately represent the relationship between process parameters (temperature, force, and velocity) and tack for Hexcel HiTape ® material. The overpredictions and underpredictions in different regions suggest that the model needs to be adapted for the HiTape ® material. As the physical equation assumes that tack forces are inversely proportionate to the velocity, the model accounts for high tack forces at lower velocities. However, for the Hexcel material, high velocities show increased tack. Groups 1, 3,10,11 and 12 possessing the lower velocity of 0.04 m/s are estimated to have a higher tack according to the predicted model as the Solvay TX1100 dry fibre material showed this response. However, the largest difference in predicted tack versus the actual tack are seen in point 9 which denotes tack force at a velocity of 0.2 m/s. The difference is around 7N. The predicted tack force is much lower as compared to the observed tack.

This indicates that adjustments are needed to improve the model's accuracy for the Hexcel HiTape ® material.

Recommended model Adjustments

- **Temperature threshold term**: Adding a term that captures the sharp increase in tack once the material reaches its binder activation temperature would help the model account for the rapid rise in tack as seen in groups 6-10. This term would differ for different dry fibre materials based on their binder type. However, the sharp increase in tack values may be due to the temperature of 64 °C chosen for the material being too low to completely activate the binder.

- **Revised speed term**: Shifting the velocity term to the numerator of the equation would align the model with the Hexcel HiTape ® observed behaviour where higher speeds show increased tack values.

5.5 Discussion

In this section, the key findings from the peel tests and statistical analysis are critically examined. The section is structured to discuss the peel test results, the interaction effects and the relationship between the process parameters of nip point temperature, layup speed and compaction forces on the tack behaviour of the Hexcel HiTape® dry fibre material. This section also addresses the limitations of the investigation.

The primary objective of this study was to investigate the tack behaviour of the Hexcel HiTape® dry fibre material at varying nip point temperatures, layup speeds and Compaction forces and to check whether the proposed tack model for the Solvay TX1100 holds well for the Hexcel HiTape ® dry fibre material.

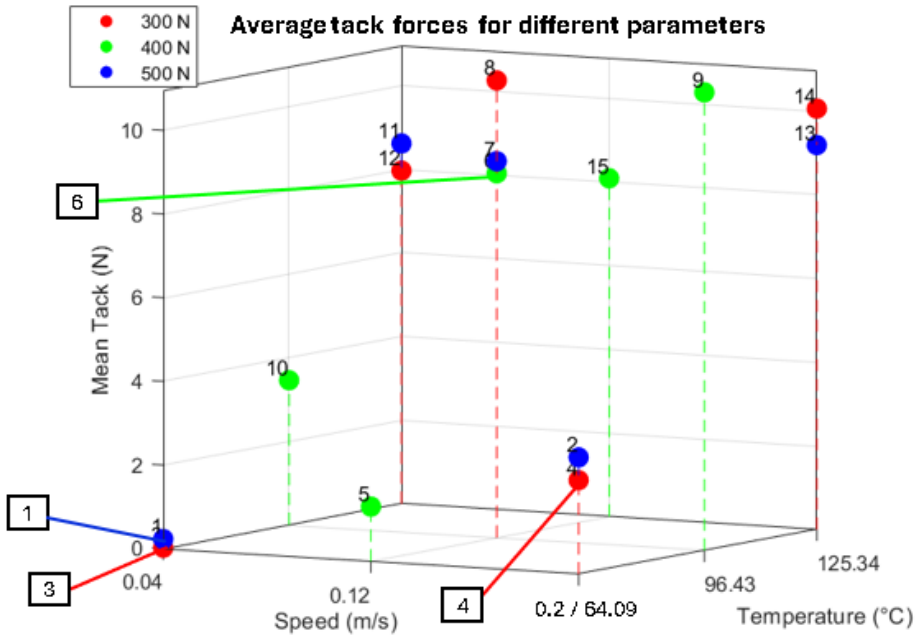

Figure 5.7: 3D score plot showing the average forces for different parameter combinations of groups 1-15

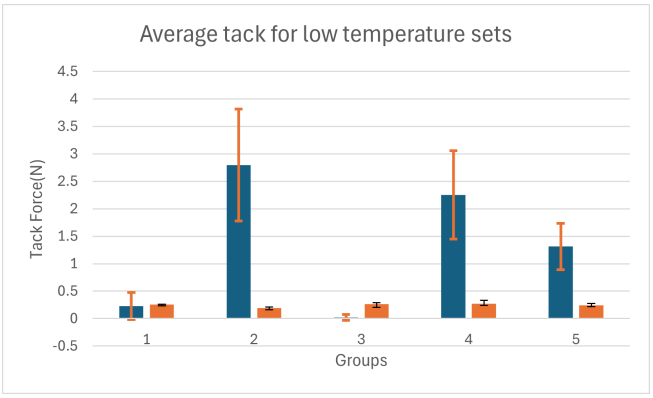

Figure 5.8: Average tack force for low temperature sets 64 °C)

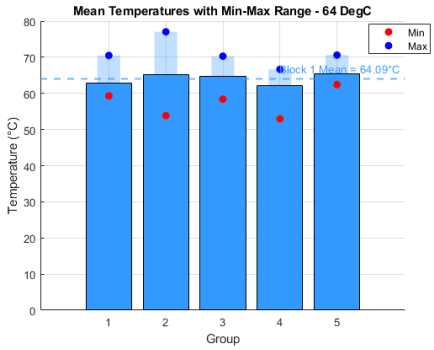

Figure 5.9: Mean temperatures with min-max range for low temperature block

5.5.1 Role of temperature on tack force

The findings from Chapter 5 subsection 5.1 and from the figure 5.7 of the peel test results indicate the dominance of temperature on the tack forces. Higher temperature sets show higher tack forces and vice versa.

Groups 1-5 (64°C temperature block) of the figure 5.1 show very low tack force values, with groups 1 and 3 showing almost no tack. This could indicate that the binder of the dry fibre tape was not completely activated during the ADFP process. The temperatures obtained by the lamps during the temperature setting of the experiment are shown in figure 4.14. This figure indicates the temperatures and the range of temperatures that could be reached for each

set. Looking at figure 5.9, for groups 1-5 where nip point temperature was around the average (64 °C), the temperature settings suggest that the variability in nip point temperatures for this set is low. This contradicts the observations found from the peel test.

The 64°C temperature set suggests the start of tack formation, as the binder may not be completely activated. The score plot in figure 5.7 shows that the threshold for effective tack occurs above the lower temperature block(64 °C). This temperature can be used as a baseline for the investigation of the actual binder activation temperature for the Hexcel HiTape ®. To conduct future investigations, a slightly higher temperature should be used as a lower temperature set while investigating this dry fibre material.

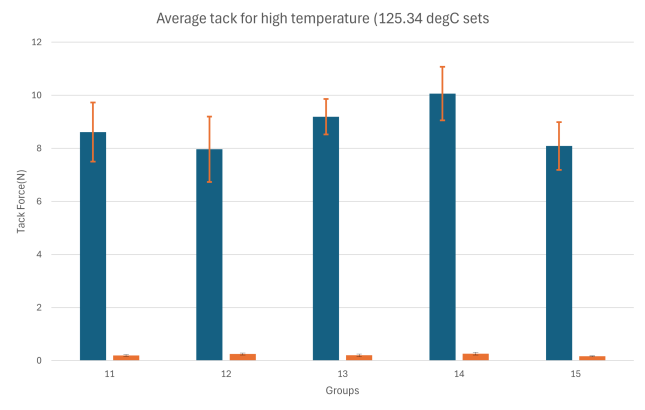

Figure 5.10: Average tack force for high temperature sets 125°C)

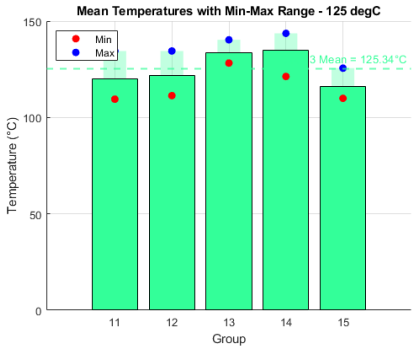

Figure 5.11: Mean temperatures with min-max range for high-temperature block

Higher temperature blocks show higher tack forces compared to the 64 °C groups. The difference between the average tack force of the groups of high (125 °C) and low(64 °C) temperature are around 8 N. This may suggest that more binder is activated in the 95 °C settings. The statistical significance of the temperature effect is further confirmed as the higher temperatures promote softening of the binder. This results in more intimate contact between the plies. This may suggest that higher temperatures result in a higher degree of polymer diffusion at 95 °C temperature setting, aligning with the proposed hypothesis of increasing temperatures increasing tack strength.

In figure 5.12, it can be observed that group 10 shows significantly lower tack compared to groups 5 to 9 of temperature block of 95 °C. This deviation could be explained by the figure 5.13 representing the nip point temperatures recorded for each setting. Group 10 (T=95 °C, V=0.04 m/s, F=400N), has the lowest minima of 84.4 °C recorded among the other temperature blocks. This could suggest that during the manufacturing of the specimen for the group, the temperature reached around this value causing a lower tack force magnitude.

5.5.2 Role of layup speed on tack force

The layup speed governs the interaction time of the ply interface under heating during the dry fibre deposition. In the peel test analysis, it is observed that a higher layup speed gives rise to a larger tack force. This is seen in groups 2,4,9,13 and 14 in the figure 5.7. Group 9 (T-95°C, V-0.2 m/s, F-400 N) reports the highest tack force out of all the sets of 10.96 N. This indicates the positive effect of layup speed on tack behaviour. This behaviour contradicts the

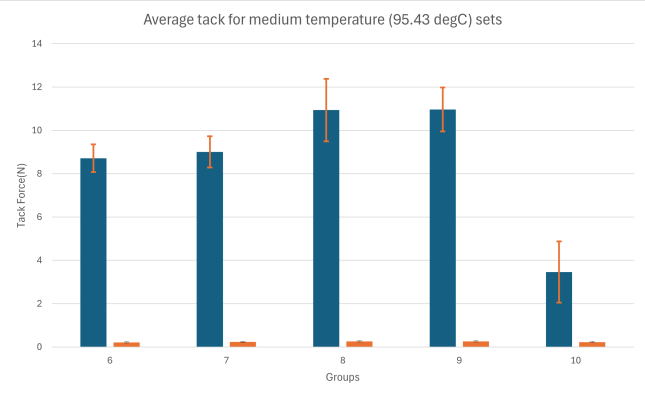

Figure 5.12: Average tack force for medium temperature sets 95°C)

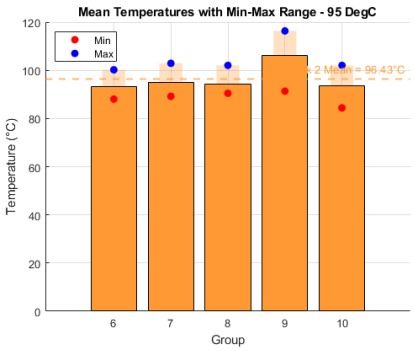

Figure 5.13: Mean temperatures with min-max range for medium-temperature block

predicted behaviour of low speed favouring better tack. It can be seen in all the temperature sets figure 5.7, that higher speeds result in higher tack forces.

The statistical analysis supports this observation revealing a positive increase of 1.87 N increase in tack for an increase in layup speed from 0.04 m/s to 0.2 m/s. This contradicts the tack behaviour obtained for the Solvay TX1100 material as seen in the chapter 2, section 2.5, where the speed shows a negative effect on tack force, with increasing speeds, decreasing tack force by an effective of 0.61 N for an increase in speed from 0.04 m/s to 0.2 m/s. An explanation for the behaviour of Hexcel HiTape ® could be because of the material architecture of the Hexcel HiTape® dry fibre material. As seen in figure 4.3, the dry fibre material contains perforations throughout the material. These perforations could be causing the seepage of the binder through the material after reaching its melting point. The dwell time or the time of the deposited substrate under heating is directly influenced by layup speed. A lower layup speed gives rise to a higher dwell time and vice versa. This could mean that a lower dwell time denoting a higher speed could lead to the binder not having enough time to seep through the material and consolidate quickly. The binder stays in the interface and polymer diffusion enhances the tack behaviour. A higher dwell time denoting a lower speed gives enough time for the binder to melt and seep through the perforations. This would cause the binder to not stay at the interface, resulting in areas without binder at the interface, causing lower tack force values.

It could be argued that, with more seepage of the binder across the interface, it may result in a higher degree of mechanical interlocking causing higher tack. This mechanical interlocking could be the reason for fibre fraying which shows higher values of tack as seen in figure 4.29. However, this investigation considered only the tack force data in the non-frayed region while accounting for tack. Further investigations accounting for the frayed regions as well are required to make a more definitive conclusion on the relationship between temperature, speed, and binder flow.

It should be noted that the seeping of the binder through the material is influenced not only by the time under the heating lamps but also by the viscosity of the melted binder. At higher temperatures, the binder's viscosity is significantly reduced, which would initially suggest that binder seepage through the material's thickness should be more pronounced at elevated

temperatures.

Looking at the tack measurement results in figure 5.1 and figure 5.7, there is a clear trend of increased tack at higher temperatures. However, contrary to expectations, the difference in binder flow rates between different speeds appears less pronounced at higher temperatures than at lower temperatures. At lower temperatures, the temperature effect is less dominant and the velocity effect is more pronounced. This effect is illustrated in the score plot in figure 5.7 where higher speeds yield slightly better tack than lower speeds (eg., Group 2 vs Group 1). In higher temperature blocks, especially the 125 °C block, as illustrated in figure 5.7 the tack force appears less sensitive to changes in layup speed, likely because the binder is sufficiently activated and adheres well, regardless of the speed. This indicates that, at elevated temperatures, the influence of layup speed diminishes as the temperature becomes the dominant factor affecting tack force.

5.5.3 Role of Compaction Force on tack force

From the peel tests, the influence of compaction forces on tack behaviour is found to be minimal compared to the effects of nip point temperature (T) and layup speed (V). This can be seen in figure 5.7. At low temperatures, there is an increase in tack force with compaction force for both low-speed and high-speed settings. For instance, the tack force rises slightly from 300 N (groups 3 and 4) to 500 N (groups 1 and 2), suggesting that higher compaction force slightly improves tack in the lowest temperature block (64 °C). At this temperature, the binder remains relatively viscous and does not flow freely. Applying compaction force helps create better contact between the binder and fibre surfaces which compensates for the limited flow, resulting in a slightly increased tack.

However, for groups 13 and 14 at high temperature (125 °C) and high speed (0.2 m/s) with different compaction forces(300N and 500 N), it can be observed in figure 5.7 that the tack force is higher at lower compaction force 300N and decreases as the compaction force increases to 500N. This could be explained by the low viscosity of the binder at higher temperatures. When the binder is fully activated and fluid, the high compaction force may push the binder into the fibre structure or may even cause binder displacement, this effect may be increased by the presence of perforations in the Hexcel HiTape ® tow surface. This could reduce the amount of binder available at the interface, resulting in lower tack. In contrast, a lower compaction force allows the softened binder to stay at the surface, enhancing the tack without the binder seeping through the tow. However, as mentioned in subsection 5.5.2 the frayed area was not considered in the analysis. This behaviour may have an effect on tack and has to be investigated further.

The statistical analysis of the peel test data showed that the compaction force had minimal effect on tack behaviour, with no statistically significant increase in tack observed with increasing force. This could suggest that once a minimum compaction force is reached, further increases do not increase tack.

5.6 Addressing the binder seepage hypothesis

Upon observing the trend of higher tack forces at higher layup speeds after conducting the experiments, there was an effort to investigate if this hypothesis held true to the observed effect from the peel tests as seen in section 5.5.2.

The laid up specimen was cut along its thickness and embedded in resin. Following this, cross-sectional microscopy was conducted to observe the binder distribution after the peel test.

Figure 5.14: resin cast specimen for cross-section microscopy

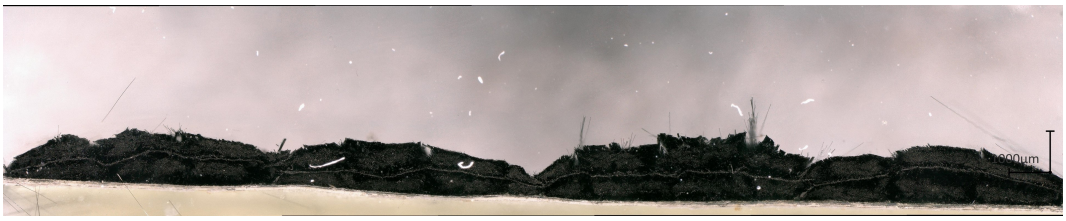

Figure 5.15: resin cast specimen for cross-section microscopy

Figures 5.14 and 5.15 show the cross-sectional specimen, and its microscopy to identify binder seepage. However, the resin likely permeated into the specimen, significantly obscuring the visibility of the binder material. It could also be because the binder got dissolved by the resin. This unintended resin infiltration reduced the contrast between the binder and the surrounding fibres, making it difficult to accurately identify and assess the extent of the binder seepage.

The act of slicing through the dry fibre across its thickness resulted in an uneven surface profile. The unevenness created topographical variations, such as protruding fibres and depressions, which introduced difficulties in achieving proper focus under the digital microscope. This surface irregularity affected the microscope's ability to maintain consistent focal depth, leading to issues with image clarity and resolution. As a result, the microscopy images exhibited reduced sharpness, particularly around the fibres, compromising the quality of the analysis.

To address the issue of binder visibility, a 3D clamping rig was constructed where a section of the tow from the deposited specimen could be securely clamped and cut. This setup was expected to enhance the visibility of the binder by reducing fibre misalignment during cutting.

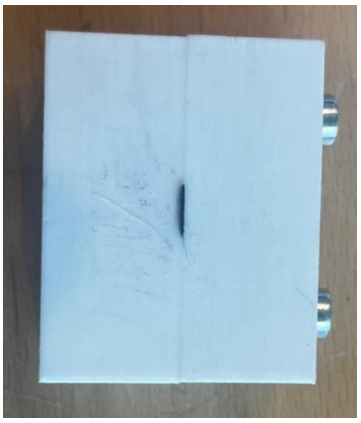

Figure 5.16: 3D printed clamp for cross-sectional dry fibre specimen

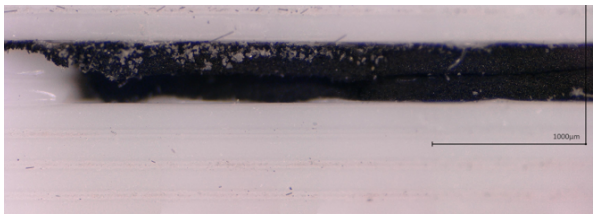

Figure 5.17: microscopy image of cross-sectional dry fibre specimen

However, the surface unevenness persisted and continued to cause focus problems with the digital microscope. Despite the clamping rig minimising handling errors, the nature of the fibrous material led to irregularities in the cut surface. These uneven surfaces introduced multiple focal planes, which prevented the microscope from achieving consistent focus on the fibres. This is seen in figure 5.17. As a result, the uneven topography remained a limiting factor, making it difficult to capture clear and focused images of the binder distribution within the fibre matrix. The extent and pattern of binder seepage remain inconclusive due to the challenges in achieving the images. The uneven fibre surface and the resin's interference in binder visibility suggest that the binder may have moved through the material unevenly, potentially concentrating in some regions while thinning in others. However, the inability to clearly discern these areas prevents definitive conclusions about the seepage behaviour.

Future work will require more precise specimen preparation techniques or alternative imaging methods like Micro CT, that would allow for a more accurate assessment of binder seepage within the fibre matrix.

5.7 Attempt to quantify fraying behaviour

Fraying was observed in some specimen sets during the peel tests as seen in section 4.7 suggesting an interesting finding of the Hexcel HiTape ® material. To quantify this fraying behaviour, the frayed specimens were examined under a digital microscope as seen in figure 5.18, to explore potential patterns. Due to the specimen length of 480 mm, the VR series 3D microscope, with a 150 mm scanning bed, was chosen over the higher resolution laser confocal microscope, which has a smaller 50 mm scanning bed. Cutting the specimens to fit

the smaller microscope would have damaged the frayed areas, so maintaining the full specimen was prioritised. Although the VR series 3D microscope has a lower resolution, this trade-off was necessary to ensure specimen integrity for accurate analysis However, several challenges were encountered in reliably measuring the extent of fraying.

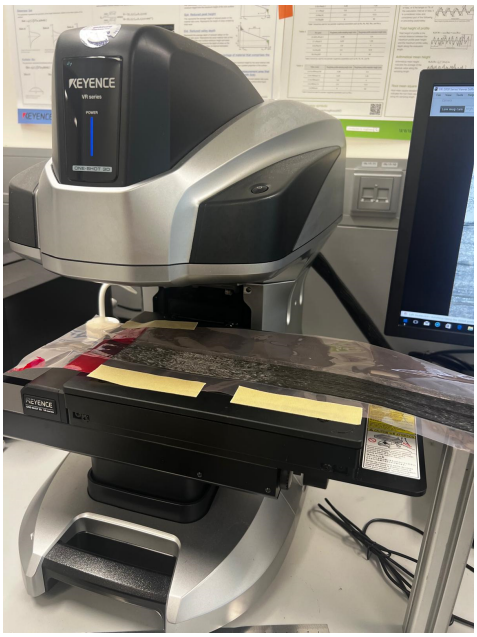

Figure 5.18: Microscope setup for analysing frayed specimen

Challenges in Quantifying Fraying

- **Lack of Consistent Fraying Patterns**: Despite the visual inspection through digital microscopy, no consistent or identifiable fraying pattern could be observed across the specimens. This irregularity in the frayed regions made it difficult to define specific criteria for measuring fraying behaviour, limiting the accuracy of direct microscopy-based quantification.

- **Complexity of Greyscale Image Analysis:** Greyscale analysis was also explored as a method for distinguishing frayed regions from intact fibre areas. This is shown in figures 5.19 and 5.20. The dark region is the fraying seen in figure 5.19. However, the irregular greyscale values introduced by frayed fibres and fibre perforations of the Hexcel HiTape ® complicated the analysis as seen in figure 5.20, as these features produced similar dark regions in the images, leading to inconsistent measurements.

Potential Methods for Future Quantification

While initial attempts at quantification were inconclusive, there are alternative methods that may offer more accurate measurement of fraying behaviour:

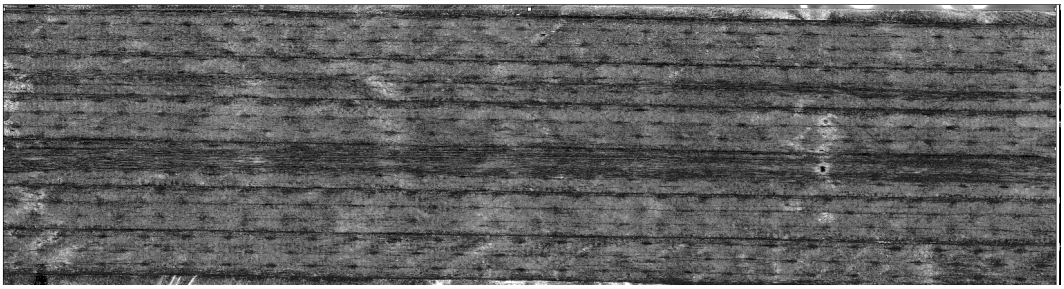

Figure 5.19: Microscope image of a slightly frayed specimen of group 4

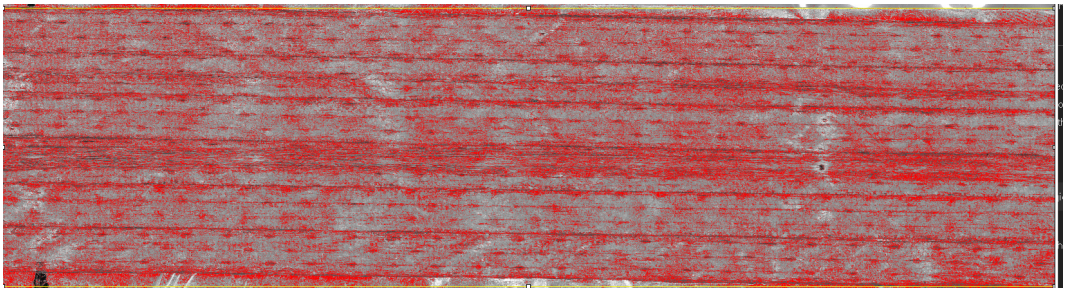

Figure 5.20: grayscale analysis of frayed specimen of group 4 specimen

- Slope Analysis from Peel Force Graphs: The slope in the frayed region of the peel force graph as seen in figure 4.29 may serve as an indirect measure of fraying. A sharp rise in the slope of the peel force graph could indicate areas where fraying influences the material's resistance. By examining these changes in the slope of the peel force graphs and correlating it to the area of frayed region to non-frayed region of the material, it may be possible to estimate a relative magnitude of fraying across specimens. Further calibration would be needed to validate this approach, but it could be a possible method to quantify the fibre fraying and account for it in future investigations.
- Microscopic analysis of Frayed vs. Non-frayed Areas: A more refined approach using microscopy could involve calculating the area ratio of frayed to non-frayed regions. This method would allow for a relative assessment of the fraying extent by comparing the affected regions to intact fibre areas. By quantifying these areas, a comparative measure of fraying could be developed, providing insight into how temperature and processing conditions affect fibre stability.

5.8 Limitations

- The design of experiments for the 3 factors and 3 levels were limited to 15 combinations out of the full factorial 27 combinations of parameters. Investigation of all 27 parameters could prove to give more data points for understanding the non-linear behaviour and the interactions between the parameters.
- As the datasheet for the Hexcel HiTape ® material was not accessible, a series of heating

trials had to be conducted to find an approximate activation temperature for the binder. The process was time-intensive.

- Thermocouples employed for temperature measurement were sensitive and the nip point temperatures recorded along the length of the ply had differences. Even using a different diameter of the same k-type thermocouple altered the measured values of the temperatures recorded during the power setting of parameters for the 3 IR lamps on the AFP unit.
- Fraying during the peel test reduced the number of usable data points for each group.
- Traditional AFP systems, such as the Coriolis C1, typically use open-loop heating control, which doesn't include a feedback system to adjust for temperature changes in real-time. This can cause uneven heating. The setup of IR lamp arrays has a major impact on how heat is distributed across the layup. Without feedback, these systems can't respond to sudden temperature shifts in the material, causing temperature gradients and a complex relationship between heating power, feed speed, and how the material absorbs heat. This makes it difficult to achieve even temperatures, especially in units like the Coriolis C1, which uses three IR heaters, adding to the challenge of maintaining consistent heat.

Chapter 6

Conclusions

The chapter begins by highlighting the findings of the study summarised in section 6.1, providing insights into how temperature, layup speed, and compaction force influence tack behaviour. In section 6.2 the research questions formulated in chapter 3 are answered.

6.1 Summary of Findings

This study investigated the influence of process parameters—temperature, velocity, and compaction force—on the tack behaviour of Hexcel HiTape® in Automated Dry Fibre Placement (ADFP). The following findings summarize the key insights from the results and analysis:

Dominant Influence of Temperature on Tack: Temperature was confirmed to be the most significant factor affecting tack. Higher temperatures consistently produced higher tack forces. This validates the initial hypothesis of the dominance of nip point temperature on the tack behaviour. This effect is attributed to reduced binder viscosity at elevated temperatures, which facilitates binder flow and promotes polymer diffusion at the interface.

Influence of velocity on tack behaviour: Following temperature, velocity emerged as the next most influential parameter. At lower temperatures, velocity had a stronger impact on tack, while at higher temperatures, temperature remained the dominant factor. This relationship suggests that velocity's effect on tack is somewhat conditional upon the temperature level. This contradicts the initial hypothesis that proposed a lower speed giving rise to higher tack force.

Effects of Compaction Force on Tack: From the peel tests, compaction force exhibited a dual influence on tack depending on the levels of temperature and velocity. At low temperatures and low speeds, increasing compaction force raised tack. Conversely, at high temperatures and high speeds, reducing compaction force appeared to enhance tack. However, from the statistical analysis in section 4.7.1, compaction force was shown to be statistically insignificant. Therefore, the hypothesis that predicted increase of tack forces with increasing tack is not supported.

Non-linear behaviour across parameters: The relationship between tack and each parameter—temperature, velocity, and compaction force—was found to be non-linear. This non-linearity indicates that the impact of each parameter on tack does not follow a simple, linear trend, underscoring the need for optimised parameter control within specific ranges to achieve consistent adhesion.

Limitations of the Solvay TX1100 Model for Hexcel HiTape®: The tack model originally developed for Solvay TX1100 material was not a good fit for Hexcel HiTape®. Specifically, the model's assumption of an inverse relationship between velocity and tack force did not align with Hexcel HiTape® behaviour, where higher velocities increased tack force. This divergence highlights the need for a material-specific model to accurately predict tack behaviour for Hexcel HiTape®. This finding contradicts the initial hypothesis. The tack model of the Solvay TX1100 material cannot be generalised to the Hexcel HiTape ®.

Hypothesized Influence of Material Structure on Tack: The positive effect of velocity on tack force is likely linked to Hexcel HiTape® 's perforated structure. At lower speeds, the binder may seep through the perforations due to prolonged exposure, resulting in less binder at the bonding interface. Higher speeds, however, help retain the binder on the surface, increasing tack. This hypothesis provides a plausible explanation for Hexcel HiTape® 's unique response to velocity.

Observations on Temperature Threshold for Binder Activation: At the lowest tested temperature (64 °C), tack remained very low, likely due to incomplete binder activation. To ensure full binder activation, a slightly higher temperature should used for future investigations. This finding offers an initial guideline for the processing range of Hexcel HiTape®, especially in the absence of data sheet specifications.

6.2 Answers to the research questions

This research focused on investigating the influence of the process parameters—nip point temperature, compaction force, and layup speed—on the tack behaviour of Hexcel HiTape® dry fibre material in the Automated Dry fibre Placement (ADFP) process. The study utilized a 90-degree peel test to quantify tack forces across various parameter combinations. The study examined how these factors, both independently and in combination, shape tack behaviour of the Hexcel HiTape ® material. Below are the conclusions drawn from the results, addressing the primary research question and supporting sub-questions.

Main research Question 1: How do the process parameters influence tack behaviour in Hexcel HiTape ®?

Sub-question 1: How does the variation in nip point temperature affect the tack behaviour of Hexcel HiTape® Dry fibre Material?

Answer: From the peel test data and the statistical analysis, it is seen that nip point temperature has the most influence on the tack behaviour of the Hexcel HiTape ® ® material. This validates the initial hypothesis of temperature having a dominant effect over all the other parameters. The higher tack force is mostly due to the reduced binder viscosity and increased degree of polymer diffusion across the ply interface that strengthens the tack bond.

Sub question 2: How does the layup speed influence the tack behaviour of the Hexcel HiTape ® dry fibre material?

Answer: Contrary to the initial hypothesis, the peel tests and statistical analysis revealed a positive correlation between layup speed and tack force for AFP-deposited Hexcel HiTape®. Higher speeds resulted in increased tack forces, likely due to the material's perforated structure, which retains binder at the interface at higher speeds, reducing binder seepage. This finding contradicts the original hypothesis that lower speeds would yield stronger tack and indicates that Hexcel HiTape® 's architecture may be the reason for positive speed-related tack behaviour.

Sub question 3: How does the compaction pressure influence the tack behaviour of the Hexcel HiTape® dry fibre material?

Answer: The hypothesis that increased compaction force would increase tack is not supported by the results. From the statistical analysis of the main effect, compaction force is not statistically significant, falling below the 95% confidence interval.

Sub question 4: Do the interaction between the parameters show significance in understanding the tack behaviour ?

Answer: Analysis of both peel force and statistical data shows that interactions between temperature, speed, and compaction force have no statistically significant impact on tack behaviour. This suggests that each parameter primarily influences tack independently, with no meaningful interaction effects observed.

Main Research Question 2: Does the unique fibre architecture and binder distribution of the Hexcel HiTape ® dry fibre material in comparison to the Solvay TX1100 dry fibre material give rise to different tack behaviour?

Answer: The unique fibre architecture and binder type of Hexcel HiTape® produce distinct tack behaviour compared to Solvay TX1100. Modelling Hexcel HiTape® data using the Solvay TX1100 tack model showed poor alignment, especially concerning layup speed effects. Unlike Solvay TX1100, where lower speeds yield higher tack, Hexcel HiTape® demonstrated increased tack at higher speeds—likely due to its perforated structure, which may help retain binder at the interface. While this initial observation points to the impact of Hexcel HiTape® 's structure on tack, further investigation is needed to confirm this hypothesis. This finding underscores the importance of material-specific models to accurately represent Hexcel HiTape® 's unique response.

Main research Question 3: Can the Solvay TX1100 tack model be applied to Hexcel HiTape®, or is a new model needed?

Answer: The Solvay TX1100 tack model does not adequately predict tack behavior for Hexcel HiTape® without modification. Significant discrepancies between predicted and observed values, particularly concerning layup speed, highlight the model's limitations. The Solvay TX1100 model assumes a negative correlation between speed and tack, which does not apply to Hexcel HiTape®, where speed positively impacts tack. Modifying the model equation to reflect this relationship is essential for achieving accurate predictions with Hexcel HiTape®.

Conclusion

This study evaluated the influence of nip point temperature, velocity, and compaction force on the tack behaviour of Hexcel HiTape® dry fibre material in the Automated Dry Fibre Placement (ADFP) process. It also assessed the suitability of the existing Solvay TX1100 tack model for this material. Results indicate that nip point temperature is the most dominant factor influencing tack force, with observed values consistently exceeding the 99.9% confidence interval. Higher nip point temperatures enhance tack by promoting binder melt and adhesion between fibre layers. This aligned with the initially proposed hypothesis. However, the Solvay TX1100 model, which predicted an inverse relationship between velocity and tack force, did not fit Hexcel HiTape's behaviour accurately. Instead, a positive relationship was observed, where increased speeds led to higher tack, suggesting that Hexcel HiTape's fibre structure and binder characteristics likely caused the unique interactions.

The results also revealed a nonlinear relationship between increasing levels of temperature and velocity. Compaction force had a minimal direct impact on tack force. The statistical analysis further confirmed that tack force in Hexcel HiTape ® is largely independent of specific parameter combinations and compaction force, underscoring temperature as the primary driver of tack performance, followed by velocity.

Chapter 7

Future recommendations

- **Model Adaptation for Hexcel HiTape ®**: In future investigations, the model developed for the Solvay TX1100 material can be modified to account for the distinct tack behaviour observed in Hexcel HiTape ® dry fibre. Calibration of the model specific to Hexcel HiTape ® will allow for the development of a generalised framework that can be applied to other dry fibre materials as well.

- **Quantifying fraying after peel test**: Fraying observed during peel tests on Hexcel HiTape® dry fibre material provides insights into its tack behaviour in Automated Dry Fibre Placement (ADFP). In this context, fraying is beneficial, indicating strong bonding within AFP layers, and enhancing structural stability. However, for quality control during rework, manufacturers need to understand how process parameters affect fraying when rework has to be done.

  To quantify fraying, force-displacement curves from peel tests can be analysed, where the frayed region can be assigned a relative fraying intensity for each parameter combination. This can be done by analysing the slope of the force vs time graphs from peel testing and comparing it with the frayed region to the non-frayed region. Surface roughness measurements may also offer a quantitative metric for fibre disruption.

- **Investigation of the binder seepage hypothesis**: To investigate the binder seepage hypothesis linked to the material's perforations, additional plies of the fibre could be laid up, and microscopy could be used to observe the extent of seepage or confirm if it occurs. Micro-CT analysis could also be applied for a non-destructive, high-resolution view of internal binder distribution and any voids created by perforations. This combined approach would provide insights into how binder migration interacts with the fibre architecture, helping clarify its impact on tack behaviour.

- **Setting temperature slightly higher than 64 °C as the minimum Temperature for Future Investigations:**: The initial tests at 64°C revealed insufficient tack, suggesting incomplete binder activation in the HiTape ® material. In the absence of a datasheet specifying the binder's activation range, this study indicates that a slightly

higher temperature should be established as a baseline temperature for future testing. This threshold would ensure complete activation of the binder, allowing for a more precise evaluation of tack behaviour and a clearer understanding of the material's adhesive performance across varied conditions.

References

[1] Alex Brasington, Christopher Sacco, Joshua Halbritter, Roudy Wehbe, and Ramy Harik. Automated fiber placement: A review of history, current technologies, and future paths forward. *Composites Part C: Open Access*, 6:100182, 10 2021.

[2] K Kozaczuk Prace Instytutu Lotnictwa and undefined 2016. Automated fiber placement systems overview. *bibliotekanauki.plK KozaczukPrace Instytutu Lotnictwa, 2016 • bibliotekanauki.pl*.

[3] Jinglan Guo and Siyuan Wang. Multiphase Flow Coupling Behavior of Bubbles Based on Computational Fluid Dynamics during AFP Process: The Behavior Characteristics of Bubbles during AFP Process. *Advances in Materials Science and Engineering*, 2021, 2021.

[4] Daniel. Saar. Development of a Model Approach to Describe the Tack Behaviour in Dry Fibre Placement. *DLR(german Aerospace Center),*, 2021.

[5] Nima Bakhshi and Mehdi Hojjati. An experimental and simulative study on the defects appeared during tow steering in automated fiber placement. *Composites Part A: Applied Science and Manufacturing*, 113:122–131, 10 2018.

[6] Stefan Neunkirchen and Ralf Schledjewski. Tack measurement of bindered rovings for the dry fiber winding process. *Polymer Composites*, 42(9):4607–4616, 9 2021.

[7] J. S.U. Schell, J. Guilleminot, C. Binetruy, and P. Krawczak. Computational and experimental analysis of fusion bonding in thermoplastic composites: Influence of process parameters. *Journal of Materials Processing Technology*, 209(11):5211–5219, 6 2009.

[8] Yi Di Boon, Sunil Chandrakant Joshi, and Somen Kumar Bhudolia. Review: Filament Winding and Automated Fiber Placement with In Situ Consolidation for Fiber Reinforced Thermoplastic Polymer Composites. *Polymers 2021, Vol. 13, Page 1951*, 13(12):1951, 6 2021.

[9] Klaus Heller, David Colin, and Klaus Drechsler. Quantifying the Influence of Out-Time on Prepreg Material Properties and Out-Of-Plane Steering Defects During Automated Fiber Placement. *Frontiers in Materials*, 9:825809, 5 2022.

[10] Peel Testing | An Introduction | Instron.

[11] Aleksandar Sekulic. Experimental identification of adhesive properties between epoxy and glass. 11 2008.

[12] RJ Crossley, PJ Schubel, NA Warrior The 17th International, and undefined 2009. The experimental characterisation of prepreg tack. *iccm-central.orgRJ Crossley, PJ Schubel, NA WarriorThe 17th International Conference on Composite Materials (ICCM-17), 2009 • iccm-central.org.*

[13] Klaus Heller. Influence of Material Property Changes on Thermoset Automated Fiber Placement Processing | Request PDF, 12 2022.

[14] Chenping Zhang, Yugang Duan, Hong Xiao, Ben Wang, Yueke Ming, Yansong Zhu, and Fugan Zhang. The effects of processing parameters on the wedge peel strength of CF/PEEK laminates manufactured using a laser tape placement process. *International Journal of Advanced Manufacturing Technology*, 120(11-12):7251–7262, 6 2022.

[15] Nima Bakhshi. *Investigation of prepreg tack through development of an AFP simulator using in-situ sensing and physics-based simulation.* PhD thesis, 2023.

[16] Anis Baz Radwan. Experimental Analysis of the Automated Fiber Placement Manufacturing Parameters for High and Low Tack Prepreg Material. *Theses and Dissertations*, 7 2019.

[17] D. Budelmann, H. Detampel, C. Schmidt, and D. Meiners. Interaction of process parameters and material properties with regard to prepreg tack in automated lay-up and draping processes. *Composites Part A: Applied Science and Manufacturing*, 117:308–316, 2 2019.

[18] S. Rao, R. Umer, J. Thomas, and W. J. Cantwell. Investigation of peel resistance during the fibre placement process. *Journal of Reinforced Plastics and Composites*, 35(4):275–286, 2 2016.

[19] Francisco Sacchetti. *Interlaminar toughness of fusion bonded thermoplastic composites.* PhD thesis, University of Twente, Enschede, The Netherlands, 9 2017.

[20] C. Soutis. Fibre reinforced composites in aircraft construction. *Progress in Aerospace Sciences*, 41(2):143–151, 2 2005.

[21] F. C. Campbell. Manufacturing Processes for Advanced Composites. *Manufacturing Processes for Advanced Composites*, pages 1–517, 1 2003.

[22] Ronald F. Gibson. PRINCIPLES OF COMPOSITE MATERIAL MECHANICS, FOURTH EDITION. *Principles of Composite Material Mechanics, Fourth Edition*, pages 1–657, 1 2016.

[23] J Summerscales and T J Searle. Low-pressure (vacuum infusion) techniques for moulding large composite structures. *Proceedings of the Institution of Mechanical Engineers, Part L: Journal of Materials: Design and Applications*, 219(1):45–58, 1 2005.

[24] Ivan V Terekhov and Evgeniy M Chistyakov. Binders Used for the Manufacturing of Composite Materials by Liquid Composite Molding. *Polymers*, 14(1), 2022.

[25] Oliver Rimmel, David Becker, and Peter Mitschang. Maximizing the out-of-plane-permeability of preforms manufactured by dry fiber placement. *Advanced Manufacturing: Polymer & Composites Science*, 2(3-4):93–102, 10 2016.

[26] Dirk H.J.A. Lukaszewicz, Carwyn Ward, and Kevin D. Potter. The engineering aspects of automated prepreg layup: History, present and future. *Composites Part B: Engineering*, 43(3):997–1009, 4 2012.

[27] Michael Assadi and Tyler Field. AFP Processing of Dry Fiber Carbon Materials (DFP) for Improved Rates and Reliability. *SAE Technical Papers*, 2020-March(March), 3 2020.

[28] P. K. Mallick. Processing of Polymer Matrix Composites. *Processing of Polymer Matrix Composites: Processing and Applications*, pages 1–341, 1 2017.

[29] M. Y. Matveev, P. J. Schubel, A. C. Long, and I. A. Jones. Understanding the buckling behaviour of steered tows in Automated Dry Fibre Placement (ADFP). *Composites Part A: Applied Science and Manufacturing*, 90:451–456, 11 2016.

[30] R. Crossley, P. Schubel, and N. Warrior. THE EXPERIMENTAL CHARACTERISATION OF PREPREG TACK. 2009.

[31] Advanced Composite Structures | Northrop Grumman.

[32] Firefly Aerospace to Automate Composite Rocket Production with Ingersoll Machine Tools - Firefly Aerospace.

[33] A. Beakou, M. Cano, J. B. Le Cam, and V. Verney. Modelling slit tape buckling during automated prepreg manufacturing: A local approach. *Composite Structures*, 93(10):2628–2635, 9 2011.

[34] Omid Aghababaei Tafreshi, Suong Van Hoa, Farjad Shadmehri, Duc Minh Hoang, and Daniel Rosca. Determination of convective heat transfer coefficient for automated fiber placement (AFP) for thermoplastic composites using hot gas torch. *Advanced Manufacturing: Polymer & Composites Science*, 6(2):86–100, 4 2020.

[35] R. Funck and M. Neitzel. Improved thermoplastic tape winding using laser or direct-flame heating. *Composites Manufacturing*, 6(3-4):189–192, 1 1995.

[36] Khaled Yassin and Mehdi Hojjati. Processing of thermoplastic matrix composites through automated fiber placement and tape laying methods. *https://doi.org/10.1177/0892705717738305*, 31(12):1676–1725, 11 2017.

[37] Robert H. Rizzolo and Daniel F. Walczyk. Ultrasonic consolidation of thermoplastic composite prepreg for automated fiber placement. *http://dx.doi.org/10.1177/0892705714565705*, 29(11):1480–1497, 1 2015.

[38] B. Lauke and K. Friedrich. Evaluation of processing parameters of thermoplastic composites fabricated by filament winding. *Composites Manufacturing*, 4(2):93–101, 6 1993.

[39] Dominik Deden, Fabian Bruckner, Lars Brandt, and Frederic Fischer. COMPARISON OF HEAT SOURCES FOR AUTOMATED DRY FIBRE PLACEMENT: XENON FLASHLAMP VS. INFRARED HEATING. 2019.

[40] Vivek Agarwal, R. L. Mccullough, and J. M. Schultz. The thermoplastic laser-assisted consolidation process - Mechanical and microstructure characterization. *Journal of Thermoplastic Composite Materials*, 9(4):365–380, 1996.

[41] W. J.B. Grouve, L. L. Warnet, B. Rietman, H. A. Visser, and R. Akkerman. Optimization of the tape placement process parameters for carbon–PPS composites. *Composites Part A: Applied Science and Manufacturing*, 50:44–53, 7 2013.

[42] C. M. Stokes-Griffin and P. Compston. A combined optical-thermal model for near-infrared laser heating of thermoplastic composites in an automated tape placement process. *Composites Part A: Applied Science and Manufacturing*, 75:104–115, 5 2015.

[43] Francesca Lionetto, Riccardo Dell'Anna, Francesco Montagna, and Alfonso Maffezzoli. Modeling of continuous ultrasonic impregnation and consolidation of thermoplastic matrix composites. *Composites Part A: Applied Science and Manufacturing*, 82:119–129, 3 2016.

[44] Somen K. Bhudolia, Goram Gohel, Kah Fai Leong, and Aminul Islam. Advances in Ultrasonic Welding of Thermoplastic Composites: A Review. *Materials 2020, Vol. 13, Page 1284*, 13(6):1284, 3 2020.

[45] Humm3® for composites.

[46] Duy Chinh Nguyen, Andreas Kolbe, and Constantin Bäns. Application of Lightning Strike Protection on Thermoplastic Structures by Automated Fiber Placement. 9 2020.

[47] Mattia Di Francesco, Laura Veldenz, Giuseppe Dell'Anno, and Kevin Potter. Heater power control for multi-material, variable speed Automated Fibre Placement. *Composites Part A: Applied Science and Manufacturing*, 101:408–421, 10 2017.

[48] Helena Rocha, Agnieszka Rocha, Joana Malheiro, Bruno Sousa, Andreia Vilela, Filipa Carneiro, and Paulo Antunes. Development and Manufacturing of a Fibre Reinforced Thermoplastic Composite Spar Produced by Oven Vacuum Bagging. *Polymers 2024, Vol. 16, Page 2216*, 16(15):2216, 8 2024.

[49] Marco Valente, Ilaria Rossitti, and Matteo Sambucci. Different Production Processes for Thermoplastic Composite Materials: Sustainability versus Mechanical Properties and Processes Parameter. *Polymers 2023, Vol. 15, Page 242*, 15(1):242, 1 2023.

[50] Ya-Nan Liu, Chongxin Yuan, Chenxiao Liu, Jie Pan, and Qinghai Dong. Study on the resin infusion process based on automated fiber placement fabricated dry fiber preform. *Scientific Reports*, 9, 10 2019.

[51] (PDF) On the development of multi-material automated fibre placement technology - ICMAC2015.

[52] Laura Veldenz, Mattia Di Francesco, Peter Giddings, Byung Chul Kim, and Kevin Potter. Material selection for automated dry fiber placement using the analytical hierarchy process. *Advanced Manufacturing: Polymer & Composites Science*, 4(4):83–96, 10 2018.

[53] (PDF) CHARACTERISTICS AND PROCESSABILITY OF BINDERED DRY FIBRE MATERIAL FOR AUTOMATED FIBRE PLACEMENT.

[54] Ajay Kumar Kadiyala, Alexandre Portela, Keith Devlin, Stephen Lee, Anthony O'Carroll, David Jones, and A J Comer. Journal Pre-proof Mechanical evaluation and failure analysis of composite laminates manufactured using automated dry fibre tape placement followed by liquid resin infusion, 11 2020.

[55] Xin Liu, Shimeng Qian, Yaoyao Ye, Qiang Xu, and Xiangqian Li. Effect of process parameters on mode-II interlaminar fracture toughness and fractographic features of automated fibre placement prepreg laminates. *Journal of Composite Materials*, 55(30):4489–4501, 8 2021.

[56] Nima Bakhshi and Mehdi Hojjati. Effect of compaction roller on layup quality and defects formation in automated fiber placement. *Journal of Reinforced Plastics and Composites*, 39(1-2):3–20, 1 2020.

[57] Ozan Çelik, Daniël Peeters, Clemens Dransfeld, and Julie Teuwen. Intimate contact development during laser assisted fiber placement: Microstructure and effect of process parameters. *Composites Part A: Applied Science and Manufacturing*, 134:105888, 2020.

[58] O J Nixon-Pearson, Jonathan Belnoue, Dmitry Ivanov, K D Potter, and Stephen Hallett. An experimental investigation of the consolidation behaviour of uncured prepregs under processing conditions. *Journal of Composite Materials*, 51, 11 2016.

[59] Adrian P Mouritz. Introduction to Aerospace Materials - Adrian P Mouritz - Google Books.

[60] Tauseef Aized and Bijan Shirinzadeh. Robotic fiber placement process analysis and optimization using response surface method. *International Journal of Advanced Manufacturing Technology*, 55(1-4):393–404, 7 2011.

[61] Magd Abdel Wahab. *Joining composites with adhesives: theory and applications*. 11 2015.

[62] Zhaoyi Sun, Zhiyuan Mei, Zheng Huang, and Guorong Wang. Preparation and Mechanical Properties of Flexible Prepreg Resin with High Strength and Low Creep. *Polymers 2024, Vol. 16, Page 558*, 16(4):558, 2 2024.

[63] C. M. Stokes-Griffin and P. Compston. Investigation of sub-melt temperature bonding of carbon-fibre/PEEK in an automated laser tape placement process. *Composites Part A: Applied Science and Manufacturing*, 84:17–25, 5 2016.

[64] Philip He, Dara Alfred, and C Loos. Thermoplastic matrix composite processing model, 1985.

[65] P. G. De Gennes. Reptation of a Polymer Chain in the Presence of Fixed Obstacles. *The Journal of Chemical Physics*, 55(2):572–579, 7 1971.

[66] F. Yang and R. Pitchumani. Healing of Thermoplastic Polymers at an Interface under Nonisothermal Conditions. *Macromolecules*, 35(8):3213–3224, 4 2002.

[67] R. P. Wool, B. -L Yuan, and O. J. McGarel. Welding of polymer interfaces. *Polymer Engineering & Science*, 29(19):1340–1367, 1989.

[68] Christopher J Wohl, Curtis W. Hickmott, Victoria E Hutton, Alireza Forghani, Frank L Palmieri, and Brian W. Grimsley. Characterization of Prepreg Tack for Composite Manufacturing by Automated Fiber Placement. *NASA Langley Research Center*.

[69] A. Zosel. Adhesion and tack of polymers: Influence of mechanical properties and surface tensions. *Colloid and Polymer Science*, 263(7):541–553, 7 1985.

[70] O. Dubois, J. B. Le Cam, and A. Béakou. Experimental analysis of prepreg tack. *Experimental Mechanics*, 50(5):599–606, 6 2010.

[71] Yi Wang, Sarthak Mahapatra, Jonathan P.H. Belnoue, Dmitry S. Ivanov, and Stephen R. Hallett. Understanding tack behaviour during prepreg-based composites' processing. *Composites Part A: Applied Science and Manufacturing*, 164:107284, 1 2023.

[72] R. J. Crossley, P. J. Schubel, and D. S.A. De Focatiis. Time–temperature equivalence in the tack and dynamic stiffness of polymer prepreg and its application to automated composites manufacturing. *Composites Part A: Applied Science and Manufacturing*, 52:126–133, 9 2013.

[73] D8336 Standard Test Method for Characterizing Tack of Prepregs Using a Continuous Application-and-Peel Procedure.

[74] Probe Tack Test of Adhesive Tape | SHIMADZU (Shimadzu Corporation).

[75] Anthony J. Comer, Peter Hammond, Dipa Ray, John Lyons, Winifred Obande, David Jones, Ronan O Higgins, and Michael Mccarthy. Wedge Peel Interlaminar Toughness of Carbon- Fibre / Peek Thermoplastic Laminates Manufactured By Laser- Assisted Automated-Tape-Placement. *SETEC 14*, (November 10-11th), 2014.

[76] Duy Chinh Nguyen and Christian Krombholz. Influence of Process Parameters and Material Aging on the Adhesion of Prepreg in AFP Processes. 2016.

[77] Chinh D Nguyen and Dominik Delisle. FIRST PLY TACK OF AN AUTOMATED FIBRE PLACEMENT PROCESS-INFLUENCE OF HEATABALE MOULD SURFACE, RELEASE FILMS AND PROCESS PARAMETERS. Technical report, 2017.

[78] Benno Böckl, Christian Jetten, Klaus Heller, Christoph Ebel, and Klaus Drechsler. ONLINE MONITORING SYSTEM FOR THE TACK OF PREPREG SLIT TAPES USED IN AUTOMATED FIBER PLACEMENT. Technical report, 2018.

[79] Andreas Endruweit, Gabriel Y.H. Choong, Sayata Ghose, Brice A. Johnson, Douglas R. Younkin, Nicholas A. Warrior, and Davide S.A. De Focatiis. Characterisation of tack for uni-directional prepreg tape employing a continuous application-and-peel test method. *Composites Part A: Applied Science and Manufacturing*, 114:295–306, 11 2018.

[80] I. Y. Chang and J. K. Lees. Recent Development in Thermoplastic Composites: A Review of Matrix Systems and Processing Methods. *http://dx.doi.org/10.1177/089270578800100305*, 1(3):277–296, 7 1988.

[81] Christopher Wohl, Frank L. Palmieri, Alireza Forghani, Curtis Hickmott, Houman Bedayat, Brian Coxon, Anoush Poursartip, and Brian Grimsley. Tack Measurements of Prepreg Tape at Variable Temperature and Humidity, 2017.

[82] Dharmaraja Selvamuthu and Dipayan Das. Introduction to Probability, Statistical Methods, Design of Experiments and Statistical Quality Control. 2024.

[83] Anup K. Das and Saikat Dewanjee. Optimization of Extraction Using Mathematical Models and Computation. *Computational Phytochemistry*, pages 75–106, 1 2018.

[84] Coriolis C1.2 - Coriolis Composites.

[85] Klaus Heller, Simon Seyfferth, Kalle Kind, and Klaus Drechsler. A Post Lay-up Tack Peel Test for Aerospace Grade Prepreg Tapes. 9 2020.

[86] R. J. Crossley, P. J. Schubel, and N. A. Warrior. The experimental determination of prepreg tack and dynamic stiffness. *Composites Part A: Applied Science and Manufacturing*, 43(3):423–434, 3 2012.

[87] Asghar Ghasemi and Saleh Zahediasl. Normality Tests for Statistical Analysis: A Guide for Non-Statisticians. *International journal of endocrinology and metabolism*, 10:486–489, 11 2012.

[88] D. C. Montgomery. Design and Analysis of Experiments, John Wiley & Sons. *Mycological Research*, 106(11):1323–1330, 2017.

[89] Simo Puntanen. Regression Analysis by Example, Fifth Edition by Samprit Chatterjee, Ali S. Hadi. *International Statistical Review*, 81, 11 2013.

Appendix A

Appendix A

No.	V (Speed)	T (Temperature)	F (Force)	y
1	-	-	+	y_1
2	+	-	+	y_2
3	-	-	-	y_3
4	+	-	-	y_4
5	0	-	0	y_5
6	0	0	0	y_6
7	0	0	+	y_7
8	0	0	-	y_8
9	+	0	0	y_9
10	-	0	0	y_{10}
11	-	+	+	y_{11}
12	-	+	-	y_{12}
13	+	+	+	y_{13}
14	+	+	-	y_{14}
15	0	+	0	y_{15}

Table A.1: Combinations of Speed (V), Temperature (T), and Force (F) for the face centred central composite design

Block	Group	T (°C)	V (m/s)	F (N)	Cube Group
1	Group 1	64	0.04	500	G1
1	Group 2	64	0.2	500	G10
1	Group 3	64	0.04	300	G3
1	Group 4	64	0.2	300	G4
1	Group 5	64	0.12	400	G11
2	Group 6	95	0.12	400	G6
2	Group 7	95	0.12	500	G7
2	Group 8	95	0.12	300	G8
2	Group 9	95	0.2	400	G15
2	Group 10	95	0.04	400	G5
3	Group 11	125	0.04	500	G2
3	Group 12	125	0.04	300	G9
3	Group 13	125	0.2	500	G13
3	Group 14	125	0.2	300	G14
3	Group 15	125	0.12	400	G12

Table A.2: Group Distribution Based on Temperature (T), Speed (V), Force (F), and Cube Group with Correct Color Coding

GROUP	SPECIMEN	MEAN PEEL	STD DEVIATION PEEL	MEAN fibre BEND	VARIANCE BEND	STD DEVIATION BEND	MEAN TACK	VARIANCE TACK	STD DEVIATION TACK
1	11	0.485378699	0.249146138	0.257254163	0.000495111	0.022251081	0.228124536	0.062073798	0.249146138
2	12	2.985489469	1.018206236	0.188621856	0.000767616	0.027705879	2.796867613	1.03674394	1.018206236
3	13	0.286119425	0.053439123	0.263569562	0.00370113	0.060836915	0.022549863	0.00285574	0.053439123
4	14	2.524898654	0.80683136	0.273173667	0.000953742	0.030882714	2.251724986	0.650976844	0.80683136
5	15	1.555962318	0.421672217	0.243904757	0.000540269	0.023243695	1.3125.3457562	0.177807458	0.421672217
6	21	8.926505531	0.640220117	0.210532712	0.000905127	0.030085325	8.715972818	0.409881798	0.640220117
7	22	9.239803427	0.718561191	0.23441387	0.000766288	0.027681913	9.005389558	0.516330186	0.718561191
8	23	11.1947829	1.439095874	0.258720295	0.001031022	0.03210953	10.93606261	2.070996935	1.439095874
9	24	11.21756942	1.010763439	0.256946138	0.000991537	0.031488681	10.96062328	1.021642729	1.010763439
10	25	3.688360565	1.41048976	0.228283381	0.001393668	0.037331866	3.460077184	1.989481363	1.41048976
11	31	8.810996967	1.11067716	0.195399922	0.000946971	0.030772894	8.615597045	1.233603754	1.11067716
12	32	8.21556652	1.233500211	0.249394172	0.001577354	0.039715911	7.966172348	1.521522771	1.233500211
13	33	9.392913525	0.043807376	0.20081941	0.001919086	0.043807376	9.192094115	0.448665162	0.669824725
14	34	10.32459852	1.011967774	0.260713008	0.002708531	0.052043552	10.06388551	1.024078775	1.011967774
15	35	8.257518133	0.897966079	0.166608443	0.000436247	0.020886535	8.09090969	0.806343079	0.897966079

Table A.3: Summary of the mean peel force, bending force, and tack force with standard deviations and variances for each specimen group.

S	**T**	**F**	**Lamp 1**	**Lamp 2**	**Lamp 3**
0.04	64	500	10	7	7
0-2	64	500	32	30	30
0-04	64	300	10	7	7
0-2	64	300	32	30	30
0.12	64	400	20	20	20
0.12	95	400	35	36	36
0-12	95	500	35	36	36
0-12	95	300	35	36	36
0.2	95	400	63	55	55
0.04	95	400	8	10	10
0.04	125	500	25	20	20
0-04	125	300	25	20	20
0-2	125	500	86	86	86
0-2	125	300	86	86	86
0.12	125	400	30	50	50

Table A.4: Power outputs of the lamps under various conditions.

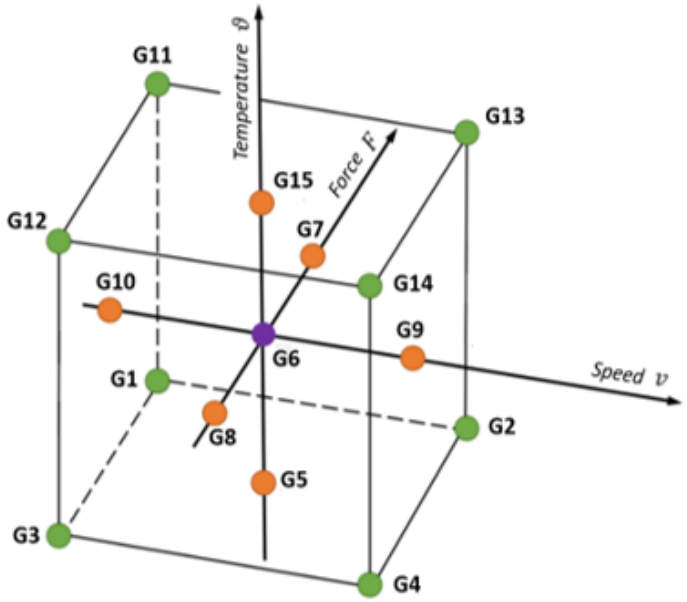

Figure A.1: face centered cube representing the groups chosen for the design of experiments

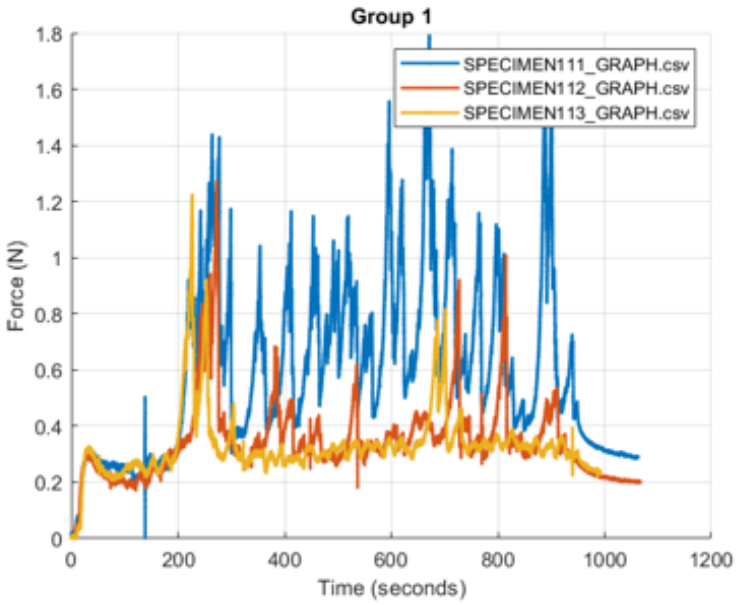

Figure A.2: Peel force vs time data for group 1

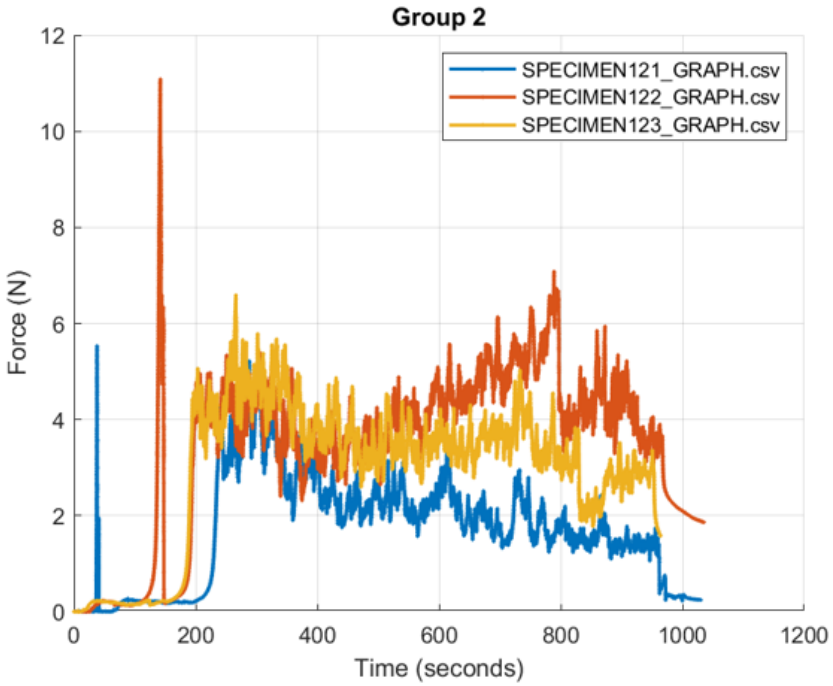

Figure A.3: Peel force vs time data for group 2

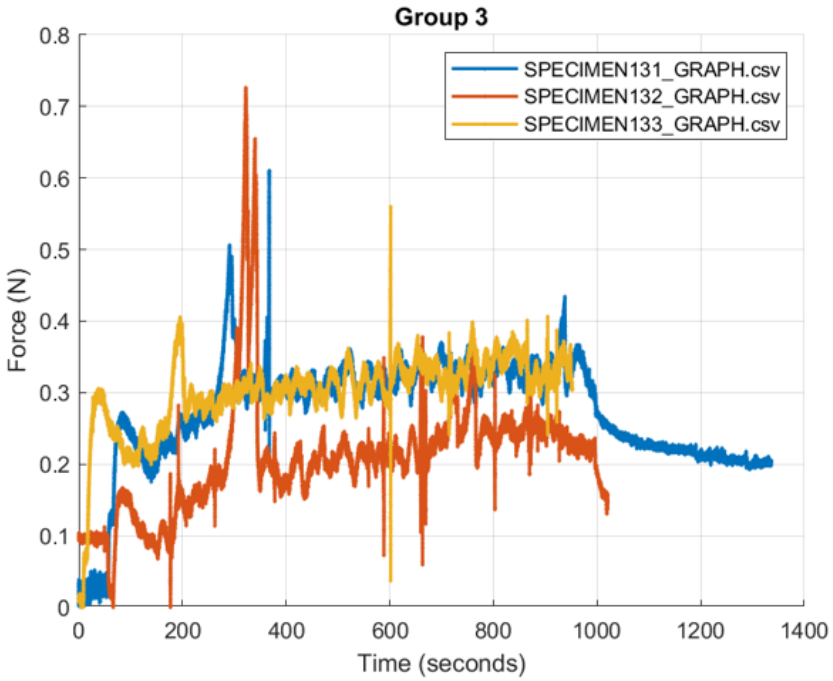

Figure A.4: Peel force vs time data for group 3

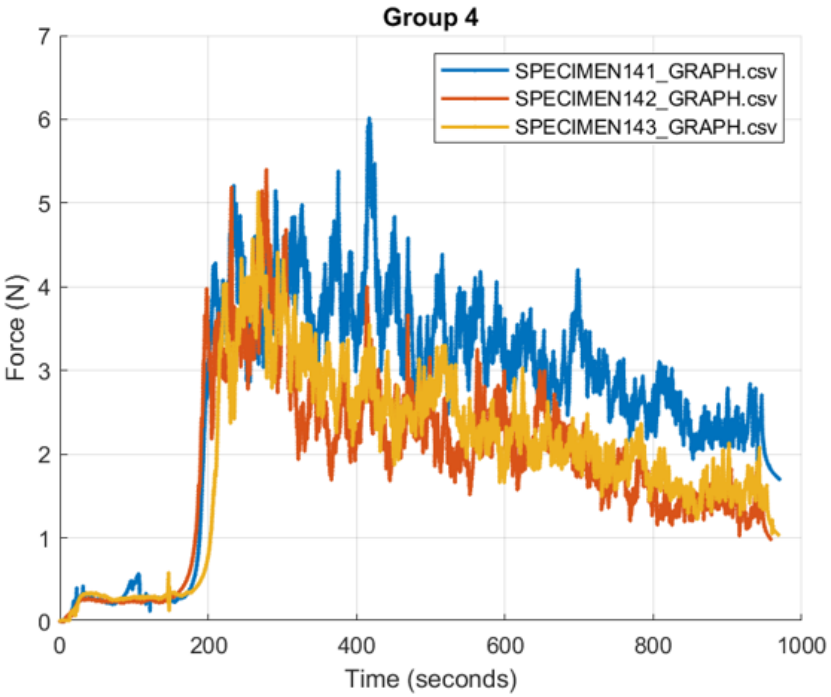

Figure A.5: Peel force vs time data for group 4

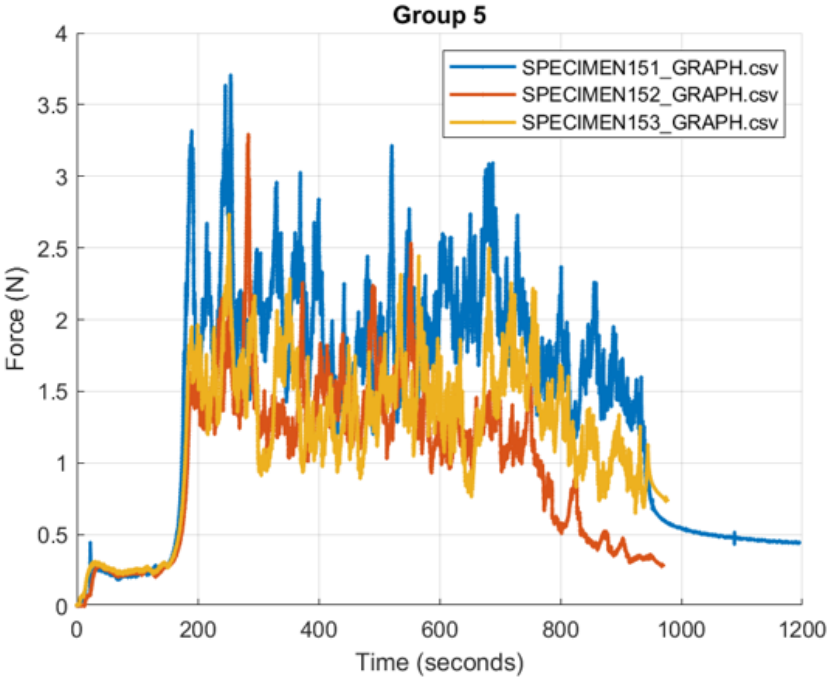

Figure A.6: Peel force vs time data for group 5

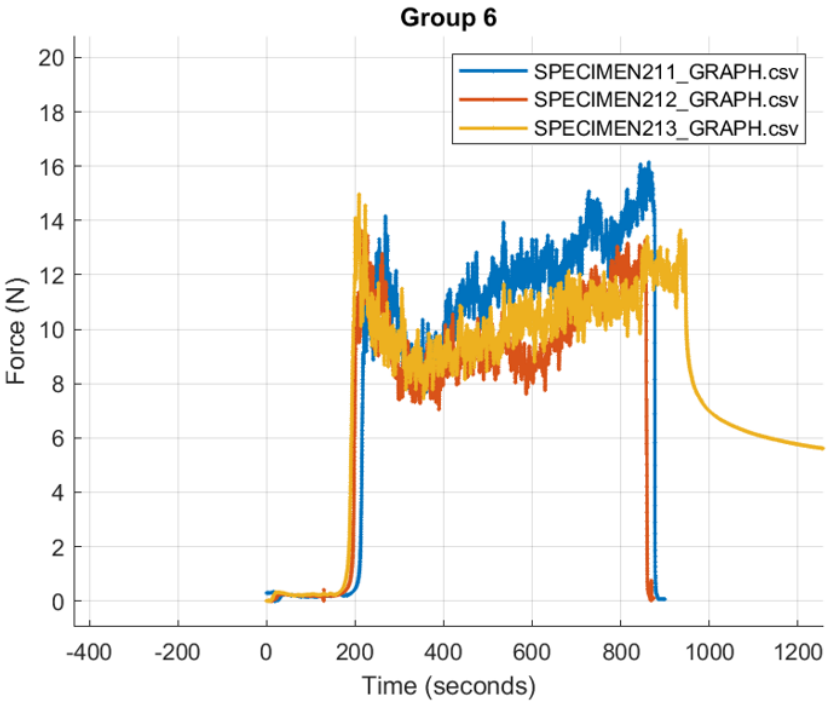

Figure A.7: Peel force vs time data for group 6

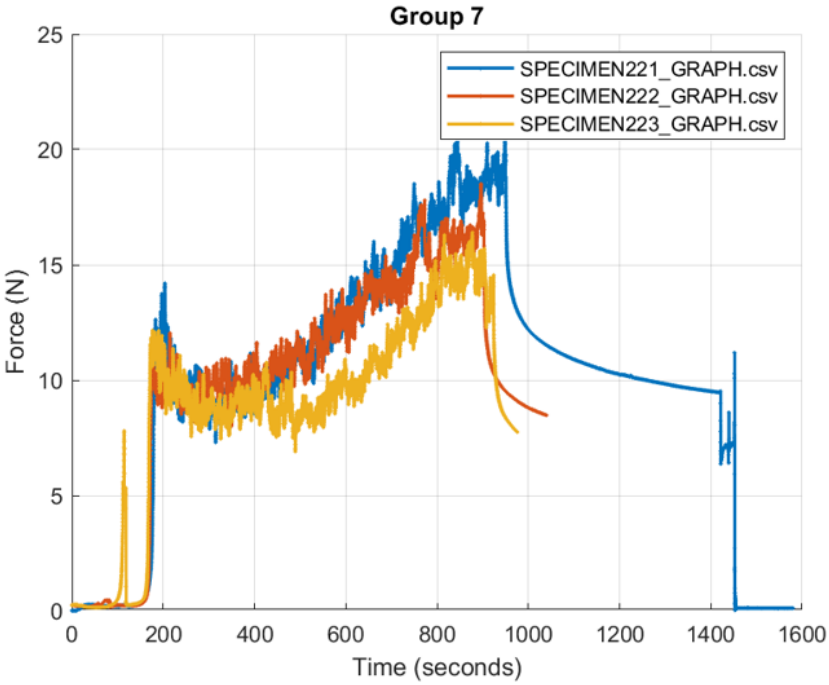

Figure A.8: Peel force vs time data for group 7

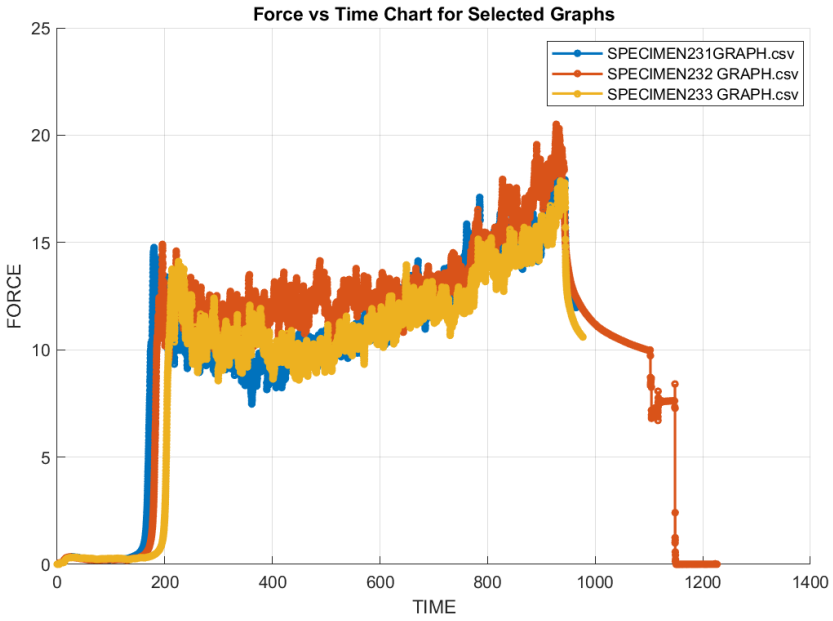

Figure A.9: Peel force vs time data for group 8

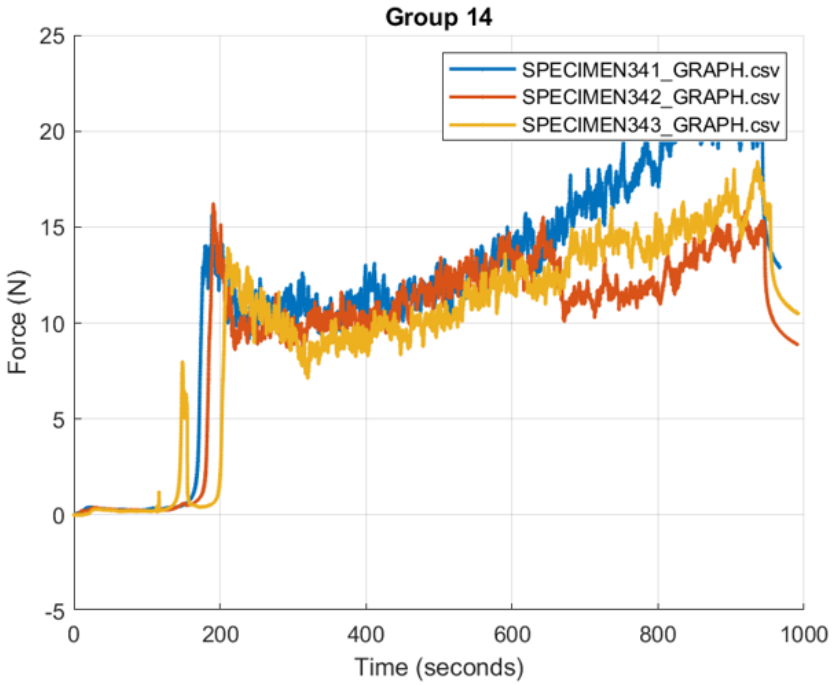

Figure A.10: Peel force vs time data for group 9

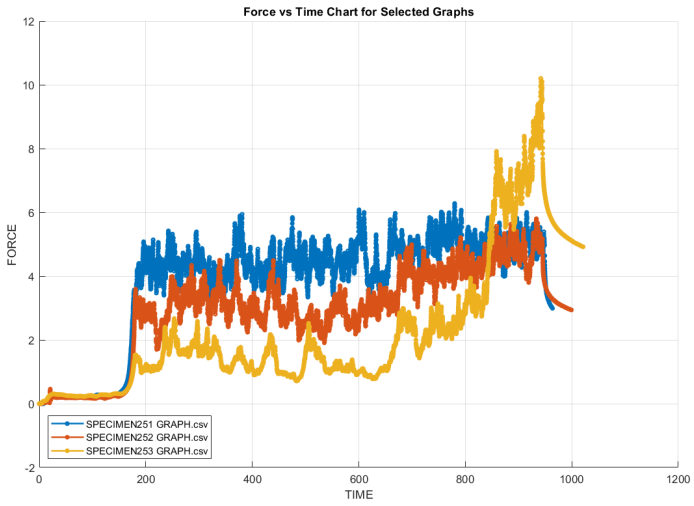

Figure A.11: Peel force vs time data for group 10

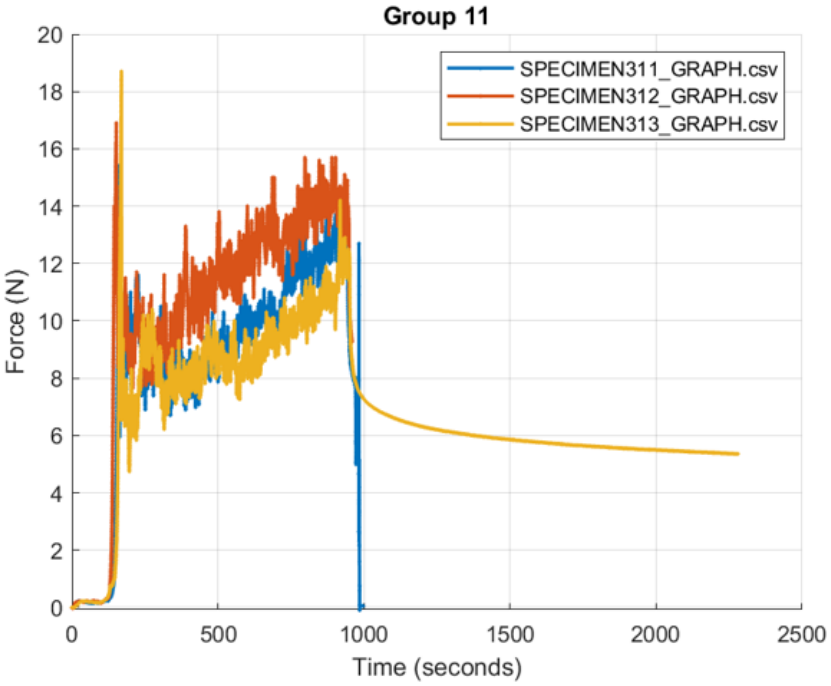

Figure A.12: Peel force vs time data for group 11

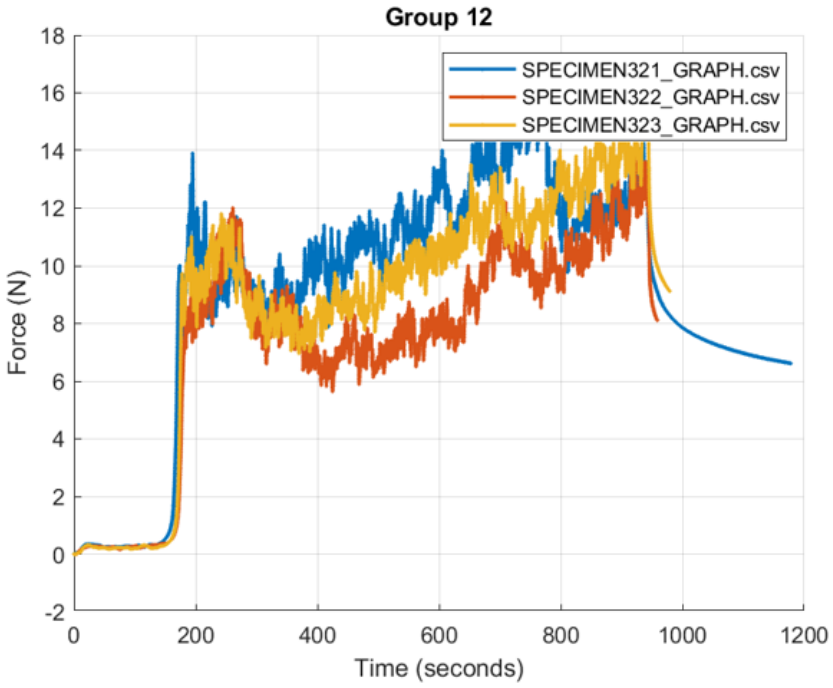

Figure A.13: Peel force vs time data for group 12

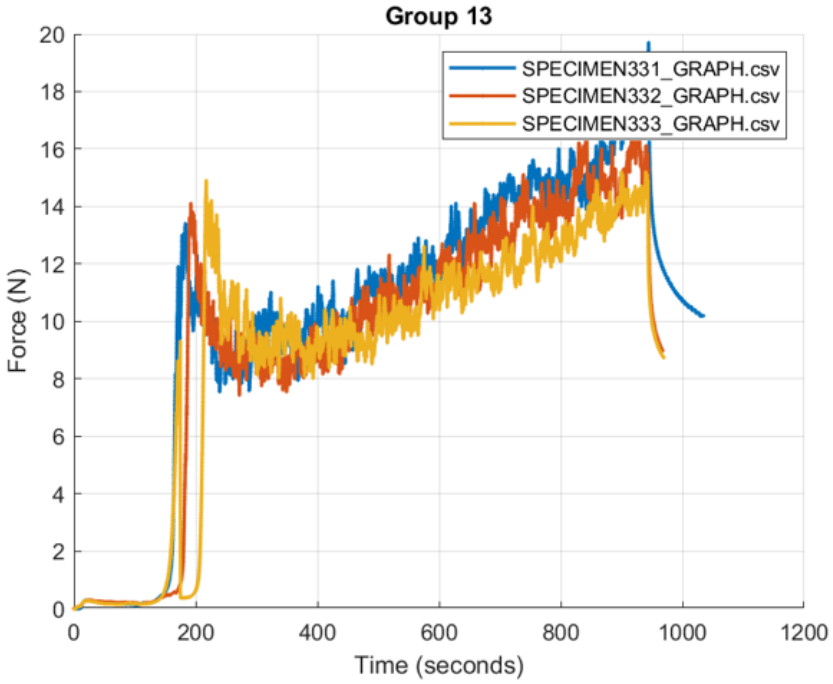

Figure A.14: Peel force vs time data for group 13

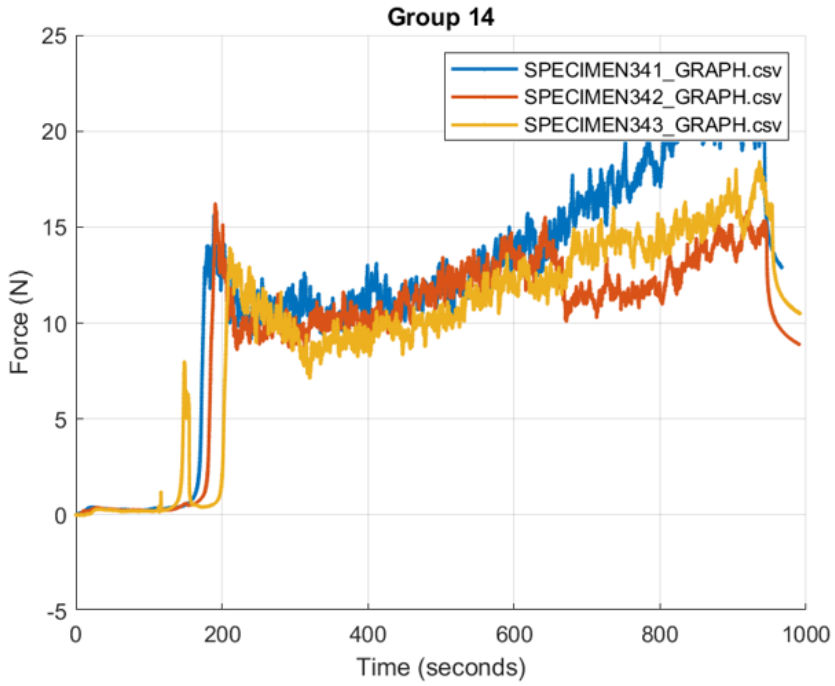

Figure A.15: Peel force vs time data for group 14

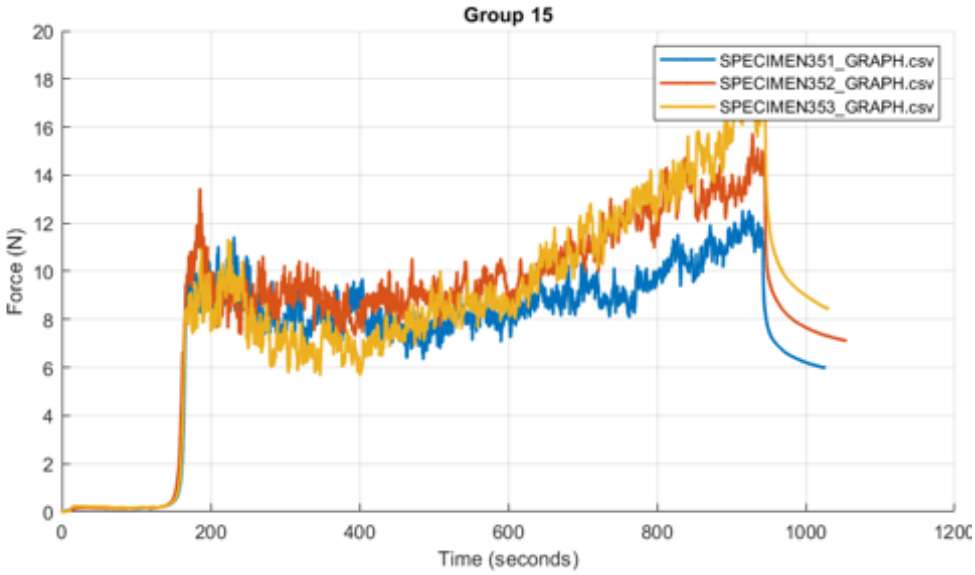

Figure A.16: Peel force vs time data for group 15

Group	Specimen	Mean Tack Force	i	$\frac{i-0.5}{n} \times 100\%$
3	13	0.022549863	1	3.33
1	11	0.228124536	2	10.00
5	15	1.312057562	3	16.67
4	14	2.251724986	4	23.33
2	12	2.796867613	5	30.00
10	25	3.460077184	6	36.67
12	32	7.966172348	7	43.33
13	33	8.09090969	8	50.00
11	31	8.615597045	9	56.67
6	21	8.715972818	10	63.33
7	22	9.005389558	11	70.00
15	35	8.09090969	12	76.67
9	24	10.93606232	13	83.33
14	34	10.06388551	14	90.00
8	23	10.96062328	15	96.67

Table A.5: Quantile distribution sorted in ascending order for the mean tack forces.

Group	Specimen	Mean Bending Force	i	$\frac{i-0.5}{n} \times 100\%$
15	35	0.166608443	1	3.33
2	12	0.188621856	2	10.00
11	31	0.195399922	3	16.67
13	33	0.20081941	4	23.33
6	21	0.210532712	5	30.00
10	25	0.228283381	6	36.67
8	23	0.23441387	7	43.33
5	15	0.243904757	8	50.00
12	32	0.249394172	9	56.67
9	24	0.256946138	10	63.33
1	11	0.257254163	11	70.00
7	22	0.258720295	12	76.67
3	13	0.263569562	13	83.33
14	34	0.260713008	14	90.00
4	14	0.273173667	15	96.67

Table A.6: Mean Bending Force quantile distribution sorted in ascending order

	TACK	BEND
$\sum$ Var Bend	5.980520785	0.12861199
S^2	0.747565098	0.016076499
$S_{\bar{d}}$	0.352979012	0.05176308

Table A.7: Calculation of standard deviation for 2^k factorial set.

	Area two tailed										
df	0	0.5	0.6	0.7	0.8	0.9	0.95	0.98	0.99	0.998	0.999
1	0	1	1.376	1.963	3.078	6.314	12.71	31.82	63.66	318.31	636.62
2	0	0.816	1.061	1.386	1.886	2.92	4.303	6.965	9.925	22.327	31.599
3	0	0.765	0.978	1.25	1.638	2.353	3.182	4.541	5.841	10.215	12.924
4	0	0.741	0.941	1.19	1.533	2.132	2.776	3.747	4.604	7.173	8.61
5	0	0.727	0.92	1.156	1.476	2.015	2.571	3.365	4.032	5.893	6.869
6	0	0.718	0.906	1.134	1.44	1.943	2.447	3.143	3.707	5.208	5.959
7	0	0.711	0.896	1.119	1.415	1.895	2.365	2.998	3.499	4.785	5.408
8	0	0.706	0.889	1.108	1.397	1.86	2.306	2.896	3.355	4.501	5.041
9	0	0.703	0.883	1.1	1.383	1.833	2.262	2.821	3.25	4.297	4.781
10	0	0.7	0.879	1.093	1.372	1.812	2.228	2.764	3.169	4.144	4.587
11	0	0.697	0.876	1.088	1.363	1.796	2.201	2.718	3.106	4.025	4.437
12	0	0.695	0.873	1.083	1.356	1.782	2.179	2.681	3.055	3.93	4.318
13	0	0.694	0.87	1.079	1.35	1.771	2.16	2.65	3.012	3.852	4.221
14	0	0.692	0.868	1.076	1.345	1.761	2.145	2.624	2.977	3.787	4.14
15	0	0.691	0.866	1.074	1.341	1.753	2.131	2.602	2.947	3.733	4.073
16	0	0.69	0.865	1.071	1.337	1.746	2.12	2.583	2.921	3.686	4.015

Figure A.17: student's two-sided t-distribution table

Factors	Mean -	Mean 0	Mean +	Effect
Temperature T	1.3248	8.6156	8.9594	7.6346
Force F	6.2481	6.5079	5.9676	-0.2805
Velocity v	4.0585	7.6121	7.0530	2.9945

Table A.8: Mean Effects of Temperature, Force, and Velocity on Tack Force

T+	T0	T-	V-	V0	V+	F-	F0	F+
0.5182	0.5744	0.3209	0.5065	0.4686	0.4723	0.5302	0.4834	0.4194

Table A.9: Standard Deviation of Main Parameters

Appendix B

Appendix B

B.1 MATLAB Code for Model Fitting

```
T = [64.09, 64.09, 64.09, 64.09, 64.09, 95.43, 95.43, 95.43, 95.43, 95.43,
    125.34, 125.34, 125.34, 125.34, 125.34]'; % Temperature
F = [500, 500, 300, 300, 400, 400, 500, 300, 400, 400, 500, 300, 500, 300,
    400]'; % Applied force
Mean_tack = [0.2281, 2.7969, 0.0225, 2.2517, 1.3121, 8.7160, 9.0054, 10.9361,
    10.9606, 3.4601, 8.6156, 7.9662, 9.1921, 10.0639, 8.0909]'; % Observed
    tack

% Define the Model Equation
% This function defines the model for tack based on T, F, and V with
    parameters a, b, and c
tackModel = @(params, T, F, V) (params(3) * F.^0.2) ./ ...
                                (params(1) * exp(params(2) ./ (5 * T)) .* V
                                    .^0.5);

% Initial parameter guesses for a, b, and c
initialParams = [0.3, 1488, 0.24]; % [a, b, c]

% Perform nonlinear regression to fit the model
opts = optimoptions('lsqcurvefit', 'Display', 'off');
[fitParams, resnorm, residuals, exitflag, output] = lsqcurvefit(@(params, X)
    ...
    tackModel(params, X(:,1), X(:,2), X(:,3)), initialParams, [T, F, V],
        Mean_tack, [], [], opts);

% Extract estimated parameters
a_estimated = fitParams(1);
b_estimated = fitParams(2);
c_estimated = fitParams(3);

% Display estimated parameters
fprintf('Estimated parameter a: %.4f\n', a_estimated);
fprintf('Estimated parameter b: %.4f\n', b_estimated);
```

```
fprintf('Estimated parameter c: %.4f\n', c_estimated);
fprintf('Residual norm (SSE): %.4f\n', resnorm);

% Calculate Goodness of Fit (R-squared)
sse = sum(residuals.^2);
sst = sum((Mean_tack - mean(Mean_tack)).^2);
rsquare = 1 - (sse / sst);
fprintf('R-squared: %.4f\n', rsquare);

% Calculate error metrics
MAE = mean(abs(residuals));
RMSE = sqrt(mean(residuals.^2));
fprintf('Mean Absolute Error (MAE): %.4f\n', MAE);
fprintf('Root Mean Squared Error (RMSE): %.4f\n', RMSE);

% Fit Evaluation Criteria
is_good_fit = true;

if rsquare < 0.5
    fprintf('R-squared is low (R^2 = %.4f): Model does not explain much variability in the data.\n', rsquare);
    is_good_fit = false;
end

if MAE > 2 * mean(Mean_tack)
    fprintf('High Mean Absolute Error (MAE = %.4f): Predictions deviate significantly from observed values.\n', MAE);
    is_good_fit = false;
end

if RMSE > std(Mean_tack)
    fprintf('High RMSE (RMSE = %.4f): Error distribution is larger than standard deviation of observed values.\n', RMSE);
    is_good_fit = false;
end

% Summary of Fit Quality
if is_good_fit
    fprintf('The model is a GOOD fit for the data based on the criteria.\n');
else
    fprintf('The model is NOT a good fit for the data based on the criteria.\n');
end

% Calculate predicted tack values using the fitted parameters
predicted_tack = tackModel(fitParams, T, F, V);

% Plot Observed vs. Predicted Tack Values with Points Only
figure;
plot(1:length(Mean_tack), Mean_tack, 'bo', 'MarkerSize', 8, 'DisplayName', 'Observed Tack'); % Observed tack as points only
hold on;
plot(1:length(predicted_tack), predicted_tack, 'r*', 'MarkerSize', 8, 'DisplayName', 'Predicted Tack'); % Predicted tack as points only
xlabel('Data Point');
ylabel('Tack');
title('Observed vs. Predicted Tack Values');
```

```
77 legend('Observed Tack', 'Predicted Tack');
78 xticks(1:15); % Ensure all 15 points are displayed on the x-axis
79 xticklabels(1:15); % Label each x-tick from 1 to 15
80 hold off;
81
82 % Plot Residuals with Zero Reference Line and Custom X-Axis Labels
83 figure;
84 x_values = 1:length(residuals);
85 plot(x_values, residuals, 'o', 'MarkerSize', 8, 'DisplayName', 'Residuals'); %
       Plot residuals as points only
86 hold on;
87 yline(0, '--', 'LineWidth', 1.5, 'DisplayName', 'Zero Reference Line'); % Add
      reference line at y = 0
88 xlabel('Data Point');
89 ylabel('Residual');
90 title('Residuals of the Fit');
91 xticks(1:15); % Ensure all 15 points are displayed on the x-axis
92 xticklabels(1:15); % Label each x-tick from 1 to 15
93 legend('Residuals', 'Zero Reference Line');
94 hold off;
```

Listing B.1: MATLAB code for nonlinear model fitting